A&A manuscript no.
(will be inserted by hand later)

Your thesaurus codes are:

ASTRONOMY
AND
ASTROPHYSICS
1.2.2008

Galactic chemical enrichment with new metallicity dependent stellar yields

L. Portinari[1], **C. Chiosi**[2,1], **and A. Bressan**[3]

[1] Department of Astronomy, University of Padova, Vicolo dell'Osservatorio 5, 35122 Padova, Italy
[2] European Southern Observatory, K-Schwarzschild-strasse 2, D-85748, Garching bei München, Germany
[3] Astronomical Observatory of Padova, Vicolo dell'Osservatorio 5, 35122 Padova, Italy
e-mail: portinari, chiosi, bressan@pd.astro.it

Received December 1997; accepted

Abstract. New detailed stellar yields of several elemental species are derived for massive stars in a wide range of masses (from 6 to 120 $M_{\odot}$) and metallicities (Z =0.0004, 0.004, 0.008, 0.02, 0.05). Our calculations are based on the Padova evolutionary tracks and take into account recent results on stellar evolution, such as overshooting and quiescent mass-loss, paying major attention to the effects of the initial chemical composition of the star. We finally include modern results on explosive nucleosynthesis in SNæ by Woosley & Weaver 1995. The issue of the chemical yields of Very Massive Objects (from 120 to 1000 $M_{\odot}$) is also addressed.

Our grid of stellar yields for massive stars is complementary to the results by Marigo et al. (1996, 1997) on the evolution and nucleosynthesis of low and intermediate mass stars, also based on the Padova evolutionary tracks. Altogether, they represent a complete set of stellar yields of unprecedented homogeneity and self-consistency.

Our new stellar yields are inserted in a code for the chemical evolution of the Galactic disc with infall of primordial gas, according to the formulation first suggested by Talbot & Arnett (1971, 1973, 1975) and Chiosi (1980). As a first application, the code is used to develop a model of the chemical evolution of the Solar Vicinity, with a detailed comparison to the available observational constraints.

Key words: Stars: evolution, nucleosynthesis – stars: mass loss – stars: supernovæ – Galaxy: Solar Neighbourhood – Galaxy: evolution – Galaxy: abundances

Send offprint requests to: L. Portinari

1. Introduction

In modelling the chemical evolution of our own Galaxy as well as of external galaxies, we deal with three basic ingredients: (1) the Star Formation Rate (SFR), (2) the Initial Mass Function (IMF) and (3) the stellar ejecta of different elements. Indeed, the chemical enrichment of galaxies is basically due to stars: while primordial nucleosynthesis produced mainly light elements, say up to ^7Li (Adouze 1986, Walker et al. 1991), heavier species (metals) are due to stellar nucleosynthesis, either hydrostatic or explosive as in the case of supernovæ (SNæ). Therefore, a chemical model should estimate accurately the role of stars of different masses in enriching the interstellar medium (ISM) with various elemental species. To this aim, one needs to consider the main nucleosynthetic processes taking place in stellar interiors, combined with a modelling of stellar evolution.

New extended sets of stellar tracks for fine grids of masses and metallicities have recently become available from various research groups. The body of these models shows that the initial chemical composition of a star bears on the details of its evolution. Therefore, we expect that stellar ejecta depend not only on the mass of a star, but also on its metallicity. In spite of this evidence, most chemical evolution models rest upon grids of stellar yields derived for stars with solar composition, and only few examples of metallicity-dependent yields can be found in literature (Maeder 1992, hereinafter M92; Maeder 1993; Woosley & Weaver 1995, hereinafter WW95).

In order to improve upon this, we derive here a wide and up-to-date set of ejecta in which the effect of the initial chemical composition is taken into account. We adopt the stellar models from the Padua library (Bressan et al. 1993; Fagotto et al. 1994a,b), which span the mass range from 0.6 to 120 $M_{\odot}$. Full sets are available for the metallicities Z=0.0004, Z=0.004, Z=0.008, Z=$Z_{\odot}$=0.02 and Z=0.05, and we derive five corresponding sets of stel-

lar ejecta. Thus we get coherent prescriptions for stellar yields deduced from a unique and homogeneous grid of stellar models covering all mass ranges, instead of patching together data from different sources. In addition, in the range of massive stars we take the effects of quiescent mass-loss starting from the ZAMS into account. We also point out that, unlike most stellar yields adopted in chemical models up to now, here we refer to evolutionary tracks calculated with convective overshooting.

As a first application of our grid of stellar yields, we develop a chemical evolution model for the Solar Neighbourhood, which is the first template environment where nucleosynthetic yields and chemical models are to be calibrated and tested.

This paper is organized as follows. In Sec. 2 we briefly summarize the various groups in which stars of different mass can be classified according to the dominant physical process and type of evolution. In Sec. 3 we deal with the role of mass loss in the evolution and nucleosynthesis of massive stars, and calculate the ejecta of the stellar winds predicted by our stellar models. In Sec. 4 we discuss the effects of mass loss on the outcoming SNæ and outline a recipe to calculate the explosive ejecta of SNæ originating from our pre-SN models. Sec. 5 summarizes and comments upon the total ejecta of mass losing massive stars with different initial metallicity. Sec. 6 describes the adopted prescriptions for the yields of low and intermediate mass stars. By means of simple semi-analytical prescriptions, in Sec. 7 we extend our grid of ejecta to Very Massive Objects up to 1000 $M_\odot$ (if they can form now or have existed in the past), since in some particular astrophysical problems it can be useful to consider the possibility of chemical enrichment by these stars. Sec. 8 introduces the mathematical formulation of our chemical model. In Sec. 9 we apply our model to the Solar Neighbourhood, discuss the space of parameters with respect to the available observational constraint and comment upon the chemical abundances and abundance ratios our model predicts. Finally, in Sec. 10 we draw some concluding remarks.

2. Definition of the mass intervals

For the sake of better understanding, we summarize here how stars are classified according to the dominant physical processes governing their evolution and fate. This is especially needed since we adopt models with convective overshoot for which the mass grouping is different as compared to standard models (cf. Chiosi 1986; Woosley 1986; Chiosi et al. 1992; and references therein).

Low mass stars: They develop degenerate He-cores, undergo core He-flash, proceed to the formation of a degenerate CO-core, and after the AGB phase terminated by the loss of the envelope by stellar wind, become white dwarfs. In models with overshoot the upper mass limit (M_{HeF}) for this to occur is about $1.6 \div 1.7$ $M_\odot$, depending on the chemical composition.

Intermediate mass stars: They avoid core He-flash (helium is ignited in a non degenerate core), proceed to the formation of a degenerate CO-core, undergo the TP-AGB phase, and losing mass by stellar wind end up as white dwarfs. In models with convective overshoot the upper mass limit (M_{up}) of this group is about 5 $M_\odot$ depending on the chemical composition.

Quasi-massive stars: In models with convective overshoot, stars in the range 6 to 8 $M_\odot$ undergo core C-burning in non degenerate conditions, but develop highly degenerate O-Ne-Mg-cores. They become dynamically unstable to *e-capture* instability and explode as supernovae.

Massive stars: In the mass range 9 to 120 $M_\odot$ there is the simultaneous occurrence of two phenomena: the dominant mass loss by stellar wind during the whole evolutionary history, and the completion of the nuclear sequence down to the formation of an iron core in presence of strong neutrino cooling. The supernova explosion is triggered by core collapse induced by *e-captures* on heavy nuclei, *photo-dissociation* of Fe into α-particles, and rapid neutronization of the collapsing material. This is the range of classical Type II SNæ. Either a neutron star of about 1.4 $M_\odot$ or a black hole of larger mass is left over, depending on the efficiency of neutrino cooling during the previous stages.

Very massive stars: Starting from the very initial stages, objects more massive than, say, 120 $M_\odot$ are strongly pulsationally unstable, suffer from violent mass loss, and undergo *pair-creation* instability during core O-burning. The final outcome is regulated by the mass of the CO-core: at decreasing core mass, these stars can either collapse later to a black hole, or suffer complete thermonuclear explosion, or recover the behaviour of the massive stars above.

3. Ejecta from the stellar wind of massive stars

Massive stars contribute to the chemical enrichment of the ISM mainly by means of their final explosion in supernova (SN). Anyway, mass loss is also known to play a major role in the evolution of massive stars and stellar winds can have a non–negligible influence on stellar ejecta (Chiosi & Maeder 1986, hereinafter CM86; Chiosi & Caimmi 1979; Chiosi 1979; Maeder 1981, 1983, 1992, 1993). Mass loss has got two main effects on final ejecta:

(1) stellar layers peeled off by stellar winds directly mix with and enrich the surrounding ISM, and evade further burning stages (direct effect);

(2) mass loss affects the final mass M_{fin} of the star and the final masses of its He– and CO–core (M_{He} and M_{CO}, respectively), thus affecting the resulting SN (indirect effect).

In our adopted models, stars more massive than $M >$ 12 $M_\odot$ are affected by stellar winds during their core H-

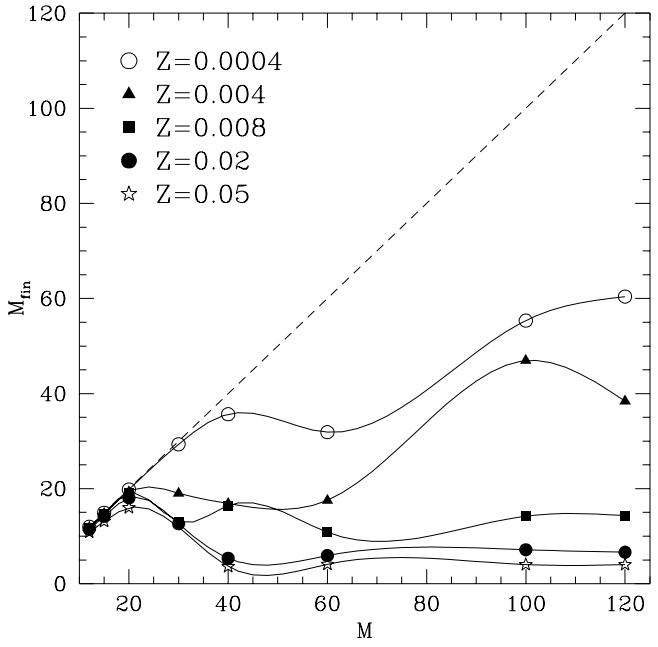

Fig. 1. Final mass vs. initial mass relation (in $M_\odot$) for massive stars of five metallicities (legend on top left). The dashed line corresponds to the case of constant mass

and He-burning phases. All remaining evolutionary stages are so short-lived that mass loss has in practice no effect at all and the mass of star is frozen to the value with which it will undergo the final supernova explosion. This value of the mass is thereinafter referred to as the final mass M_{fin}. The mass loss rates are included according to de Jager et al. (1988) from the ZAMS up to the de Jager limit; beyond such limit the star becomes a LBV candidate and its mass loss rate is increased up to 10^{-3} $M_\odot$/yr. When the surface hydrogen abundance falls below 0.3, the star is considered to enter its Wolf–Rayet stage and from then on the assumed mass loss rate follows Langer (1989). Since metallicity affects the bound–free and line opacity in the surface layers of massive stars, the efficiency of radiation pressure driven winds is expected to depend on metallicity according to $\dot{M} \propto Z^\alpha$, $\alpha \sim 0.5 \div 1.0$ (Kudritzki et al. 1989; Kudritzki 1997; Leitherer & Langer 1991; Lamers & Cassinelli 1996). Evidence for the dependence of mass loss rates on metallicity comes from statistics of blue and red supergiants and of WR stars in our own Galaxy, in the Magellanic Clouds and in other galaxies of the Local Group (Maeder & Conti 1994). In our models, mass loss rates are scaled with metallicity according to Kudritzki et al. (1989, $\dot{M} \propto Z^{0.5}$), therefore wind ejecta and the structure of SN precursors sensitively depend on the initial metallicity of the star, as shown by M92. For more details on the evolution of massive stars in presence of mass loss the reader is referred to CM86, Chiosi et al. (1992), Chiosi (1997).

Table 1. Initial masses and corresponding final masses

M	M_{fin}				
	Z=0.0004	Z=0.004	Z=0.008	Z=0.02	Z=0.05
12	11.97	11.84	11.77	11.46	10.85
15	14.94	14.76	14.63	14.21	13.11
20	19.83	19.30	19.03	18.06	16.00
30	29.35	19.05	13.03	12.63	—
40	35.65	16.86	16.44	5.35	3.62
60	31.88	17.55	10.81	5.93	4.09
100	55.35	46.93	14.23	7.16	4.03
120	60.41	38.43	14.35	6.63	4.04

In Fig. 1 we plot the final mass M_{fin} versus the initial mass M for our five sets of models between 12 and 120 $M_\odot$; the corresponding values are listed in Tab. 1. As expected, higher metallicities correspond to lower final masses, due to larger mass loss rates. In particular, the most massive stars ($M > 40$ $M_\odot$) in the higher metallicity sets end up with quite low final masses, typically $4 \div 6$ $M_\odot$. These stars go through a WR phase, during which mass loss rates are high and strongly dependent on the stellar mass ($\dot{M} \propto M^{2.5}$, Langer 1989); in this stage the stellar mass is decreasing rapidly, and the mass loss rate is also correspondingly decreasing, until all these stars reach very similar final masses. The final mass is very low especially in the case of high metallicity, because a more efficient wind during the Main Sequence phase allows the WR stage to be reached sooner and the intense WR mass loss to be active for a longer time. Indeed, to reach the final convergence mass the star needs to lose its H–rich envelope soon enough (before the helium abundance in the core gets to $Y \sim 0.5$, according to Woosley et al. 1995).

The ejecta due to stellar winds are calculated as

$$E_{iM}^{wind} = \int_0^{\tau_M} \dot{M}(M,t)\, X_i^S(t)\, dt \qquad (1)$$

where E_{iM}^{wind} is the amount (in $M_\odot$) of species i expelled in the wind by a star of mass M, $\dot{M}$ is the mass loss rate and X_i^S is the surface abundance of species i. The integration runs over the whole lifetime τ_M of a star of mass M. In practice, τ_M is the time when carbon ignites in the core, i.e. when the track ends. Wind ejecta are calculated for H, ^{3}He, ^{4}He, ^{12}C, ^{13}C, ^{14}N, ^{15}N, ^{16}O, ^{17}O, ^{18}O, ^{20}Ne, ^{22}Ne and are listed in Tab. 2.

The amount and the chemical composition of the expelled wind change with the mass and with the metallicity of the star; in order to explain this effect better, we consider stellar yields rather than ejecta. The stellar yield of a species i, p_{iM}, is defined as the mass fraction of a star of mass M that has been newly synthesized as species i and then ejected (Tinsley 1980). If i has been converted into other species rather than produced, its yield p_{iM} is

Table 2. Ejecta (in $M_\odot$) of the stellar wind for our model massive stars

Z=**0.0004**

M	^{1}H	^{3}He	^{4}He	^{12}C	^{13}C	^{14}N	^{15}N	^{16}O	^{17}O	^{18}O	^{20}Ne	^{22}Ne
12	0.024	4.23E-07	0.007	2.13E-06	1.09E-07	1.93E-06	1.58E-09	6.47E-06	6.24E-09	1.22E-08	9.55E-07	1.28E-07
15	0.049	5.18E-07	0.015	5.10E-06	2.21E-07	2.84E-06	3.81E-09	1.32E-05	1.09E-08	2.71E-08	1.93E-06	2.59E-07
20	0.128	1.52E-07	0.038	1.63E-05	2.00E-07	4.28E-06	1.62E-08	3.50E-05	1.39E-08	8.03E-08	5.07E-06	6.80E-07
30	0.500	6.70E-07	0.150	6.43E-05	7.74E-07	1.62E-05	5.94E-08	1.37E-04	8.84E-08	2.99E-07	1.99E-05	2.67E-06
40	3.34	6.62E-06	1.00	4.28E-04	5.45E-06	1.11E-04	3.21E-07	9.17E-04	9.67E-07	1.92E-06	1.33E-04	1.78E-05
60	17.08	1.09E-05	11.03	1.01E-03	6.42E-05	5.60E-03	8.11E-07	2.64E-03	2.53E-05	3.31E-06	8.59E-04	1.15E-04
100	27.44	5.20E-05	17.19	1.73E-03	2.05E-04	8.61E-03	1.14E-06	4.26E-03	1.23E-05	7.59E-06	1.36E-03	1.83E-04
120	32.52	5.05E-05	27.06	1.65E-03	1.43E-04	1.38E-02	1.77E-06	4.03E-03	5.15E-05	8.80E-06	1.82E-03	2.45E-04

Z=**0.004**

M	^{1}H	^{3}He	^{4}He	^{12}C	^{13}C	^{14}N	^{15}N	^{16}O	^{17}O	^{18}O	^{20}Ne	^{22}Ne
12	0.115	2.43E-06	0.042	1.08E-04	5.26E-06	1.26E-04	8.37E-08	2.90E-04	6.35E-07	6.09E-07	4.80E-05	6.44E-06
15	0.173	2.36E-06	0.064	1.78E-04	6.20E-06	1.75E-04	1.82E-07	4.42E-04	6.42E-07	1.01E-06	7.27E-05	9.76E-06
20	0.509	6.76E-06	0.185	5.69E-04	1.82E-05	4.18E-04	4.95E-07	1.34E-03	1.58E-06	3.02E-06	2.13E-04	2.86E-05
30	7.68	8.21E-05	3.23	7.91E-03	2.85E-04	9.52E-03	4.33E-06	1.90E-02	8.61E-05	3.44E-05	3.35E-03	4.49E-04
40	14.39	7.77E-05	8.66	1.03E-02	5.55E-04	3.80E-02	8.09E-06	2.82E-02	3.57E-04	3.31E-05	7.07E-03	9.50E-04
60	19.54	1.73E-04	15.95	4.33	1.28E-03	5.77E-02	1.53E-05	2.51	2.05E-04	8.42E-05	1.30E-02	1.74E-03
100	28.02	1.26E-04	24.84	1.78E-02	8.75E-04	0.118	1.50E-05	3.83E-02	3.97E-04	6.04E-05	1.62E-02	2.18E-03
120	31.93	1.20E-04	49.09	0.127	1.55E-03	0.214	2.01E-05	0.147	3.03E-04	6.12E-05	2.49E-02	3.62E-03

Z=**0.008**

M	^{1}H	^{3}He	^{4}He	^{12}C	^{13}C	^{14}N	^{15}N	^{16}O	^{17}O	^{18}O	^{20}Ne	^{22}Ne
12	0.168	5.94E-06	0.065	3.36E-04	1.61E-05	3.54E-04	2.82E-07	8.78E-04	5.09E-07	1.88E-06	1.43E-04	1.93E-05
15	0.262	8.42E-06	0.103	5.74E-04	2.01E-05	5.02E-04	4.87E-07	1.39E-03	7.44E-07	2.98E-06	2.26E-04	3.03E-05
20	0.693	1.53E-05	0.272	1.61E-03	4.66E-05	1.17E-03	1.44E-06	3.71E-03	8.32E-06	8.15E-06	5.94E-04	7.98E-05
30	10.81	1.14E-04	6.02	1.81E-02	7.55E-04	4.52E-02	1.27E-05	4.96E-02	4.19E-04	5.51E-05	1.78E-03	1.39E-03
40	13.92	2.19E-04	9.46	2.41E-02	9.89E-04	7.23E-02	2.63E-05	5.95E-02	4.83E-04	1.19E-04	1.44E-02	1.93E-03
60	18.80	2.67E-04	21.53	7.02	1.97E-03	0.133	2.96E-05	1.50	6.99E-04	1.37E-04	3.01E-02	4.04E-03
100	25.91	—	38.38	15.5	3.79E-03	0.267	—	5.28	—	—	—	—
120	30.12	3.51E-04	49.28	19.2	4.79E-03	0.349	5.54E-05	6.19	8.41E-04	1.93E-04	6.51E-02	0.295

Z=$Z_\odot$=**0.02**

M	^{1}H	^{3}He	^{4}He	^{12}C	^{13}C	^{14}N	^{15}N	^{16}O	^{17}O	^{18}O	^{20}Ne	^{22}Ne
12	0.365	2.00E-05	0.168	2.01E-03	9.45E-05	1.89E-03	1.84E-06	5.17E-03	3.30E-05	1.14E-05	8.32E-04	1.12E-04
15	0.532	2.93E-05	0.246	3.11E-03	1.15E-04	2.55E-03	2.93E-06	7.56E-03	3.29E-05	1.69E-05	1.21E-03	1.63E-04
20	1.29	7.19E-05	0.609	7.89E-03	2.11E-04	6.06E-03	7.51E-06	1.84E-02	6.68E-05	4.09E-05	2.96E-03	3.98E-04
30	10.31	3.96E-04	6.72	5.37E-02	1.83E-03	0.103	4.07E-05	0.131	1.41E-03	2.31E-04	2.65E-02	3.56E-03
40	12.62	4.72E-04	18.81	2.39	3.50E-03	0.211	5.37E-05	0.280	3.35E-03	7.00E-03	5.29E-02	0.264
60	16.42	5.27E-04	31.95	4.28	5.30E-03	0.343	7.79E-05	0.440	3.82E-03	2.89E-04	8.26E-02	0.318
100	23.84	5.51E-04	55.35	10.7	9.68E-03	0.682	9.96E-05	1.14	5.56E-03	3.04E-04	0.142	0.596
120	28.57	1.37E-03	73.88	7.93	1.15E-02	1.01	1.92E-04	0.781	2.15E-03	7.53E-04	0.173	0.525

Z=**0.05**

M	^{1}H	^{3}He	^{4}He	^{12}C	^{13}C	^{14}N	^{15}N	^{16}O	^{17}O	^{18}O	^{20}Ne	^{22}Ne
12	0.668	9.06E-05	0.426	1.13E-02	4.86E-04	7.72E-03	9.45E-06	2.90E-02	2.45E-04	6.08E-05	4.40E-03	5.90E-04
15	1.09	1.53E-04	0.712	1.89E-02	7.73E-04	1.29E-02	1.62E-05	4.70E-02	3.88E-04	9.92E-05	7.24E-03	9.72E-04
20	2.26	3.45E-04	1.53	4.04E-02	1.19E-03	2.88E-02	3.72E-05	9.74E-02	7.06E-04	2.07E-04	1.53E-02	2.05E-03
40	10.05	1.17E-03	22.56	1.82	7.50E-03	0.484	1.50E-04	0.507	1.39E-02	7.61E-03	0.139	0.608
60	13.95	6.47E-04	35.83	3.07	1.12E-02	1.06	1.25E-04	0.711	3.38E-02	3.67E-04	0.213	0.523
100	26.92	8.60E-04	60.69	3.22	1.92E-02	1.79	1.84E-04	1.14	5.51E-02	3.23E-02	0.366	1.23
120	38.44	1.15E-03	68.13	3.28	2.59E-02	2.11	2.26E-04	1.62	6.30E-02	0.177	0.443	1.23

negative. On the basis of this definition, the total amount of species i ejected by a star of mass M is:

$$E_{iM} = (M - M_r)\, X_i^0 \; + \; M p_{iM} \qquad (2)$$

where M_r is the remnant mass and X_i^0 is the initial abundance of species i in the star when it was born. The first term is the amount of "original" species i eventually expelled, while the second term is the positive or negative contribution of newly synthesized i. Therefore, yields allow us to estimate the nucleosynthetic production due to the star itself, by distinguishing the newly synthesized fraction from the fraction that was already present in the gas whence the star formed. The stellar yields of the wind for our set of masses and metallicities are calculated according to:

$$M\, p_{iM}^{wind} = \int_0^{\tau_M} \dot{M}(M,t)\, [X_i^S(t) - X_i^0]\, dt \qquad (3)$$

The yields formalism is basically due to Tinsley (1980), but the previous formulæ are taken as revised by M92. The wind yields we obtain are listed in Tab. 3 and can be commented on as follows (see also M92).

- ^{1}**H:** Hydrogen yields are always negative and increase in modulus with increasing mass and metallicity, since the more efficient mass loss is, the larger amount of new helium and metals (synthesized at the expense of ^{1}H) is revealed on the surface and released in the wind.
- ^{3}**He:** The abundance of ^{3}He increases at the very outer edge of the H–burning region, due to the first reactions

Table 3. Yields p_{iM}^{wind} (see Eq. 3) of the stellar wind for our massive stars. When the amount of a newly synthesized/consumed element is less than 1% of its initial one, the corresponding yield is assumed to be not significative, i.e. is set equal 0

Z=0.0004

M	^{1}H	^{3}He	^{4}He	^{12}C	^{13}C	^{14}N	^{15}N	^{16}O	^{17}O	^{18}O	^{20}Ne	^{22}Ne
12	0	0	0	0	0	0	0	0	0	0	0	0
15	0	0	0	0	0	0	0	0	0	0	0	0
20	0	3.23E-10	0	0	0	0	0	0	0	0	0	0
30	0	3.26E-09	0	0	0	0	-1.35E-10	0	1.13E-09	-5.28E-10	0	0
40	0	6.99E-08	0	0	0	0	-2.59E-09	0	1.50E-08	-4.68E-09	0	0
60	-7.60E-02	-2.31E-07	7.60E-02	-2.95E-05	5.15E-07	8.18E-05	-3.22E-08	-5.50E-05	3.82E-07	-1.72E-07	0	0
100	-6.92E-02	1.27E-07	6.92E-02	-2.68E-05	1.52E-06	7.50E-05	-3.21E-08	-5.18E-05	8.52E-08	-1.40E-07	0	0
120	-0.111	-1.63E-08	0.111	-3.53E-05	6.02E-07	1.03E-04	-3.37E-08	-7.14E-05	3.87E-07	-1.67E-07	0	0

Z=0.004

M	^{1}H	^{3}He	^{4}He	^{12}C	^{13}C	^{14}N	^{15}N	^{16}O	^{17}O	^{18}O	^{20}Ne	^{22}Ne
12	-3.34E-04	8.70E-08	3.34E-04	-3.95E-06	2.83E-07	7.29E-06	-5.79E-09	-3.45E-06	4.20E-08	-1.26E-08	0	0
15	-4.91E-04	1.76E-08	4.91E-04	-3.80E-06	2.26E-07	7.73E-06	-3.38E-09	-4.08E-06	2.95E-08	-9.34E-09	0	0
20	-8.96E-04	3.13E-08	8.96E-04	-5.98E-06	4.99E-07	1.22E-05	-9.28E-09	-6.65E-06	4.98E-08	-1.79E-08	0	0
30	-2.00E-02	-4.77E-07	2.00E-02	-9.74E-05	5.18E-06	2.27E-04	-2.12E-07	-1.37E-04	2.56E-06	-6.22E-07	0	0
40	-7.76E-02	-3.15E-06	7.76E-02	-3.14E-04	7.01E-06	8.06E-04	-3.62E-07	-5.17E-04	8.43E-06	-1.97E-06	0	0
60	-2.09	-3.34E-06	9.60E-02	7.14E-02	1.29E-05	7.85E-04	-4.36E-07	4.04E-02	2.82E-06	-2.02E-06	0	0
100	-0.121	-3.41E-06	1.21	-3.46E-04	2.47E-06	1.05E-03	-3.68E-07	-7.39E-04	3.52E-06	-1.97E-06	0	0
120	-0.248	-4.98E-06	2.46	3.83E-04	4.90E-06	1.61E-03	-4.96E-07	-2.14E-04	1.95E-06	-2.78E-06	0	2.25E-06

Z=0.008

M	^{1}H	^{3}He	^{4}He	^{12}C	^{13}C	^{14}N	^{15}N	^{16}O	^{17}O	^{18}O	^{20}Ne	^{22}Ne
12	-5.11E-04	1.51E-07	5.11E-04	-1.06E-05	8.77E-07	1.98E-05	-1.46E-08	-9.49E-06	9.52E-09	-3.27E-08	0	0
15	-7.33E-04	1.28E-07	7.33E-04	-1.04E-05	7.60E-07	2.13E-05	-1.56E-08	-1.14E-05	8.24E-09	-3.97E-08	0	0
20	-1.44E-03	-9.11E-08	1.44E-03	-1.55E-05	1.18E-06	3.43E-05	-2.30E-08	-2.02E-05	3.34E-07	-6.36E-08	0	0
30	-5.92E-02	-6.15E-06	5.92E-02	-5.14E-04	1.18E-05	1.23E-03	-6.82E-07	-7.36E-04	1.30E-05	-3.64E-06	0	0
40	-8.91E-02	-4.90E-06	8.92E-02	-5.62E-04	1.08E-05	1.51E-03	-4.93E-07	-1.00E-03	1.11E-05	-2.74E-06	0	0
60	-2.95	-9.98E-06	0.154	0.115	1.33E-05	1.81E-03	-1.11E-06	2.15E-02	1.03E-05	-5.66E-06	0	0
100	-0.377	—	0.169	0.154	1.76E-05	2.24E-03	—	4.92E-02	—	—	—	—
120	-0.402	-1.26E-05	0.191	0.158	1.91E-05	2.47E-03	-1.26E-06	4.79E-02	5.53E-06	-6.92E-06	0	2.38E-03

Z=Z$_{\odot}$=0.02

M	^{1}H	^{3}He	^{4}He	^{12}C	^{13}C	^{14}N	^{15}N	^{16}O	^{17}O	^{18}O	^{20}Ne	^{22}Ne
12	-1.32E-03	-3.29E-07	1.32E-03	-5.70E-05	5.19E-06	1.01E-04	-6.80E-08	-4.86E-05	2.56E-06	-1.47E-07	0	0
15	-1.58E-03	-3.75E-07	1.57E-03	-5.42E-05	4.57E-06	1.04E-04	-6.26E-08	-5.48E-05	1.97E-06	-1.54E-07	0	0
20	-3.29E-03	-6.74E-07	3.28E-03	-8.46E-05	4.80E-06	1.83E-04	-9.78E-08	-1.05E-04	2.94E-06	-3.04E-07	0	0
30	-6.17E-02	-1.23E-05	6.17E-02	-1.07E-03	2.67E-05	2.72E-03	-1.47E-06	-1.74E-03	4.45E-05	-6.31E-06	0	0
40	-0.291	-2.63E-05	0.228	5.55E-02	3.63E-05	4.21E-03	-2.88E-06	-2.15E-03	8.01E-05	1.54E-04	0	6.42E-03
60	-0.357	-3.09E-05	0.280	6.69E-02	3.50E-05	4.61E-03	-3.10E-06	-2.18E-03	5.99E-05	-1.70E-05	0	5.12E-03
100	-0.411	-3.53E-05	0.294	0.102	4.18E-05	5.67E-03	-3.53E-06	1.58E-03	5.17E-05	-1.94E-05	0	5.77E-03
120	-0.423	-3.02E-05	0.351	6.14E-02	3.99E-05	7.27E-03	-3.01E-06	-3.48E-03	1.39E-05	-1.66E-05	0	4.18E-03

Z=0.05

M	^{1}H	^{3}He	^{4}He	^{12}C	^{13}C	^{14}N	^{15}N	^{16}O	^{17}O	^{18}O	^{20}Ne	^{22}Ne
12	-1.73E-03	-3.00E-06	1.71E-03	-2.46E-04	2.63E-05	3.46E-04	-3.83E-07	-1.20E-04	1.94E-05	-7.43E-07	0	0
15	-3.00E-03	-3.67E-06	2.98E-03	-2.98E-04	3.29E-05	4.67E-04	-4.59E-07	-2.02E-04	2.46E-05	-1.03E-06	0	0
20	-6.31E-03	-4.73E-06	6.30E-03	-4.49E-04	3.00E-05	8.19E-04	-5.79E-07	-4.11E-04	3.32E-05	-1.75E-06	0	0
40	-0.293	-7.08E-05	0.244	3.44E-02	5.28E-05	9.27E-03	-7.35E-06	-1.14E-02	3.37E-04	1.35E-04	0	1.47E-02
60	-0.325	-9.17E-05	0.269	3.97E-02	4.83E-05	1.47E-02	-9.28E-06	-1.28E-02	5.53E-04	-5.03E-05	0	8.25E-03
100	-0.305	-9.70E-05	0.269	2.03E-02	5.01E-05	1.49E-02	-9.86E-06	-1.39E-02	5.41E-04	2.65E-04	0	1.18E-02
120	-0.258	-9.67E-05	0.228	1.54E-02	7.28E-05	1.46E-02	-9.90E-06	-1.20E-02	5.15E-04	1.42E-03	0	9.74E-03

of the p-p chain; then ^{3}He is rapidly turned to ^{4}He. Its yields are generally negative, except in some cases of low mass loss where the ^{3}He–enriched layers are lost, rather than inner ones.

^{4}He: Helium yields are larger for larger masses and, at any given mass, for higher metallicities, because strong winds can take large amounts of new ^{4}He away.

^{12}C—^{16}O: Carbon yields are negative in most cases, since the CNO cycle turns ^{12}C into ^{14}N. Only when mass loss gets very efficient, i.e. for high masses and metallicities, carbon yields can be positive because He–burning products can be revealed on the surface (WC and WO stars). Quite the same holds for oxygen, whose yields are seldom positive. If mass loss is extreme, anyway, ^{12}C and ^{16}O yields may even decrease because most of the mass is rapidly lost in the wind in the form of ^{4}He.

^{14}N—^{13}C—^{17}O: In our models of massive stars, nitrogen is produced only as a secondary element, therefore its yields sensitively grow with metallicity. The same holds for ^{13}C and for ^{17}O, which are secondary products of the CNO cycle as well.

^{15}N: ^{15}N is quickly destroyed in the CNO cycle, therefore its yields are always negative (although small) and increasing in modulus with metallicity, as the efficiency of the CNO cycle increases.

^{18}O: ^{18}O is destroyed in the CNO cycle; it is later produced by α capture on ^{14}N during He–burning, but then it is turned into ^{22}Ne by a new α capture, so that the abundance peak of ^{18}O is very thin (CM86). Therefore, even when mass loss is so efficient as to reveal He–burning products on the surface, ^{18}O yields usually remain negative.

^{22}Ne: ^{22}Ne yields are negligible for relatively low masses and/or metallicities, while when mass loss gets very efficient there is a sensitive ejection of new ^{22}Ne as a by-product of He–burning remained uncovered on the surface of WR stars.

^{20}Ne: ^{20}Ne yields are always negligible because, although ^{20}Ne can be produced by α capture on ^{16}O during He–burning, this holds for so advanced stages that even an extreme mass loss can't peel off the layers where ^{20}Ne is synthesized.

4. The supernova explosion

To determine the contribution of quasi-massive and massive stars in the chemical enrichment of the ISM we need

Table 4. He–core mass (in $M_\odot$) of model stars in four different evolutionary stages (see text). Here M_{He} is defined as the mass–point where the hydrogen content falls to 0

Z=0.0004	6	7	9	12	15	20	30	40	60	100	120
$M_{He}(1)$	0.01	0.01	0.06	0.71	1.90	3.97	7.85	12.62	21.44	39.83	48.10
$M_{He}(2)$	0.82	1.00	1.40	2.10	2.95	4.64	8.51	12.77	21.54	39.83	48.10
$M_{He}(3)$	1.69	2.03	2.80	4.04	5.36	7.62	12.36	17.31	25.84	49.54	56.76
$M_{He}(4)$	1.69	2.03	2.80	4.04	5.36	7.62	12.33	16.98	25.40	49.16	56.67
Z=0.004	6	7	9	12	15	20	30	40	60	100	120
$M_{He}(1)$	0.01	0.02	0.38	1.16	2.16	3.76	7.58	11.63	19.47	37.72	46.71
$M_{He}(2)$	0.90	1.12	1.62	2.45	3.39	5.12	8.70	12.56	20.39	37.72	46.71
$M_{He}(3)$	1.70	2.08	2.88	4.18	5.44	7.65	12.02	16.52	17.77	45.84	39.70
$M_{He}(4)$	1.70	2.08	2.88	4.18	5.43	7.64	11.62	16.48	17.55	45.47	38.43
Z=0.008	6	7	9	12	15	20	30	40	60	100	120
$M_{He}(1)$	0.01	0.05	0.35	1.06	1.98	3.85	7.77	11.12	19.58	38.82	48.26
$M_{He}(2)$	0.91	1.14	1.66	2.54	3.52	5.22	8.79	12.93	20.41	38.82	49.20
$M_{He}(3)$	1.60	1.98	2.82	4.13	5.41	7.58	11.99	16.26	10.76	14.03	14.16
$M_{He}(4)$	1.60	1.98	2.82	4.13	5.40	7.57	11.08	15.98	10.65	13.83	13.95
Z=0.02	6	7	9	12	15	20	30	40	60	100	120
$M_{He}(1)$	0.008	0.06	0.38	1.198	2.13	3.68	7.36	10.78	19.08	39.82	38.52
$M_{He}(2)$	0.94	1.19	1.75	2.72	3.74	5.55	9.26	12.93	21.19	39.82	38.52
$M_{He}(3)$	1.51	1.91	2.78	4.11	5.47	7.66	12.36	5.29	5.86	7.07	6.55
$M_{He}(4)$	1.51	1.91	2.78	4.10	5.46	7.64	12.07	5.20	5.77	6.96	6.44
Z=0.05	6	7	9	12	15	20	30	40	60	100	120
$M_{He}(1)$	0.01	0.08	0.40	1.26	2.24	3.90	—	11.03	10.76	19.22	19.65
$M_{He}(2)$	1.05	1.34	2.00	3.10	4.21	6.21	—	14.40	14.06	22.42	22.88
$M_{He}(3)$	1.59	2.03	2.99	4.51	6.00	8.47	—	3.63	4.08	4.03	4.03
$M_{He}(4)$	1.59	2.03	2.99	4.48	5.98	8.46	—	3.53	3.98	3.92	3.93

to know the ejecta of the final SN explosion, which actually plays the major role. Although mass loss is well known to have substantial effects in the evolution of massive stars, SN models usually start from constant mass pre-SN structures. Only few examples are found in literature of stellar models with mass loss followed up to the very final stages and the explosion (e.g. Woosley et al. 1993, 1995), but no extended studies exist yet of explosive nucleosynthesis of mass losing massive stars for wide sets of masses and metallicities. To get the global nucleosynthetic production for these stars one is generally forced to link, somehow, pre-SN models evolved including stellar winds and SN models based on constant mass calculations. Since our tracks stop at the beginning of C–ignition in the core, here we need to perform such a link as well.

Under the hypothesis that the stellar core, which drives the explosion mechanism, evolves uncoupled from the envelope, SN models were calculated letting He–cores, i.e. pure helium stars, evolve (Arnett 1978, 1991; Nomoto & Hashimoto 1986; Thielemann et al. 1996; Woosley & Weaver 1986). These bare helium stars are later identified with the helium core (M_{He}) of stars with initial, total mass M. By means of a suitable relation between the total mass M of the star and its M_{He}, the ejecta obtained for bare He–cores were then shifted into a scale of stellar masses. The envelope layers, and also the wind contribution in the case of mass losing stellar models, were added to the ejecta of the corresponding He–core (Chiosi & Caimmi 1979; Chiosi 1979; Baraffe & El Eid 1991). Yet, as pointed out by Maeder (1981, 1984, 1992), this method leads to some inconsistency, because a stellar core does not necessarily evolve like an isolated one. Unlike a bare He–core, its size may change during stellar evolution: it can grow or recede in time, depending also on dredge-up episodes and mass loss. Table 4 shows this effect by displaying M_{He} values in four evolutionary stages of our tracks: (1) when H is exhausted in the centre, (2) when He ignites in the core, (3) when He is exhausted in the centre and (4) when C ignites in the core. M_{He} gets growing in the course of evolution for less massive and/or low metallicity stars; in stars where mass loss is very efficient, M_{He} falls in later stages.

Therefore, it's hard to find an univocal relation between the total initial mass of the star and M_{He}. The meaningful value of M_{He} for the sake of the resulting SN might be the one corresponding to the end of core He–burning or to C–ignition, since following stages are so fast that mass loss cannot alter the structure of the star any more. However, even the "final" He–core mass may be inadequate to fix the resulting explosion. In particular, in the WR stage the strong mass loss proceeding after the He–core is uncovered can alter the evolution of the core and the final nucleosynthesis. Woosley et al. (1993) follow the evolution of a mass losing 60 $M_\odot$ star evolving through a WR stage and ending as a 4.25 $M_\odot$ bare He–core at the time of explosion. Such a structure is compared to a 4.25 $M_\odot$ pure He star evolved without mass loss. The final thermal and dynamical structure of the two objects results very similar, but their chemical structure is different: although the mass of the pre-SN He–core is the same, M_{CO} is different and this affects all subsequent burning stages, the resulting entropy distribution and the final explosion.

Therefore, here we prefer to choose M_{CO} as the characterizing parameter for the resulting SN, as suggested by M92. Indeed, C–burning and following burning stages are

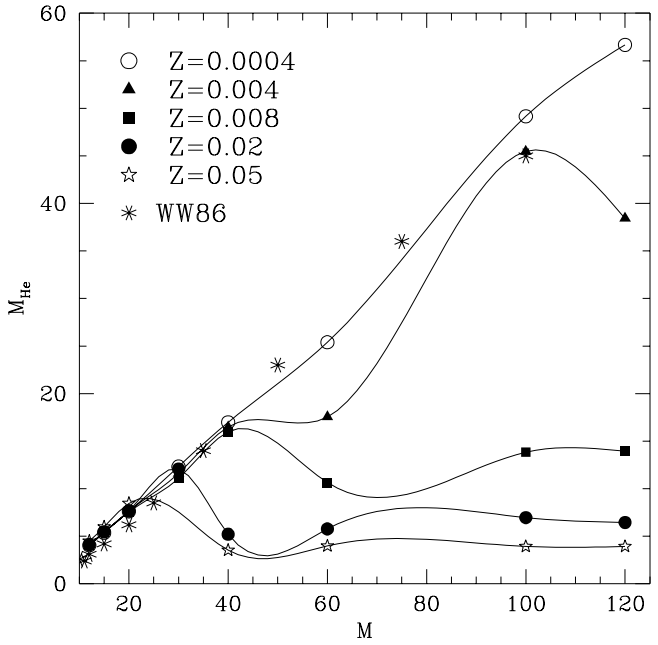

Fig. 2. He–core mass vs. initial mass relation (in $M_\odot$) for massive stars of five metallicities. Asterisks indicate He–core masses from Woosley & Weaver 1986, relevant to constant mass pre-SN models

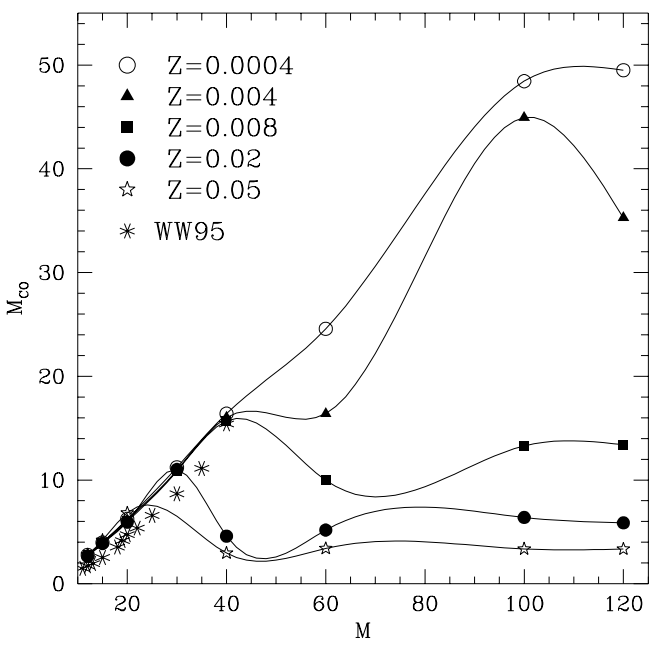

Fig. 3. CO–core mass vs. initial mass relation (in $M_\odot$) for massive stars of five metallicities. Asterisks indicate CO–core masses from Woosley & Weaver 1995, relevant to constant mass pre-SN models

so quick that mass loss hasn't got time enough to influence inner cores and can be ignored (see also Woosley et al. 1993, 1995). M_{CO} at carbon ignition well corresponds to M_{CO} at the time of explosion. Basing on M_{CO} we perform a link with SN models for all our massive stars, i.e. for our models with M $\geq 6\ M_\odot$. Even though our models include quiescent mass loss only for M $\geq 12\ M_\odot$, a link with SN models is made also for $6\ M_\odot \leq$ M $\leq 12\ M_\odot$, since in our models with overshooting $M_{\rm up} \sim 5\ M_\odot$ and all higher masses are expected to undergo SN explosion. In general, we remind that due to overshooting any given M here corresponds to larger M_{He} and M_{CO} with respect to "standard" models, and since the final fate of a star is ultimately related to the size of its core the significant mass ranges implying different kinds of SN are shifted downward in mass.

Table 5. Initial masses and corresponding He–core masses

M	M_{He}				
	Z=0.0004	Z=0.004	Z=0.008	Z=0.02	Z=0.05
6	1.69	1.70	1.60	1.51	1.59
7	2.03	2.08	1.98	1.91	2.03
9	2.80	2.88	2.82	2.78	2.99
12	4.04	4.18	4.13	4.10	4.48
15	5.36	5.43	5.40	5.46	5.98
20	7.62	7.64	7.57	7.64	8.46
30	12.33	11.62	11.08	12.07	—
40	16.98	16.48	15.98	5.20	3.53
60	25.40	17.55	10.65	5.77	3.98
100	49.16	45.47	13.83	6.96	3.92
120	56.67	38.43	13.95	6.44	3.93

Table 6. Initial masses and corresponding CO–core masses

M	M_{CO}				
	Z=0.0004	Z=0.004	Z=0.008	Z=0.02	Z=0.05
6	1.11	1.11	1.05	1.01	1.00
7	1.28	1.20	1.22	1.10	1.16
9	1.80	1.83	1.75	1.68	1.71
12	2.78	2.82	2.73	2.64	2.79
15	3.97	3.96	3.89	3.89	4.19
20	6.25	6.15	6.02	5.94	6.84
30	11.23	10.95	10.86	11.02	—
40	16.39	16.03	15.70	4.59	2.95
60	24.58	16.40	9.97	5.18	3.41
100	48.45	44.94	13.29	6.39	3.36
120	49.51	35.28	13.40	5.87	3.35

Table 7. Total ejecta (in $M_\odot$) for quasi-massive stars of 6 and 7 $M_\odot$, for different metallicities

Z=0.0004

M	^{1}H	^{3}He	^{4}He	^{12}C	^{13}C	^{14}N	^{15}N	^{16}O	^{17}O	^{18}O	^{20}Ne	^{22}Ne	M_r
6	3.22	1.70E-04	1.48	2.42E-04	1.48E-05	5.23E-04	1.82E-07	8.12E-04	3.94E-06	1.35E-06	1.93E-05	5.13E-06	1.30
7	3.68	1.45E-04	2.00	2.67E-04	1.71E-05	7.25E-04	2.02E-07	9.10E-04	4.37E-06	1.49E-06	2.34E-05	5.99E-06	1.30

Z=0.004

M	^{1}H	^{3}He	^{4}He	^{12}C	^{13}C	^{14}N	^{15}N	^{16}O	^{17}O	^{18}O	^{20}Ne	^{22}Ne	M_r
6	3.16	1.80E-04	1.52	2.80E-03	1.65E-04	4.72E-03	2.04E-06	8.17E-03	3.99E-05	1.56E-05	1.93E-04	4.73E-08	1.30
7	3.61	1.64E-04	2.07	3.22E-03	1.99E-04	6.42E-03	2.34E-06	9.35E-03	3.93E-05	1.80E-05	2.34E-04	5.45E-08	1.30

Z=0.008

M	^{1}H	^{3}He	^{4}He	^{12}C	^{13}C	^{14}N	^{15}N	^{16}O	^{17}O	^{18}O	^{20}Ne	^{22}Ne	M_r
6	3.15	1.97E-04	1.51	5.97E-03	3.30E-04	8.53E-03	4.43E-06	1.69E-02	1.09E-04	3.33E-05	3.86E-04	1.03E-04	1.30
7	3.59	1.80E-04	2.06	6.73E-03	3.98E-04	1.21E-02	4.93E-06	1.91E-02	1.25E-04	3.79E-05	4.68E-04	1.20E-04	1.30

$Z=Z_\odot$=0.02

M	^{1}H	^{3}He	^{4}He	^{12}C	^{13}C	^{14}N	^{15}N	^{16}O	^{17}O	^{18}O	^{20}Ne	^{22}Ne	M_r
6	3.02	2.46E-04	1.58	1.60E-02	8.49E-04	1.84E-02	1.18E-05	4.38E-02	5.24E-04	8.83E-05	9.64E-04	2.57E-04	1.30
7	3.44	2.34E-04	2.15	1.79E-02	1.00E-03	2.72E-02	1.32E-05	4.97E-02	5.71E-04	9.89E-05	1.17E-03	2.99E-04	1.30

Z=0.05

M	^{1}H	^{3}He	^{4}He	^{12}C	^{13}C	^{14}N	^{15}N	^{16}O	^{17}O	^{18}O	^{20}Ne	^{22}Ne	M_r
6	2.49	3.37E-04	1.97	4.03E-02	2.08E-03	4.39E-02	3.02E-05	0.111	1.66E-03	2.21E-04	2.41E-03	6.42E-04	1.30
7	2.88	3.59E-04	2.53	4.61E-02	2.51E-03	6.13E-02	3.38E-05	0.129	1.99E-03	2.53E-04	2.92E-03	7.49E-04	1.30

4.1. The adopted $M_{He}(M)$ and $M_{CO}(M)$ relations

In Fig. 2 we plot the relation between the initial mass M and the corresponding He–core mass M_{He} at the end of the evolutionary track. For the sake of comparison, asterisks indicate M_{He} values given by Woosley & Weaver 1986 for pre–SN models calculated at constant mass. Up to $\sim$ 30 $M_\odot$ the He–cores are more massive in our models due to overshooting, while for larger masses the effects of mass loss dominate. Indeed, in the range 10 $\div$ 30 $M_\odot$ stellar evolution is more sensitive to the treatment of convection, while for larger masses the assumptions about mass loss have an overwhelming influence (CM86).

In Fig. 3 we plot M_{CO} at the end of the track versus M; in our models, we define M_{CO} as the mass interior to the outer edge of the He–burning region. Asterisks indicate M_{CO} values deduced from the recent SN models by WW95 (see App. A), calculated from pre–SN structures with no mass loss and with no overshooting.

In Tab. 5 and Tab. 6 we list the values of M_{He} and of M_{CO} respectively, for our quasi-massive and massive stars ($M > M_{up}$ =5 $M_\odot$). In models with overshooting all these stars eventually give SNæ, and their core masses are prerequisite to characterize the outcoming supernova and its ejecta.

4.2. Electron capture supernovæ

Quasi-massive stars (8 $\div$ 10 $M_\odot$ in standard models and 6 $\div$ 8 $M_\odot$ in models with overshoot) generally develop a degenerate O-Ne-Mg core after C–burning and eventually explode as "electron capture" supernovæ (EC SNæ), leaving a neutron star of $\sim$1.3 $M_\odot$ as a remnant and expelling very few heavy elements (Nomoto 1984, 1987; Mayle & Wilson 1988). Recent calculations seem to confirm that a degenerate O-Ne-Mg core reaching 1.375 $M_\odot$, the limit mass for electron captures on ^{24}Mg and ^{20}Ne, develops density conditions extreme enough that it collapses to a neutron star, rather than undergo a thermonuclear explosion due to disruptive O-Ne burning in degenerate material (Gutierrez et al. 1996).

But the final stages of stars in this mass range are still debated. These stars develop a double–shell structure similar to that of lower mass stars, and experience a thermally pulsing, mass losing phase as well. Nomoto's models didn't include thermal pulses nor mass loss, but the detailed evolution of a model 10 $M_\odot$ star has been recently followed by Garcia–Berro & Iben (1994), Ritossa et al. (1996). Their models suggest that such a star might be unable to reach the limit core mass for electron capture and explode in an EC SN: it might rather get rid of the overlying layers through a superwind phase typical of TP-AGB stars and result in a massive (1.26 $M_\odot$) O-Ne-Mg white dwarf.

By comparing the size of our stellar cores with those of Nomoto (1984, 1987) and Ritossa et al. (1996), in our models with convective overshooting such a behaviour is expected between 6 and 8 $M_\odot$ ($M_{CO} \sim 1.0 \div 1.3\ M_\odot$ at the beginning of core C–burning). For our models in this mass range, we assume that the inner 1.3 $M_\odot$ remain locked in the remnant, either a neutron star or a white dwarf, while the overlying layers are expelled, either by a final explosion or by a superwind during the TP-AGB phase. The resulting ejecta for this mass range are presented in Tab. 7.

We thus neglect the products of explosive nucleosynthesis in case of SN explosion, which is reasonable since EC SNæ are believed to produce negligible amounts of heavy elements (not more than 0.002 $M_\odot$, Mayle & Wilson 1988). More important, we are neglecting the effects of thermal pulses and of the III dredge-up in the nucleosynthetic yields of SAGB stars (SAGB = Super-Asymptotic Giant Branch, see Garcia-Berro & Iben 1994, Ritossa et al. 1996). No full calculations of stellar yields for this kind of stars exist yet in literature, neither for standard models nor for models with overshooting. Further investigation of nucleosynthesis and mass loss in this mass range should be done.

Table 8. Remnant mass M_r and ejecta E_i^{CO} (in $M_\odot$) of CO–cores for different elements, as deduced from WW95

Z=$Z_\odot$ (case S in WW95)

M_{CO}	M_r	^{12}C	^{15}N	^{16}O	^{20}Ne	^{24}Mg	^{28}Si	^{32}S	^{40}Ca	^{56}Fe
1.49	1.26	3.13E-02	1.29E-05	6.47E-02	1.58E-02	4.34E-03	1.55E-02	5.94E-03	7.50E-04	6.93E-02
1.72	1.30	5.59E-02	3.77E-05	0.130	6.55E-03	2.92E-03	8.42E-02	7.16E-02	1.38E-02	4.34E-02
1.95	1.40	8.95E-02	4.01E-06	0.192	2.67E-02	1.07E-02	5.13E-02	2.16E-02	2.95E-03	0.133
2.53	1.40	0.134	9.20E-05	0.591	9.08E-02	2.03E-02	0.102	5.85E-02	1.03E-02	0.115
3.54	1.70	0.215	9.34E-05	1.02	0.254	4.78E-02	0.128	4.89E-02	5.95E-03	6.59E-02
4.16	1.90	0.250	6.83E-05	1.32	8.20E-02	1.75E-02	0.267	0.123	1.26E-02	0.100
4.73	2.00	0.178	8.48E-05	1.83	8.03E-02	2.34E-02	0.278	0.146	1.34E-02	8.84E-02
5.37	1.90	0.203	1.10E-04	2.26	4.33E-02	3.30E-02	0.345	0.165	1.63E-02	0.205
6.59	1.90	0.281	1.64E-04	3.12	3.64	9.65E-02	0.303	0.134	1.56E-02	0.129
8.67	4.10	0.241	9.62E-05	3.51	0.346	0.201	8.38E-02	5.35E-03	3.25E-05	4.80E-05
11.12	7.20	0.253	5.13E-05	2.92	0.476	0.111	2.60E-02	1.34E-03	2.97E-05	0
15.41	12.30	0.267	2.07E-05	2.21	0.408	5.53E-02	8.64E-03	4.62E-04	6.95E-06	0

Z=0.1 $Z_\odot$ (case P in WW95)

M_{CO}	M_r	^{12}C	^{15}N	^{16}O	^{20}Ne	^{24}Mg	^{28}Si	^{32}S	^{40}Ca	^{56}Fe
1.81	1.30	8.66E-02	9.74E-06	0.137	1.04E-02	4.95E-03	2.95E-02	1.32E-02	2.78E-03	0.177
2.01	1.20	0.106	1.65E-05	0.282	4.04E-02	1.63E-02	6.43E-02	3.11E-02	5.16E-03	0.180
2.52	1.40	0.139	4.79E-05	0.546	7.26E-02	2.11E-02	7.03E-02	3.35E-02	5.83E-03	0.194
3.43	1.60	0.222	5.82E-05	0.983	0.204	7.71E-02	0.126	4.74E-02	7.75E-03	0.136
4.32	1.90	0.242	7.17E-05	1.51	9.36E-02	5.07E-02	0.231	0.128	1.86E-02	0.121
5.11	2.00	0.228	1.01E-04	2.11	3.32E-02	1.64E-02	0.325	0.183	2.27E-02	0.123
6.06	1.90	0.263	1.25E-04	2.89	4.13E-02	2.95E-02	0.394	0.216	2.16E-02	0.202
8.06	2.60	0.299	1.28E-04	4.10	0.634	0.319	7.06E-02	1.95E-03	5.06E-05	0
10.55	6.50	0.314	5.89E-05	3.08	0.488	0.144	2.28E-02	8.32E-04	5.06E-05	0
12.65	8.90	0.332	3.55E-05	2.70	5.99	7.61E-02	6.02E-03	5.27E-04	5.51E-05	0

Z=0.01 $Z_\odot$ (case T in WW95)

M_{CO}	M_r	^{12}C	^{15}N	^{16}O	^{20}Ne	^{24}Mg	^{28}Si	^{32}S	^{40}Ca	^{56}Fe
1.80	1.30	8.98E-02	6.65E-06	0.141	9.46E-03	5.75E-03	3.12E-02	1.40E-02	2.61E-03	0.152
2.01	1.40	0.109	1.01E-05	0.209	2.48E-02	1.05E-02	4.14E-02	2.18E-02	4.89E-03	0.191
2.42	1.50	0.149	2.14E-05	0.422	4.00E-02	2.12E-02	7.32E-02	3.46E-02	6.46E-03	0.171
3.18	1.50	0.194	4.76E-05	0.951	0.185	3.58E-02	0.101	5.60E-02	9.94E-03	0.135
4.31	1.90	0.208	8.71E-05	1.62	5.46E-02	1.66E-02	0.244	0.148	1.84E-02	7.30E-02
4.83	1.90	0.248	9.57E-05	1.94	4.11E-02	5.73E-02	0.311	0.148	1.93E-02	9.88E-02
5.84	1.70	0.279	1.27E-04	2.83	4.37E-02	3.95E-02	0.385	0.205	1.94E-02	0.187
8.10	3.10	0.315	1.35E-04	3.98	0.357	0.255	0.116	3.24E-03	0	0
10.20	5.20	0.343	8.29E-05	3.67	0.711	0.180	1.78E-02	1.39E-04	0	0
12.39	8.90	0.340	3.82E-05	2.61	0.532	7.41E-02	3.60E-03	0	0	0

4.3. Iron–core collapse supernovæ

In the range $M > 8\ M_\odot$, our models go through the whole sequence of nuclear burning stages and eventually explode after iron–core collapse. Very few models explode as "pair creation" SNæ (PC SNæ) before building an iron core (see § 4.4). To get the final outcome of iron core collapse SNæ, we link our models to the recent SN models by WW95, which cover a wide range of masses and metallicities (from 11 to 40 $M_\odot$ and from Z=0 to Z=$Z_\odot$=0.02). In WW95, pre-SN models are calculated at constant mass and convective regions are treated adopting the Schwarzschild criterion and semiconvection; the models are exploded by letting a piston move outward, tuning it so that the final ejecta gain a typical kinetic energy at infinity (1.2×10^{51} erg, although for M > 30 $M_\odot$ higher energies are also considered in cases B and C).

WW95 give the total ejecta, i.e. the ejecta relevant to the whole star. In order to link the outcome of these SNæ to our models, we need to discriminate the contribution of the CO core alone in the models of WW95. We consider the following elemental species: H, ^{4}He, ^{12}C, ^{13}C, ^{14}N, ^{15}N, ^{16}O, ^{17}O, ^{18}O, ^{20}Ne, ^{22}Ne, ^{24}Mg, ^{28}Si, ^{32}S, ^{40}Ca, ^{56}Fe. By means of the method described in App. A, for various metallicities referred to in WW95 we derive suitable relations between the mass of the CO–core and the amount of different elements expelled by the core in the explosion. These E_i^{CO}—M_{CO} relations are shown in Tab. 8 and in Fig. 4. We notice quite a regular behaviour of the remnant mass and of the ejecta of most elements as a function of M_{CO}, even with varying initial metallicity. This confirms that M_{CO} is a good parameter for our link (but see also App. B).

By means of a linear interpolation with respect to M_{CO} and to metallicity in such relations, we get the ejecta E_i^{CO} from the CO–cores of *our* models. Then we add (1) the composition of the overlying layers still left in our models at the time of explosion, and (2) the ejecta E_i^{wind} from the stellar wind (Tab. 4), to get our total ejecta as the sum:

$$E_i = E_i^{CO} + E_i^{over} + E_i^{wind} \quad (4)$$

4.4. Pair creation supernovæ

Massive stars with larger cores ($M_{He} \gtrsim\ 35\ M_\odot$) are known to undergo pair creation events during O–burning. This "pair creation" instability (Fowler & Hoyle 1964) may lead either to violent pulsational instability with ejection of some external layers and later iron core collapse ($35\ M_\odot \lesssim\ M_{He} \lesssim\ 60\ M_\odot$), or to complete thermonuclear

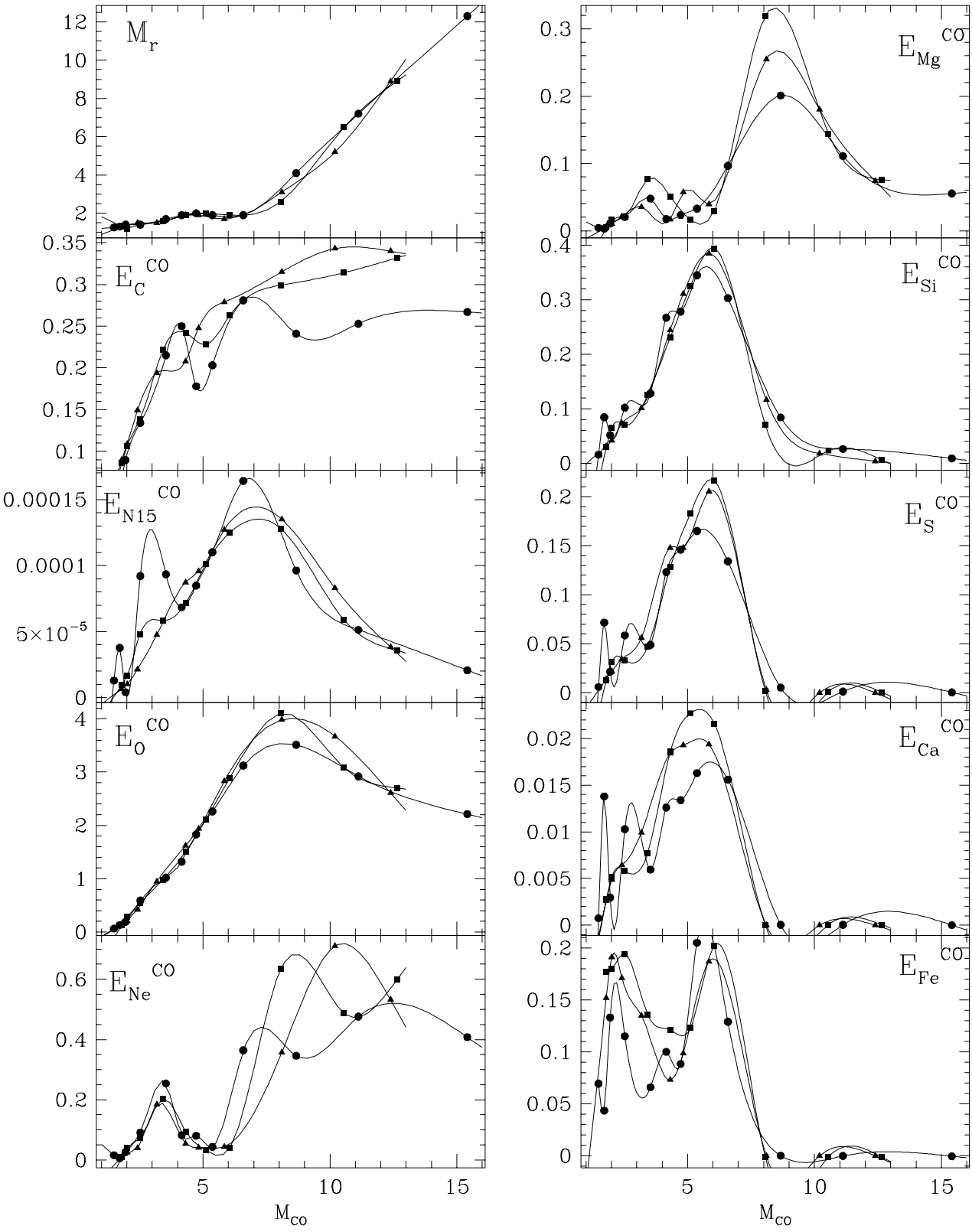

Fig. 4. Remnant mass and ejecta of the CO–core as functions of M_{CO} for three different metallicities, as deduced from WW95 (see text). Circles: case Z=$Z_{\odot}$; squares: case Z=0.1 $Z_{\odot}$; triangles: case Z=0.01 $Z_{\odot}$.

explosion (60 $M_\odot \lesssim M_{He} \lesssim$ 110 $M_\odot$), or to collapse to black hole after He–exhaustion ($M_{He} \gtrsim$ 110 $M_\odot$); for details refer to Woosley (1986). In terms of CO–core masses, up to $M_{CO}\sim$ 57 $M_\odot$ we expect pulsational instability, in the range M_{CO}=57 ÷ 106 $M_\odot$ a complete disruption is supposed to occur, while larger cores collapse to black holes.

Because of mass loss, in our stellar models we seldom face such large cores and "pair creation" supernovæ (PC SNæ) are likely to occur only in the case of the higher mass, low metallicity stars (M=100–120 $M_\odot$, Z=0.0004–0.004), as mass loss in not very efficient. These stars have He–cores in the range 35 ÷ 60 $M_\odot$ (Tab. 5); following Woosley (1986) we assume that they expel some of the external layers when pair instability develops, while whatever remains bound finally collapses to a black hole. In order to establish what is to be expelled in our CO–cores and what is to be locked in the remnant, we interpolate between the cases M_{He}=45 $M_\odot$ and 55 $M_\odot$ of Woosley (1986), corresponding to $M_{CO} \sim$ 41 $M_\odot$ and $M_{CO} \sim$ 52 $M_\odot$, respectively. For M_{CO}=41 $M_\odot$ only overlying layers are expelled, while for the M_{CO}=52 $M_\odot$ the inner 27 $M_\odot$ remain bound. Detailed ejecta of this case, as deduced from Tab. 18 of Woosley (1986), are shown in Tab. 9. The total ejecta of our stellar models experiencing a PC SN event are calculated according to Eq. (4).

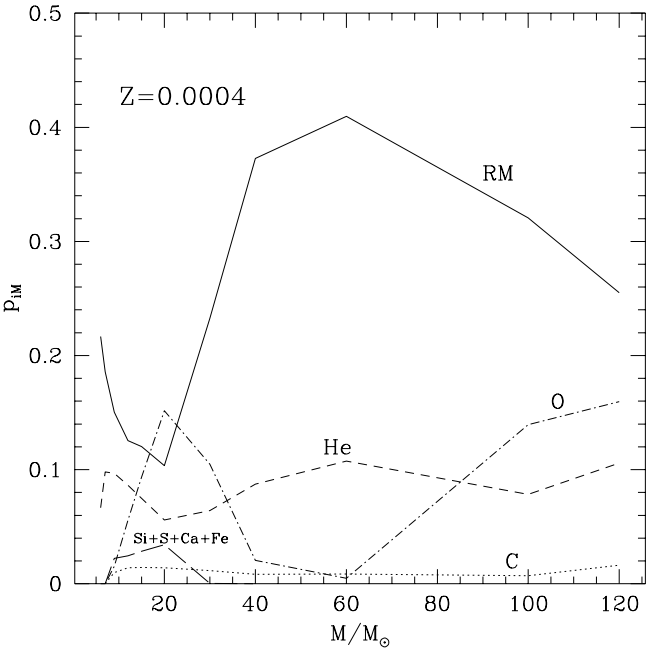

Fig. 5. Fractional remnant mass RM=M_r/M and total yields p_{iM} for some elements vs. the initial stellar mass M, for the Z=0.0004 set. Solid line: RM; dashed line: helium yields; dotted line: carbon yields; dash-dotted line: oxygen yields;long-dashed line: heavy elements yields.

Table 9. 1^{st} column: M_{He} values of PC SNæ models of Woosley (1986). 2^{nd} column: corresponding CO-core masses. 3^{rd} to 6^{th} column: ejecta from the CO–core for significant elemental species. 7^{th} column: remnant mass. All quantities are expressed in $M_\odot$

M_{He}	M_{CO}	^{12}C	^{16}O	^{20}Ne	^{24}Mg	M_r
45	41	0	0	0	0	41
55	52	1.1	21	1.5	1.1	27

5. The total ejecta of massive stars

The total ejecta for our stellar models, obtained as outlined in the previous sections, are listed in Tab. 10.

In Figures 5 to 9 we plot the fractional remnant mass M_r/M and the total yields p_{iM} for some representative elements vs. the stellar mass M, for our five sets of metallicity. A trend with metallicity is evident.

In the lower metallicity sets (Z=0.0004 and Z=0.004) remnant masses are very large due to lower mass-loss efficiency: massive CO–cores are built in the pre-SN phase, resulting in high remnant masses (i.e. black holes, cfr. Tab. 8). We notice an anti–correlation between the remnant mass and the oxygen yield: for instance, in the case Z=0.0004, M=40 and 60 $M_\odot$ ($M_{CO}\sim$ 18–24 $M_\odot$) almost the whole CO–core collapses to a black hole and a very small amount of new oxygen is released. For larger masses PC SNæ are found and oxygen yields increase again, while remnant masses decrease. This is in line with what Langer & Woosley (1996) suggest: at low metallicity (i.e. in the early phases of galactic evolution) stars in the range 30 ÷ 100 $M_\odot$ may form black holes and have a secondary role in chemical enrichment, while higher masses may give an important contribution through PC SNæ, also depending on the IMF in the early epochs. For solar metallicity, on the contrary, mass loss inhibits black hole formation and PC SNæ events.

In the case Z=0.008, the effects of mass loss are getting evident: for large masses ($M \gtrsim$ 40 $M_\odot$) remnant masses are sensibly smaller than in the previous sets, while helium and carbon yields are larger because of the contribution from the wind.

These effects are exalted in the higher metallicity sets (Z=$Z_\odot$=0.02 and Z=0.05), where large initial masses end as WR stars with small masses and small cores (cfr. Tab. 1 and Tab. 6), resulting in relatively low oxygen yields but very large helium yields. Carbon yields decrease again moving from the Z=0.008 to the Z=0.05 case, both because a higher mass loss rate is able to take more helium away before it is turned to carbon, and because with an increasing metallicity an increasing fraction of the original carbon is turned to ^{14}N in the CNO cycle.

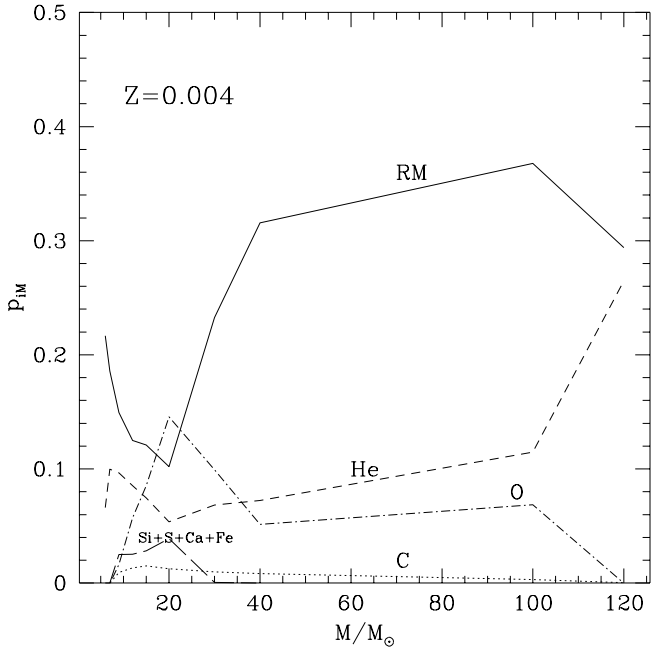

Fig. 6. Same as previous figure, for the Z=0.004 set

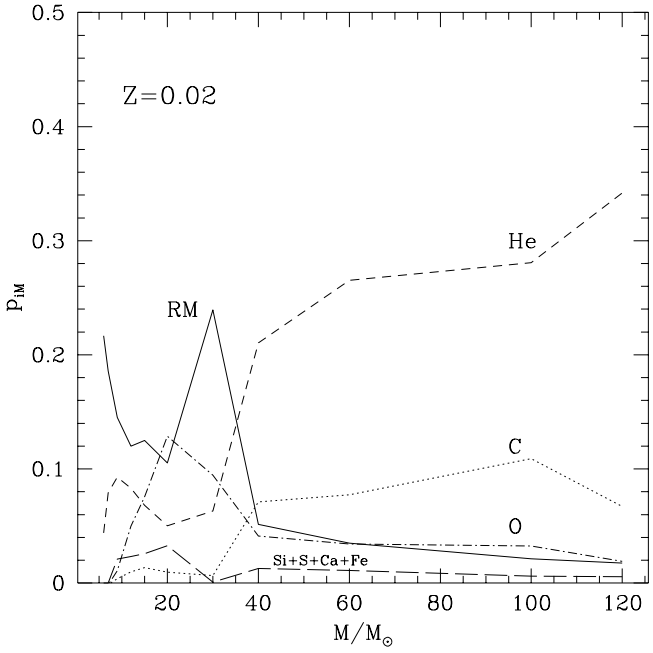

Fig. 8. Same as previous figure, for the Z=0.02 set

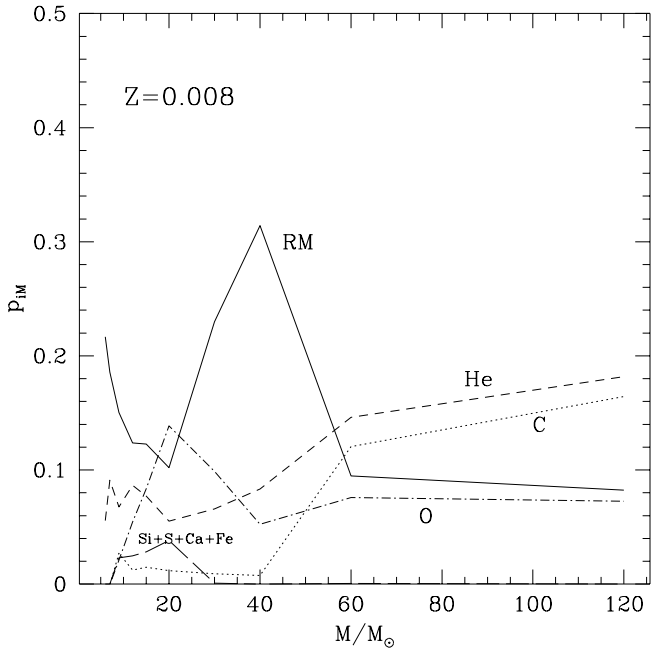

Fig. 7. Same as previous figures, for the Z=0.008 set

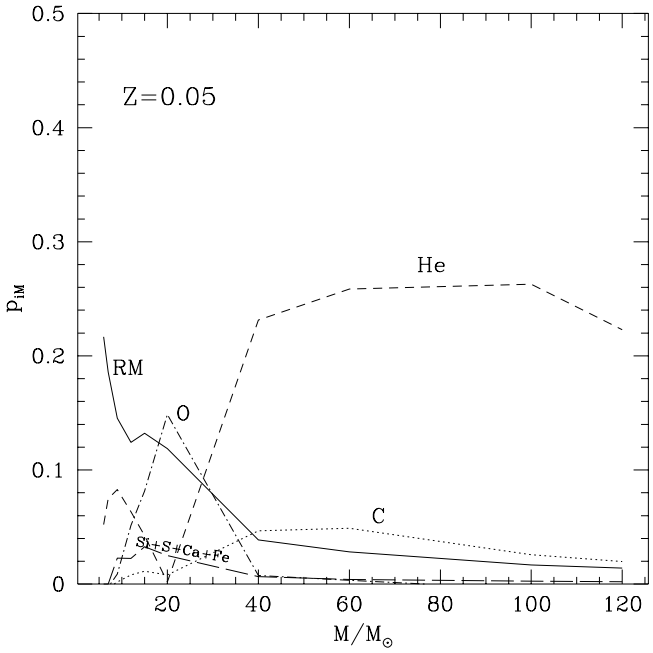

Fig. 9. Same as previous figures, for the Z=0.05 set

Table 10. Total ejecta (in $M_\odot$) for model stars between 9 and 120 $M_\odot$ for different metallicities

Z=0.0004

M	^{1}H	^{3}He	^{4}He	^{12}C	^{13}C	^{14}N	^{15}N	^{16}O	^{17}O	^{18}O	
				^{20}Ne	^{22}Ne	^{24}Mg	^{28}Si	^{32}S	^{40}Ca	^{56}Fe	M_r
9	4.57	1.22E-04	2.63	8.97E-02	2.27E-05	9.31E-04	7.16E-06	0.140	4.78E-06	2.43E-05	
				9.43E-03	2.96E-05	5.61E-03	3.08E-02	1.38E-02	2.60E-03	0.155	1.35
12	5.77	9.50E-05	3.45	0.170	2.91E-05	1.28E-03	3.58E-05	0.671	5.09E-06	2.97E-05	
				0.108	3.82E-05	2.91E-02	8.63E-02	4.39E-02	7.91E-03	0.157	1.50
15	6.86	8.02E-05	4.16	0.214	3.58E-05	1.50E-03	7.45E-05	1.41	5.80E-06	7.57E-05	
				9.92E-02	6.44E-05	2.68E-02	0.200	0.118	1.57E-02	9.59E-02	1.80
20	8.51	5.83E-05	5.24	0.284	4.21E-05	2.18E-03	1.29E-04	3.03	5.66E-06	3.01E-06	
				9.99E-02	5.64E-05	7.59E-02	0.340	0.172	1.63E-02	0.157	2.07
30	11.54	2.59E-05	7.22	0.350	4.49E-05	3.33E-03	6.14E-05	3.15	1.03E-05	1.34E-04	
				0.616	2.25E-04	0.130	1.21E-02	2.90E-04	2.42E-05	4.39E-04	6.98
40	14.33	1.73E-05	9.26	0.339	5.00E-05	4.86E-03	6.15E-07	0.824	1.71E-05	3.60E-06	
				0.271	9.69E-05	5.43E-02	3.08E-04	1.87E-04	2.83E-05	5.52E-04	14.91
60	20.01	1.09E-05	14.60	0.510	8.04E-05	7.57E-03	8.86E-07	0.288	3.08E-05	3.31E-06	
				1.14E-03	4.64E-04	3.34E-04	4.63E-04	2.81E-04	4.24E-05	8.29E-04	24.58
100	28.07	5.20E-05	23.46	0.719	2.20E-04	1.08E-02	1.21E-06	13.95	1.52E-05	7.60E-06	
				1.00	2.12E-04	0.718	6.73E-0.3	4.08E-0.3	6.18E-0.4	1.21E-03	32.0.6
120	32.80	5.05E-05	33.25	1.97	1.77E-04	1.58E-02	1.86E-06	19.16	5.69E-05	8.80E-06	
				1.33	3.03E-04	0.867	9.21E-04	5.58E-04	8.44E-05	1.65E-03	30.60

Z=0.004

M	^{1}H	^{3}He	^{4}He	^{12}C	^{13}C	^{14}N	^{15}N	^{16}O	^{17}O	^{18}O	
				^{20}Ne	^{22}Ne	^{24}Mg	^{28}Si	^{32}S	^{40}Ca	^{56}Fe	M_r
9	4.44	1.40E-04	2.71	9.03E-02	2.49E-04	8.60E-03	1.45E-05	0.162	4.00E-05	2.19E-05	
				1.54E-02	2.94E-04	6.65E-03	3.74E-02	1.90E-02	3.71E-03	0.169	1.35
12	5.59	1.15E-04	3.54	0.171	3.23E-04	1.16E-02	5.92E-05	0.707	6.26E-05	4.81E-04	
				0.121	3.86E-04	3.92E-02	9.22E-02	4.08E-02	6.86E-03	0.169	1.50
15	6.71	1.00E-04	4.28	0.240	3.73E-04	1.52E-02	7.12E-05	1.31	8.36E-05	2.95E-05	
				0.141	4.53E-04	5.86E-02	0.194	9.69E-02	1.40E-02	0.125	1.82
20	8.40	1.07E-04	5.38	0.271	4.89E-04	1.87E-02	1.33E-04	2.95	7.66E-05	3.98E-05	
				9.31E-02	5.68E-04	4.77E-02	0.374	0.200	2.02E-02	0.192	2.04
30	11.39	8.51E-05	7.58	0.319	4.35E-04	3.13E-02	5.96E-05	3.03	3.20E-04	4.12E-05	
				0.510	7.82E-04	0.131	2.32E-02	2.38E-03	2.77E-04	4.46E-03	6.98
40	14.41	7.77E-05	9.46	0.361	5.72E-04	4.06E-02	8.17E-06	2.12	3.60E-04	3.31E-05	
				0.743	9.84E-04	0.223	3.13E-03	1.90E-03	2.87E-04	5.61E-03	12.6
100	28.17	1.26E-04	26.66	0.375	9.20E-04	0.124	1.52E-05	6.98	4.04E-04	6.04E-05	
				0.515	2.26E-03	0.379	7.19E-03	4.36E-03	6.60E-04	1.29E-02	36.7
120	32.05	1.20E-04	52.10	0.127	1.63E-03	0.224	2.04E-05	0.147	3.15E-04	6.12E-05	
				2.59E-02	3.79E-03	8.00E-03	1.11E-02	6.71E-03	1.01E-03	1.98E-02	35.2

Z=0.008

M	^{1}H	^{3}He	^{4}He	^{12}C	^{13}C	^{14}N	^{15}N	^{16}O	^{17}O	^{18}O	
				^{20}Ne	^{22}Ne	^{24}Mg	^{28}Si	^{32}S	^{40}Ca	^{56}Fe	M_r
9	4.40	1.60E-04	2.52	0.259	5.06E-04	1.47E-02	2.21E-05	0.220	1.69E-04	5.25E-04	
				8.34E-03	3.25E-03	3.68E-03	4.12E-02	2.81E-02	5.68E-03	0.139	1.35
12	5.50	1.80E-04	3.67	0.168	6.69E-04	2.32E-02	7.17E-05	0.696	2.28E-05	1.91E-04	
				0.119	7.62E-04	3.42E-02	9.48E-02	4.50E-02	7.55E-03	0.158	1.48
15	6.49	1.78E-04	4.45	0.248	7.84E-04	2.92E-02	7.79E-05	1.31	2.79E-05	6.39E-05	
				0.143	9.13E-04	5.18E-02	0.204	9.92E-02	1.33E-02	0.120	1.84
20	8.27	1.55E-04	5.59	0.271	1.03E-03	3.67E-02	1.39E-04	2.85	2.42E-04	7.94E-05	
				0.107	1.15E-03	4.42E-02	0.372	0.195	2.01E-02	0.194	2.04
30	11.23	1.14E-04	7.75	0.313	8.34E-04	5.79E-02	6.87E-05	3.06	4.84E-04	5.71E-05	
				0.502	1.57E-03	0.133	2.93E-02	4.14E-03	5.03E-04	8.96E-03	6.90
40	13.90	2.19E-04	10.19	0.352	1.02E-03	7.69E-02	3.36E-05	2.21	4.89E-04	1.19E-04	
				0.656	1.99E-03	6.74E-03	6.35E-03	4.04E-03	6.25E-04	1.14E-02	12.5
60	18.91	2.67E-04	22.35	7.33	2.02E-03	0.133	1.04E-04	4.78	7.08E-04	2.33E-03	
				0.517	9.59E-03	0.184	5.35E-02	9.73E-03	1.24E-03	2.34E-02	5.69
120	30.08	3.51E-04	49.35	19.95	4.85E-03	0.349	8.52E-05	9.17	8.51E-04	1.93E-04	
				0.638	0.300	8.17E-02	3.34E-02	1.75E-02	2.60E-03	4.99E-02	9.89

$Z=Z_\odot$=0.02

M	^{1}H	^{3}He	^{4}He	^{12}C	^{13}C	^{14}N	^{15}N	^{16}O	^{17}O	^{18}O	
				^{20}Ne	^{22}Ne	^{24}Mg	^{28}Si	^{32}S	^{40}Ca	^{56}Fe	M_r
9	4.18	2.28E-04	2.99	7.27E-02	1.29E-03	4.02E-02	4.85E-05	0.178	0.748E-04	1.18E-04	
				1.95E-02	1.50E-03	6.64E-03	7.62E-02	6.22E-02	1.18E-02	5.68E-02	1.31
12	5.20	2.45E-04	3.95	0.170	1.65E-03	5.46E-02	1.12E-04	0.712	0.827E-04	1.49E-04	
				0.123	1.92E-03	2.78E-02	0.111	6.11E-02	1.04E-02	0.121	1.44
15	6.18	2.65E-04	4.70	0.266	1.95E-03	6.68E-02	1.02E-04	1.273	0.882E-04	1.66E-04	
				0.175	2.28E-03	3.62E-02	0.213	9.46E-02	1.03E-02	9.79E-02	1.87
20	7.75	3.23E-04	6.01	0.279	2.06E-03	8.84E-02	1.65E-04	2.76	1.04E-03	1.99E-04	
				0.214	2.89E-03	6.91E-02	0.335	0.156	1.68E-02	0.186	2.11
30	10.30	3.96E-04	8.28	0.307	2.01E-03	0.128	9.46E-05	3.08	1.45E-03	2.32E-04	
				0.500	3.89E-03	0.124	4.07E-02	9.02E-03	1.17E-03	2.22E-02	7.18
40	12.52	4.72E-04	19.05	3.03	3.61E-03	0.211	1.35E-04	2.05	3.37E-03	7.00E-03	
				0.135	0.282	3.86E-02	0.298	0.154	1.53E-02	0.133	2.06
60	16.49	5.27E-04	32.14	4.93	5.41E-03	0.343	1.81E-04	2.66	3.84E-03	2.89E-04	
				0.138	0.336	5.60E-02	0.360	0.181	1.87E-02	0.234	2.09
100	23.97	5.51E-04	55.48	11.40	9.79E-03	0.682	2.55E-04	4.27	5.58E-03	3.04E-04	
				0.455	0.613	0.130	0.371	0.176	2.13E-02	0.251	2.12
120	28.72	1.37E-03	74.03	8.63	1.16E-02	1.01	3.25E-04	3.52	2.17E-03	7.53E-04	
				0.349	0.542	0.113	0.402	0.197	2.28E-02	0.307	2.11

Z=0.05

M	^{1}H	^{3}He	^{4}He	^{12}C	^{13}C	^{14}N	^{15}N	^{16}O	^{17}O	^{18}O	
				^{20}Ne	^{22}Ne	^{24}Mg	^{28}Si	^{32}S	^{40}Ca	^{56}Fe	M_r
9	3.45	4.06E-04	3.45	0.111	3.19E-03	8.79E-02	7.73E-05	0.283	2.52E-03	2.14E-03	
				3.49E-02	3.74E-03	1.16E-02	9.26E-02	7.55E-02	1.42E-02	6.61E-02	1.31
12	4.25	4.92E-04	4.46	0.225	3.81E-03	0.116	1.44E-04	0.895	2.77E-03	5.47E-03	
				0.168	4.73E-03	3.83E-02	0.124	6.51E-02	1.05E-02	0.129	1.49
15	5.02	5.74E-04	5.22	0.329	4.79E-03	0.136	1.30E-04	1.57	3.37E-03	8.71E-03	
				0.123	5.63E-03	3.05E-02	0.285	0.135	1.43E-02	0.131	1.98
20	6.22	7.36E-04	6.24	0.376	4.79E-03	0.174	2.34E-04	3.44	4.24E-03	1.79E-03	
				0.412	6.75E-03	0.124	0.299	0.132	1.57E-02	0.152	2.38
40	9.98	1.17E-03	22.79	2.34	7.69E-03	0.484	2.43E-04	1.32	1.40E-02	7.61E-03	
				0.301	0.646	7.56E-02	0.173	9.11E-02	1.40E-02	0.203	1.55
60	14.06	6.47E-04	36.03	3.66	1.14E-02	1.06	2.19E-04	1.73	3.39E-02	3.67E-04	
				0.448	0.562	0.111	0.217	0.106	1.50E-02	0.238	1.70
100	26.74	8.60E-04	60.90	3.79	1.94E-02	1.79	2.78E-04	2.14	5.52E-02	3.23E-02	
				0.594	1.27	0.157	0.281	0.146	2.12E-02	0.357	1.68
120	38.07	1.15E-03	68.39	3.82	2.61E-02	2.11	3.20E-04	2.60	6.31E-02	0.177	
				0.669	1.27	0.180	0.314	0.166	2.42E-02	0.416	1.68

As far as heavy elements (^{28}Si + ^{32}S + ^{40}Ca + ^{56}Fe) are concerned, the bulk of contribution seems to come from stars between 10 and 20 $M_{\odot}$. For larger masses large remnants are found, so that most heavy elements produced remain locked in the remnant, at least for $Z \leq 0.008$. In the case of solar or super-solar metallicity, also stars with $M > 20\ M_{\odot}$ result in low CO–cores and low-mass remnants and can release some heavy elements.

6. Low and intermediate mass stars

For low and intermediate mass stars ($M \leq 5\ M_{\odot}$) we adopt the yields by Marigo et al. (1996, 1997), which are calculated basing on the same series of stellar tracks we adopt for massive stars. Specifically, by means of a semi-analytical model Marigo et al. (1996) extend the tracks of the Padua library, which stop at the end of the E-AGB phase, to the TP-AGB and III dredge-up phase. Further improvements of the semi-analytical formulation also allows to properly take into account the effects of envelope burning on the yields of stars between 4 and 5 $M_{\odot}$(Marigo et al. 1997). The related production of primary ^{14}N has remarkable effects upon the predictions of chemical models for the Solar Neighbourhood (§ 9.7).

Thus we extend our grid of stellar ejecta to the range of low and intermediate mass stars and provide a complete data-base for the chemical models of galaxies. This data-base is referred to a unique grid of stellar models for the whole range of stellar masses, which gives it coherence and homogeneity of basic physical prescriptions.

Table 11. Lifetimes, H–burning core masses and CO–core masses for Very Massive Objects

	M	τ_H	M_{Hb}	M_{CO}
Z=**0.0004**	150	3.0 10^6	75	PC SN
	200	2.7 10^6	100	PC SN
	300	2.5 10^6	150	18
	500	2.0 10^6	250	21
	1000	2.0 10^6	500	21
Z=**0.004**	150	3.0 10^6	75	35
	200	2.7 10^6	100	35
	300	2.5 10^6	150	8
	500	2.0 10^6	250	10
	1000	2.0 10^6	500	10
Z=**0.008**	150	3.0 10^6	75	13
	200	2.7 10^6	100	13
	300	2.5 10^6	150	7
	500	2.0 10^6	250	8
	1000	2.0 10^6	500	8
Z=$Z_{\odot}$=**0.02**	150	3.0 10^6	75	6
	200	2.7 10^6	100	5
	300	2.5 10^6	150	5
	500	2.0 10^6	250	5
	1000	2.0 10^6	500	5
Z=**0.05**	150	3.0 10^6	75	3.5
	200	2.7 10^6	100	3.5
	300	2.5 10^6	150	3.5
	500	2.0 10^6	250	3.5
	1000	2.0 10^6	500	3.5

7. Very Massive Objects

The structure and evolution of very massive massive objects (VMOs), i.e. stars in the mass range 120< M <1000 $M_{\odot}$, was explored in past years, mainly in the framework of a primeval Population III of very massive stars formed by metal–free gas (Bond et al. 1984; Carr et al. 1984; El Eid et al. 1983; Ober et al. 1983; Woosley & Weaver 1982). Population III was invoked to solve the G-dwarf problem and to explain the non-zero metallicity of Population II stars, to provide a substantial amount of dark matter by means of black hole formation, to account for black holes in AGNs, to explain the reionization of the Universe, to produce primordial helium and to account for some difficulties in Big Bang nucleosynthesis; for a review see Bond (1984).

Some recent interest toward stars more massive than the canonical limit of say 120 $M_{\odot}$ come from studies of chemical evolution and population synthesis in galaxies under unconventional IMFs (Chiosi et al. 1997) such as that proposed by Padoan et al. (1997) which formally allows for a non–zero, though small, probability that objects more massive than 120 $M_{\odot}$ can form.

We are not going to discuss here the possible existence of VMOs in present-day or primeval galaxies, nor the cosmological consequences of Population III; rather, we want to make reasonable assumptions about nucleosynthesis and mass loss in VMOs and to extend our five grids of ejecta up to 1000 $M_{\odot}$, for the purpose of future use if required by the particular problem under examination. Notice that we do not include chemical enrichment from VMOs in our chemical model of the Solar Neighbourhood (see Sect. 9).

VMOs are pulsationally unstable during H-burning, so once they form they are likely to undergo violent mass loss until they fall below the critical mass for pulsational stability; this limit is generally around 100 $M_{\odot}$, though depending on metallicity. We assume that VMOs lose mass at a rate of 10^{-3} $M_{\odot}$/yr (comparable to the extreme mass loss rate adopted in our stellar tracks beyond the de Jager limit), independently of metallicity since mass loss here is driven by instability rather than by radiation pressure. We stop this phase of paroxysmal mass loss when the mass has decreased down to 150 $M_{\odot}$.

Meanwhile, we assume that the star has been burning hydrogen in the inner 50% of its mass (He–cores of VMOs involve ∼0.56 of the initial mass, see the references quoted above) and that the hydrogen content X in the core has been linearly decreasing with time, consistently with the

behaviour of our high-mass stellar tracks. The hydrogen content in the core at any time t is given by:

$$X(t) = X^0 \left(1 - \frac{t}{\tau_H}\right) \quad (5)$$

where X^0 is the initial hydrogen abundance in the star and τ_H is the H–burning timescale, assumed following the references above and listed in the second column of Tab. 11.

At the end of the violent mass loss phase (i.e. when the current mass falls below 120 $M_\odot$) we adopt a rate for radiation pressure driven mass loss derived from Lamers & Cassinelli (1996):

$$\dot{M} = 2.11 \times 10^{-14} \times M^{-4.421} \quad (6)$$

scaled with metallicity in conformity with our stellar tracks for massive stars ($\dot{M} \propto Z^{0.5}$). This mass loss rate holds until the star becomes a WR star; in case it enters this stage, for the rest of its lifetime we adopt the mass loss rate by Langer (1989), scaled with metallicity. For the sake of consistency with our stellar tracks, we assume that the WR stage begins if the surface hydrogen content falls below X=0.3, i.e. when two conditions are fulfilled: (1) the H–burning or He–core is revealed on the surface (the stellar mass must have fallen below 1/2 of its initial value) and (2) the hydrogen content in the core, given by Eq. (5), is lower than X=0.3.

In the papers referenced above about VMOs, later burning processes build a CO–core which almost fills the whole He–core ($M_{CO} \sim M_{He}$). This result cannot hold here, since we include strong mass-loss and a possible WR stage which sensitively depletes the mass. The CO–core is assumed to fill the total remaining mass at the end of the lifetime. The assumed lifetimes and H–burning core masses, and the obtained CO–core masses, are listed in Tab. 11. We notice that, for the higher metallicity cases, the final masses of the CO–cores tend to converge to the same small value for all the VMOs, due to a prolonged WR stage with very efficient mass loss.

To derive the composition of the ejected material, we assume that the layers over the H–burning core have not altered their initial composition, i.e. we neglect any convective dredge-up of processed material and a possible recession of the convective core from initial masses larger than 1/2 the total mass. When the core is revealed on the surface, we assume that all initial CNO isotopes have been converted to ^{14}N, that the hydrogen content is given by Eq. (5) at any time t and that the remaining fraction is ^{4}He.

The size of the CO–core eventually drives the SN explosion, as we have assumed to hold for lower masses (§ 4). In most cases the final outcome is an iron–core collapse SN, whose ejecta are calculated as in § 4.3. The only exceptions are the cases M=150 and 200 $M_\odot$, Z=0.0004, whose CO–cores are marked "PC SN" in Tab. 11. These objects never lose enough mass to let the core uncovered; they build a 75 $M_\odot$ and a 100 $M_\odot$ He–core, respectively, which eventually explode as PC SNæ. The ejecta of such cores are taken directly from Tab. 18 of Woosley (1986), but for those of ^{14}N which are to be scaled with metallicity. In fact, Woosley's PC SNæ are calculated for solar metallicity and their initial abundances of CNO isotopes, which are turned to ^{14}N during H–burning, are solar; for our Z=0.0004 case, the initial CNO content is much lower.

The resulting ejecta for the whole set of VMOs and for the five metallicity cases included in our grid are listed in Tab. 12.

8. The chemical evolution model

Our results about stellar nucleosynthesis and ejecta described in previous sections were inserted in a model of chemical evolution, which was applied to the analysis of the Solar Neighbourhood. In this section we outline the main features and equations of the model.

We adopt an open model with continuous *infall* of primordial gas that builds the disk gradually, as suggested by dynamical studies (Larson 1976; Burkert et al. 1992; Carraro et al. 1997). Infall also provides for the better solution to the "G–dwarf problem" (Lynden-Bell 1975; Tinsley 1980; Chiosi 1978, 1980; Pagel 1989; Matteucci 1991). Our formulation follows the one framed by Talbot & Arnett (1971, 1973, 1975) and adapted to open models by Chiosi (1980). This formulation, particularly suitable for galactic discs, is also currently used by other authors (e.g. Matteucci & François 1989; Timmes et al. 1995).

The Galactic disc is divided into concentric cylindrical shells, 2 kpc wide each, which evolve independently, neglecting any possible radial flows of gas or stars. Each ring consists of a homogeneous mixture of gas and stars, so that for each ring the only independent variable is time t (*one–zone* formulation, Talbot & Arnett 1971). Galactic discs are comfortably described in terms of surface mass density $\sigma(r,t)$, which depends both on the galactocentric radius r of the ring and also on time t, since in each ring the surface density is growing in time due to gradual infall of gas. Since in this paper the model is applied only to the Solar Neighbourhood ($r = r_\odot$), for the sake of simplicity we drop the dependence on r in the following equations. If we indicate with $\sigma_g(t)$ the surface gas density, the gas fraction in the ring at any time t is the ratio:

$$\frac{\sigma_g(t)}{\sigma(t)}$$

while the surface star density is:

$$\sigma_s(t) = \sigma(t) - \sigma_g(t)$$

In closed models the total surface density σ is constant and the other quantities can be normalized with respect to it; in open models it is suitable to normalize with respect to the total surface density at the present age of the Galaxy

Table 12. Total ejecta in $M_\odot$ for VMOs (150 ÷ 1000 $M_\odot$) of different metallicities

Z=**0.0004**

M	^{1}H	^{3}He	^{4}He	^{12}C	^{13}C	^{14}N	^{15}N	^{16}O	^{17}O	^{18}O	
				^{20}Ne	^{22}Ne	^{24}Mg	^{28}Si	^{32}S	^{40}Ca	^{56}Fe	M_r
150	59.51	6.60E-05	20.95	1.31	8.88E-05	2.67E-03	7.32E-06	38.02	6.30E-06	3.63E-05	
				1.80	3.08E-04	1.60	16.00	8.90	1.30	0.612	0
200	79.82	8.80E-05	28.90	0.840	1.18E-04	1.46E-02	9.76E-06	34.02	8.40E-06	4.84E-05	
				1.50	4.10E-04	1.50	23.00	15.00	2.40	13.00	0
300	152.7	1.32E-04	129.1	1.48E-02	1.78E-04	4.48E-02	1.46E-05	3.17E-02	1.26E-05	7.27E-05	
				8.61E-03	1.16E-03	2.66E-03	3.68E-03	2.23E-03	3.38E-04	6.60E-03	18.00
500	292.2	2.20E-04	186.6	2.47E-02	2.96E-04	7.75E-02	2.44E-05	5.28E-02	2.10E-05	1.21E-04	
				1.46E-02	1.97E-03	4.52E-03	6.26E-03	3.79E-03	5.74E-04	1.12E-02	21.00
1000	596.2	4.40E-04	382.4	4.94E-02	5.92E-04	0.162	4.88E-05	0.106	4.20E-05	2.42E-04	
				2.99E-02	4.02E-03	9.24E-03	1.28E-02	7.75E-03	1.17E-03	2.29E-02	21.00

Z=**0.004**

M	^{1}H	^{3}He	^{4}He	^{12}C	^{13}C	^{14}N	^{15}N	^{16}O	^{17}O	^{18}O	
				^{20}Ne	^{22}Ne	^{24}Mg	^{28}Si	^{32}S	^{40}Ca	^{56}Fe	M_r
150	56.67	6.60E-04	57.84	7.41E-02	8.88E-04	0.153	7.32E-05	0.159	6.30E-05	3.63E-04	
				3.51E-02	4.72E-03	1.09E-02	1.50E-02	9.11E-03	1.38E-03	2.69E-02	35.00
200	75.57	8.80E-04	88.74	9.89E-02	1.18E-03	0.227	9.76E-05	0.211	8.40E-05	4.84E-04	
				5.04E-02	6.77E-03	1.56E-02	2.15E-02	1.31E-02	1.98E-03	3.86E-02	35.00
300	159.2	1.32E-03	131.6	0.442	1.78E-03	0.480	2.73E-04	4.34	1.26E-04	7.27E-04	
				0.692	1.20E-02	0.330	0.126	3.01E-02	4.10E-03	7.29E-02	2.68
500	295.9	2.20E-03	192.0	0.551	2.96E-03	0.810	3.18E-04	3.82	2.10E-04	1.21E-03	
				0.658	2.01E-02	0.226	9.95E-02	4.01E-02	5.92E-03	0.115	5.67
1000	591.9	4.40E-03	394.0	0.798	5.92E-03	1.65	5.62E-04	4.35	4.20E-04	2.42E-03	
				0.811	4.02E-02	0.273	0.165	7.97E-02	1.19E-02	0.232	5.67

Z=**0.008**

M	^{1}H	^{3}He	^{4}He	^{12}C	^{13}C	^{14}N	^{15}N	^{16}O	^{17}O	^{18}O	
				^{20}Ne	^{22}Ne	^{24}Mg	^{28}Si	^{32}S	^{40}Ca	^{56}Fe	M_r
150	55.54	1.32E-03	80.25	0.460	1.78E-03	0.423	1.75E-04	2.86	1.26E-04	7.27E-04	
				0.636	1.12E-02	9.16E-02	4.42E-02	2.22E-02	3.32E-03	6.41E-02	9.57
200	80.98	1.76E-03	104.4	0.509	2.37E-03	0.592	2.24E-04	2.97	1.68E-04	9.69E-04	
				0.667	1.53E-02	0.101	5.73E-02	3.02E-02	4.52E-03	8.75E-02	9.57
300	159.1	2.64E-03	131.9	0.572	3.35E-03	0.968	4.31E-04	3.81	2.52E-04	1.45E-03	
				0.433	2.41E-02	0.158	0.383	0.197	2.28E-02	0.279	2.15
500	292.9	4.40E-03	195.0	0.778	5.92E-03	1.63	6.13E-04	4.92	4.20E-04	2.42E-03	
				0.841	4.04E-02	0.361	0.227	9.48E-02	1.35E-02	0.244	2.96
1000	582.7	8.80E-03	401.1	1.27	1.18E-02	3.31	1.10E-03	5.97	8.40E-04	4.84E-03	
				1.14	8.14E-02	0.456	0.358	0.174	2.55E-02	0.478	2.96

Z=$Z_\odot$=**0.02**

M	^{1}H	^{3}He	^{4}He	^{12}C	^{13}C	^{14}N	^{15}N	^{16}O	^{17}O	^{18}O	
				^{20}Ne	^{22}Ne	^{24}Mg	^{28}Si	^{32}S	^{40}Ca	^{56}Fe	M_r
150	52.39	3.30E-03	88.62	0.614	4.44E-03	1.17	5.04E-04	3.50	3.15E-04	1.82E-03	
				0.429	2.95E-02	0.134	0.417	0.206	2.46E-02	0.334	2.11
200	96.71	4.40E-03	94.51	0.672	5.92E-03	1.61	5.73E-04	2.89	4.20E-04	2.42E-03	
				0.379	4.01E-02	0.116	0.406	0.223	2.51E-02	0.317	2.09
300	155.3	6.60E-03	133.4	0.919	8.88E-03	2.45	8.17E-04	3.42	6.30E-04	3.63E-03	
				0.531	6.06E-02	0.613	0.471	0.263	3.11E-02	0.434	2.09
500	281.4	1.10E-02	202.9	1.44	1.48E-02	4.12	1.33E-03	4.90	1.05E-03	6.05E-03	
				0.799	0.101	0.266	0.668	0.361	4.59E-02	0.784	2.09
1000	553.8	2.20E-02	420.2	2.67	2.96E-02	8.32	2.55E-03	7.54	2.10E-03	1.21E-02	
				1.56	0.204	0.502	0.994	0.559	7.59E-02	1.37	2.09

Z=**0.05**

M	^{1}H	^{3}He	^{4}He	^{12}C	^{13}C	^{14}N	^{15}N	^{16}O	^{17}O	^{18}O	
				^{20}Ne	^{22}Ne	^{24}Mg	^{28}Si	^{32}S	^{40}Ca	^{56}Fe	M_r
150	44.58	8.25E-03	94.29	1.14	1.11E-02	3.02	1.01E-03	3.00	7.87E-04	4.54E-03	
				0.813	7.51E-02	0.221	0.367	0.194	2.79E-02	0.494	1.74
200	87.44	1.10E-02	98.84	1.45	1.48E-02	4.07	1.31E-03	3.66	1.05E-03	6.06E-03	
				1.00	0.101	0.280	0.449	0.243	3.54E-02	0.641	1.74
300	140.9	1.65E-02	140.2	2.07	2.22E-02	6.17	1.92E-03	4.98	1.58E-03	9.08E-03	
				1.39	0.152	0.398	0.612	0.342	5.03E-02	0.933	1.74
500	246.6	2.75E-02	224.1	3.30	3.70E-02	10.37	3.14E-03	7.62	2.62E-03	1.51E-02	
				2.15	0.255	0.634	0.938	0.540	8.03E-02	1.52	1.74
1000	478.2	5.50E-02	466.6	6.39	7.40E-02	20.88	6.19E-03	14.23	5.25E-03	3.03E-02	
				4.06	0.511	1.22	1.75	1.04	0.155	2.98	1.74

t_G, i.e. at the final age of the model. So we introduce the normalized surface gas density as:

$$G(t) = \frac{\sigma_g(t)}{\sigma(t_G)}$$

In each ring the gas is assumed to be chemically homogeneous, and the normalized gas density for each chemical species i is:

$$G_i(t) = X_i(t)\, G(t)$$

where X_i is the fractionary mass abundance of species i; $\sum_i X_i$=1 by definition. The chemical evolution of the ISM is the evolution of the set of the G_i's, described by:

$$\frac{d}{dt}\, G_i(t) \;=\; -\, X_i(t)\Psi(t) \;+ \\ + \int_{M_l}^{M_u} \Psi(t-\tau_M)\, R_{Mi}(t-\tau_M)\Phi(M)\, dM \;+ \\ + \left[\frac{d}{dt} G_i(t)\right]_{inf} \qquad (7)$$

where $\Psi(t)$ is the SFR, $\Phi(M)$ is the IMF, $R_{Mi}(t)$ is the mass fraction of a star of mass M ejected into the ISM in the form of element i, M_l and M_u are the lower and upper limit for stellar mass respectively, and τ_M is the lifetime of a star of mass M. The first term on the right side represents the depletion of species i from the ISM due to star formation; the second term represents the amount of species i put in the ISM by stellar ejecta; the third term is the contribution of the infalling gas. We describe the various ingredients in the following subsections.

8.1. The infall term

In open models the surface mass density $\sigma(r,t)$ increases by slowly accreting gas at a rate $\dot\sigma_{inf}(r,t)$, until it reaches the observed present values. An infall rate exponentially decreasing in time with a timescale τ:

$$\dot\sigma_{inf}(r,t) = A(r)\, e^{-\frac{t}{\tau}} \qquad (8)$$

well reproduces the results of dynamical models (Larson 1976; Burkert et al. 1992; Carraro et al. 1997), with the exception of radial flows. $A(r)$ is obtained by integrating upon time and by imposing that at the age t_G the observed present surface mass density $\sigma(r,t_G)$ is matched:

$$A(r)\left(1-e^{-\frac{t_G}{\tau}}\right)\,\tau = \sigma(r,t_G) \qquad (9)$$

In the case of the solar ring:

$$A_\odot\left(1-e^{-\frac{t_G}{\tau}}\right)\,\tau = \sigma(r_\odot,t_G) \qquad (10)$$

The contribution of the infalling gas to the evolution of the (normalized) gas fraction $G(t)$ is:

$$\left[\frac{d}{dt}G(t)\right]_{inf} = \frac{\dot\sigma_{inf}(t)}{\sigma(t_G)} \qquad (11)$$

and, for each single chemical species i:

$$\left[\frac{d}{dt}G_i(t)\right]_{inf} \;=\; \frac{\dot\sigma_{inf}(t)\, X_{i,inf}}{\sigma(t_G)} \qquad (12)$$

which gives the third term on the right side of Eq. (7).

8.2. The Star Formation Rate

We adopt the formulation of the SFR for the Galactic disk given by Talbot & Arnett (1975):

$$\frac{d}{dt}\,\sigma_g(r,t) = \nu\,\left[\frac{\sigma(r,t)\,\sigma_g(r,t)}{\tilde\sigma(\tilde r,t)}\right]^{\kappa-1}\,\sigma_g(r,t) \qquad (13)$$

Here, κ is the exponent of the Schmidt (1959) law for star formation, $\Psi \propto \rho^\kappa$; plausible values for κ range from 1 to 2 (proportional to gas density or proportional to cloud–cloud collision events respectively, Larson 1991); $\tilde\sigma(\tilde r,t)$ is the surface mass density at a given galactocentric distance $\tilde r$, adopted as a normalization factor; ν is a parameter for the star formation efficiency, related to the choice of $\tilde r$.

Talbot & Arnett's SFR is based on Schmidt's law, but it also takes into account that the cooling due to gas accretion onto the equatorial plane is balanced by the heating due to the feed–back of massive stars. The SFR turns out to be related to the dynamical timescale, shorter where the mass density is larger, while the timescale of gas accretion onto the equatorial plane is longer than the purely dynamical one due to the feed–back from star formation. As a caveat, we remind that the formula above holds in the plane–parallel approximation, which may not be a good one in the case of open models.

In terms of the formalism introduced in previous sections, this adopted SFR

$$\Psi(r,t) = \nu\,\left[\frac{\sigma(r,t)}{\tilde\sigma(\tilde r,t)}\right]^{2(\kappa-1)}\,\left[\frac{\sigma(r,t_G)}{\sigma(r,t)}\right]^{\kappa-1}\,G^\kappa(r,t) \qquad (14)$$

Limiting to the solar ring and taking $\tilde r = r_\odot$ we get (dropping the dependence on r):

$$\Psi(t) = \nu\,\left[\frac{\sigma(t_G)}{\sigma(t)}\right]^{\kappa-1}\,G^\kappa(t) \qquad (15)$$

where ν is to be fixed so as to reproduce the features of the Solar Neighbourhood.

Table 13. The Q_{ij} matrix

	^{H} (1)	^{4}He (2)	^{12}C (3)	^{13}C (4)	^{14}N (5)	^{16}O (6)	nr (7)	^{20}Ne (8)	^{24}Mg (9)	^{28}Si (10)	^{32}S (11)	^{40}Ca (12)	^{56}Fe (13)
(1) H	$1-q_4$												
(2) ^4He	q_4-q_C	$1-q_C$											
(3) ^{12}C	$\chi_C w_C$	$\chi_C w_C$	$1-q_{C13s}$										
(4) ^{13}C	$\chi_{C13} w_C$	$\chi_{C13} w_C$	$q_{C13s}-q_{Ns}$	$1-q_{Ns}$									
(5) ^{14}N	$\chi_N w_C$	$\chi_N w_C$	$q_{Ns}-q_C$	$q_{Ns}-q_C$	$1-q_C$	$q_{Ns}-q_C$							
(6) ^{16}O	$\chi_O w_C$	$\chi_O w_C$				$1-q_{Ns}$							
(7) nr			w_C	w_C	w_C	w_C	$1-d$						
(8) ^{20}Ne	$\chi_{Ne} w_C$	$\chi_{Ne} w_C$						$1-d$					
(9) ^{24}Mg	$\chi_{Mg} w_C$	$\chi_{Mg} w_C$							$1-d$				
(10) ^{28}Si	$\chi_{Si} w_C$	$\chi_{Si} w_C$								$1-d$			
(11) ^{32}S	$\chi_S w_C$	$\chi_S w_C$									$1-d$		
(12) ^{40}Ca	$\chi_{Ca} w_C$	$\chi_{Ca} w_C$										$1-d$	
(13) ^{56}Fe	$\chi_{Fe} w_C$	$\chi_{Fe} w_C$											$1-d$

8.3. The Initial Mass Function

We adopt a Salpeter–like IMF:

$$\Phi(M)\,dM = C\,M^{-\mu}\,dM \tag{16}$$

where μ=1.35 in Salpeter's (1955) law.

Once the slope μ and the limiting masses M_l and M_u are chosen, the coefficient C is fixed by normalizing the IMF over the whole mass interval:

$$\int_{M_l}^{M_u} \Phi(M)\,dM\, = 1 \tag{17}$$

Since the bulk of chemical enrichment is due to stars with $M\ \geq$1 $M_\odot$, it is meaningful to fix the fraction ζ of the total stellar mass distributed in stars above 1 $M_\odot$, which is equivalent to fixing M_l (see below). Then we get the normalization condition:

$$\zeta\ =\ \int_{M_1}^{M_u} \Phi(M)\,dM\ =\ C\int_{M_1}^{M_u} M^{-\mu}\,dM \tag{18}$$

where M_1=1 $M_\odot$ and M_u is chosen to be 100 $M_\odot$ (no VMOs are supposed to be present). The normalization condition fixes M_l once ζ is given:

$$\int_{M_l}^{M_1} \Phi(M)\,dM + \zeta\ = 1 \tag{19}$$

The slope μ of the IMF may not be constant over the whole range of stellar masses (Miller & Scalo 1980; Scalo 1986). The model includes also the possibility of a variable μ over different mass ranges; in this case, beside the normalization condition, we impose that the IMF is continuous where the different mass ranges connect and thus determine the normalization coefficients C_1,.....C_n for the different ranges. See, for instance, Chiosi & Matteucci (1982).

8.4. The contribution of stellar ejecta

We calculate the fraction of a star of initial mass M that is ejected back in form of chemical species i

$$R_{Mi} = \frac{E_{iM}}{M} \tag{20}$$

according to our results on stellar ejecta (discussed in previous sections) and by means of the "Q_{ij} matrix" formalism, first introduced by Talbot & Arnett (1973) and later adopted by many authors (Chiosi & Matteucci 1982; Matteucci & François 1989; Ferrini et al. 1992). Each matrix element Q_{ij} is defined as the mass fraction of a star originally in form of species j which has been processed and ejected as species i. R_{Mi} is the sum over all "fuels" j:

$$R_{Mi} = \sum_{j=1}^{N} Q_{ij}(M)\,X_j \tag{21}$$

Each matrix element is defined as:

$$Q_{ij} = \frac{M_{ij,exp}}{X_j M} \tag{22}$$

where X_j is the initial mass abundance of species j and $M_{ij,exp}$ is the amount of species i synthesized starting from j and eventually expelled. The diagonal elements Q_{ii} represent the unprocessed fraction of species i that is eventually re-ejected. By summing upon all the sources of species i, one must get the total ejecta of i:

$$\sum Q_{ij} X_j M = E_{iM} \tag{23}$$

Each stellar mass M corresponds to a different Q_{ij} matrix, which generally depends also on the metallicity of the star.

The Q_{ij} matrix of Talbot & Arnett originally treated ^{1}H, ^{2}H, ^{3}He, ^{4}He, ^{12}C–^{16}O, ^{14}N, neutron rich isotopes (nr) and the bulk of heavy elements (h). Later, the dimensions

of the matrix were extended to include a higher number of chemical species (Ferrini et al. 1992). The formalism we use here is analogous to that in Ferrini et al. (1992), although the definitions of some matrix elements have been revised In our model we follow the evolution of 13 elements: ^{1}H, ^{4}He, ^{12}C, ^{13}C, ^{14}N, ^{16}O, neutron rich isotopes (nr), ^{20}Ne, ^{24}Mg, ^{28}Si, ^{32}S, ^{40}Ca, ^{56}Fe.

The set of non–zero Q_{ij} elements is displayed in Tab. 13. Here we list the various quantities entering the matrix elements:

d	mass fraction eventually locked in the remnant
q_4	mass fraction involved in H–burning
q_C	mass fraction involved in He–burning
$w_C = q_C - d$	mass fraction that has been processed by He–burning and has been ejected
q_{Ns}	mass fraction where ^{12}C, ^{13}C and ^{16}O have been turned to secondary ^{14}N by the CNO cycle
q_{C13s}	mass fraction where ^{12}C is turned to secondary ^{13}C by the CNO cycle
χ_i	fractionary mass abundance within w_C of *newly synthesized* species i

The meaning and the calculation of the non–zero elements of the Q_{ij} matrix are discussed in App. C.

8.5. Stellar lifetimes

To follow the temporal behaviour of different chemical species and isotopes, we drop the "instantaneous recycling approximation" by taking into account the role of finite lifetimes for stars of different masses. Our stellar models of different metallicities allow us to consider the effects of a different metal content not only on the ejecta but also on the lifetimes $\tau_M = \tau_M(Z)$. The dependence of lifetimes on metallicity can be up to a factor of 2 for stars around 1 $M_\odot$.

The lifetimes we adopt are calculated as the sum $\tau = t_H + t_{He}$ of the H–burning and He–burning timescales of the stellar tracks of the Padua library, and are listed in Tab. 14. The trend of τ_M with metallicity is not univocal: up to solar metallicity, τ_M increases with Z due to the effect of increasing opacity, while for super–solar metallicity (Z =0.05) τ_M decreases because the helium content Y increases, due to the assumed ratio $\Delta Y/\Delta Z$=2.5. When Y increases sensitively, (1) the hydrogen content $X = 1 - Y - Z$, i.e. the available "fuel", decreases and (2) the average molecular weight μ increases, which leads to a higher luminosity ($L \sim \mu^{7.4}$). For super–solar metallicities the effects of Y overcome those of opacity, giving shorter lifetimes with increasing Z.

In the chemical model, for each mass M and metallicity Z we calculate the corresponding lifetime $\tau_M(Z)$ by interpolating within the logarithmic relation $\log(M)$—$\log(t)$ for the tabulated metallicities, and then by interpolating with respect to Z.

Around $\sim$1 $M_\odot$ the influence of metallicity reduces lifetimes of a factor of 2 for low metallicities with respect to the solar case: low and intermediate mass stars born in early galactic stages eject their nucleosynthetic products in shorter times.

We assume that each star expels its ejecta all at once at the end of its lifetime, and that the ejected material is immediately mixed in the ISM, which remains always homogeneous. This "instantaneous mixing approximation" is suitable to reproduce the average trends of the age–metallicity relation, of abundance ratios and so on, while it can't model the observed scatter of the data around the average trend. Only few models relaxing the instantaneous mixing approximation can be found in literature (Malinie et al. 1991, 1993; Pilyugin & Edmunds 1996; van den Hoek & de Jong 1997).

8.6. The numerical solution

For the set of equations 7 we adopt the numerical solution suggested by Talbot & Arnett (1971), with the addition of the infall term (Chiosi 1980). Each equation is treated as a linear differential equation, whose analytical solution can be written as:

$$G_i(t_2) = G_i(t_1)\, e^{-\chi(t_1,t_2)} + \int_{t_1}^{t_2} W_i(t) e^{-\chi(t,t_2)}\, dt \qquad (24)$$

where:

$$\chi(t_1,t_2) \equiv \int_{t_1}^{t_2} \eta(t)\, dt\,,$$

$$\eta(t) \equiv \frac{B(t)}{G(t)} = \frac{\Psi(t)}{G(t)}$$

and

$$W_i(t) \equiv \int_{M_l}^{M_u} \Psi(t-\tau_M)\Phi(M) R_{Mi}(t-\tau_M)\, dM + \left[\frac{d}{dt} G_i(t)\right]_{inf} \qquad (25)$$

We perform the integration over a timestep $\Delta t = t^{n+1} - t^n$ by approximating η and W_i over the whole timestep with a constant value (the one estimated at time $t^{n+\frac{1}{2}} = t^n + \frac{1}{2}\Delta t$):

$$G_i(t^{n+1}) = G_i(t^n) e^{-\eta \Delta t} + \frac{W_i}{\eta}\left[1 - e^{-\eta \Delta t}\right] \qquad (26)$$

Since η and W_i are not strictly constant over Δt, an iteration is required to provide with convergency. As suggested by Talbot & Arnett (1971), we choose to iterate only with respect to η, because W_i is an integrated quantity involving all past value of $G(t)$ and is not so sensitive to the

Table 14. Stellar lifetimes in years for stars from 0.6 to 120 $M_{\odot}$, for different metallicities

M	Z=0.0004	Z=0.004	Z=0.008	Z=0.02	Z=0.05
0.6	4.28E+10	5.35E+10	6.47E+10	7.92E+10	7.18E+10
0.7	2.37E+10	2.95E+10	3.54E+10	4.45E+10	4.00E+10
0.8	1.41E+10	1.73E+10	2.09E+10	2.61E+10	2.33E+10
0.9	8.97E+09	1.09E+10	1.30E+10	1.59E+10	1.42E+10
1.0	6.03E+09	7.13E+09	8.46E+09	1.03E+10	8.88E+09
1.1	4.23E+09	4.93E+09	5.72E+09	6.89E+09	5.95E+09
1.2	3.08E+09	3.52E+09	4.12E+09	4.73E+09	4.39E+09
1.3	2.34E+09	2.64E+09	2.92E+09	3.59E+09	3.37E+09
1.4	1.92E+09	2.39E+09	2.36E+09	2.87E+09	3.10E+09
1.5	1.66E+09	1.95E+09	2.18E+09	2.64E+09	2.51E+09
1.6	1.39E+09	1.63E+09	1.82E+09	2.18E+09	2.06E+09
1.7	1.18E+09	1.28E+09	1.58E+09	1.84E+09	1.76E+09
1.8	1.11E+09	1.25E+09	1.41E+09	1.59E+09	1.51E+09
1.9	9.66E+08	1.23E+09	1.25E+09	1.38E+09	1.34E+09
2.0	8.33E+08	1.08E+09	1.23E+09	1.21E+09	1.24E+09
2.5	4.64E+08	5.98E+08	6.86E+08	7.64E+08	6.58E+08
3	3.03E+08	3.67E+08	4.12E+08	4.56E+08	3.81E+08
4	1.61E+08	1.82E+08	1.93E+08	2.03E+08	1.64E+08
5	1.01E+08	1.11E+08	1.15E+08	1.15E+08	8.91E+07
6	7.15E+07	7.62E+07	7.71E+07	7.45E+07	5.67E+07
7	5.33E+07	5.61E+07	5.59E+07	5.31E+07	3.97E+07
9	3.42E+07	3.51E+07	3.44E+07	3.17E+07	2.33E+07
12	2.13E+07	2.14E+07	2.10E+07	1.89E+07	1.39E+07
15	1.54E+07	1.52E+07	1.49E+07	1.33E+07	9.95E+06
20	1.06E+07	1.05E+07	1.01E+07	9.15E+06	6.99E+06
30	6.90E+06	6.85E+06	6.65E+06	6.13E+06	5.15E+06
40	5.45E+06	5.44E+06	5.30E+06	5.12E+06	4.34E+06
60	4.20E+06	4.19E+06	4.15E+06	4.12E+06	3.62E+06
100	3.32E+06	3.38E+06	3.44E+06	3.39E+06	3.11E+06
120	3.11E+06	3.23E+06	3.32E+06	3.23E+06	3.11E+06

exact value of $G(t^{n+1})$, and also because the resolving expression depends exponentially on η, while only linearly on W_i. If $G_i^{(k)}$ is the estimate of $G_i(t^{n+1})$ at the kth iteration, we proceed through successive corrections:

$$G_i^{(k+1)} = G_i^{(k)} \left[1 + \delta_i^{(k+1)}\right] \tag{27}$$

where

$$\delta_i^{(k+1)} = \frac{G_i^{(k)} - A_i}{\beta_i - G_i^{(k)}} \tag{28}$$

$$A_i = e^{-\eta\Delta t}\left[G_i(t^n) - \frac{W_i}{\eta}\right] + \frac{W_i}{\eta} \tag{29}$$

$$\beta_i = \frac{1}{2}\frac{\partial \ln \eta}{\partial \ln G} \times$$

$$\times \left[\left(e^{-\eta\Delta t} - 1\right)\frac{W_i}{\eta} - \eta\Delta t e^{-\eta\Delta t}\left(G_i(t^n) - \frac{W_i}{\eta}\right)\right] \tag{30}$$

and η, W_i are estimated at $t^{n+\frac{1}{2}}$. $G_i^{(k)}$ is updated until the correction $\delta_i^{(k+1)}$ is smaller than a chosen limit δ_{max}.

The timestep Δt of the model is chosen to be the minimum value between: (1) a timestep Δt_1 which guarantees that the relative variation of the $G_i(t)$'s is lower than a fixed ϵ; (2) a timestep Δt_2 which guarantees that the surface mass density $\sigma(t)$ increases no more than 5%; (3) a timestep Δt_3 which is twice the previous timestep of the model, in order to speed up the calculation when possible. In this way, the infall term in the W_i's can be assumed to be constant within Δt, and the formulation by Talbot & Arnett (1971), suited to close models, can be applied also to open models.

As for the initial conditions, we assume $\sigma(0)$ to be very small, although non–zero to avoid mathematical infinities for t=0. At the beginning the disk is formed by gas only, while star formation is not active yet: $\sigma_g(0) = \sigma(0)$. With the adopted normalization, this translates in $G(0) = G_i(0) = G_s(0) \simeq 0$.

The W_i's are calculated by integrating with respect to time, rather than with respect to mass; Eq. (25) is rewritten as:

$$W_i(t) = \int_0^{t-\tau_{M_u}} \Psi(t')\left[\Phi(M) R_{Mi}(t')\left(-\frac{dM}{d\tau_M}\right)\right]_{M(t-t')} dt' +$$

$$+ \left[\frac{d}{dt}G_i(t)\right]_{inf} \tag{31}$$

where $M(\tau)$ is the mass of a star of lifetime τ. We need to integrate with respect to time when introducing the dependence of metallicity, since all quantities then depend on $Z(t)$ as well as on M: the integral on the right hand is to be calculated on the path of the (M, t) plane fixed by the relation between mass and lifetime, or better by the $M(\tau, Z(t-\tau))$ vs. τ relation, where $Z(t)$ is built by the on–going model itself. Also the "restitution fractions" R_{Mi} depend on $Z(t)$ (§ 8.4); therefore, all the stored values

of $G_i(t^n)$, $X_i(t^n)$ and $Z(t^n)$ of all the timesteps t^n of the model enter the evaluation of $\Psi(t')$, $R_{Mi}(t')$ and $dM/d\tau_M$ for each t' in the integral.

Operatively, the integration is turned to a summation over a series of time intervals $[t^{(k-1)}, t^{(k)}]$, with $t^{(0)} = 0$ e $t^{(k_{max})} = t$ (the current age of the model). Within each time interval, the integrand is assumed to be constant and is estimated at the middle point $(t^{(k-1)}+t^{(k)})/2$. The time intervals $[t^{(k-1)}, t^{(k)}]$ are fixed as follows. The whole mass range $[M_l, M_u]$ is divided in 200 intervals $[M^{(p)}, M^{(p+1)}]$, where the $M^{(p)}$ are equidistant in logarithmic scale. At any age t of the model, we calculate the corresponding birthtimes $t^{(p)} = t - \tau_{M^{(p)}}$. The $t^{(k)}$'s defining the grid for the integration are given by the $t^{(p)}$, implemented with the previous timesteps t^n of the model.

8.7. Inserting Type Ia supernovæ

Up to now we have discussed the ejecta of single stars of different mass ranges, but in a chemical model we also need to include Type Ia supernovæ (SNæ Ia), that originate in close binary systems and contribute an important fraction of heavy elements, especially iron. We need to introduce SNæ Ia especially to explain the observed evolution of abundance ratios of α–elements with respect to iron (Sneden et al. 1979; Matteucci & Greggio 1986).

Prescriptions for the rate of SNæ Ia and for the composition of their ejecta are needed. We adopt the rate suggested by Greggio & Renzini (1983), which assumes the scenario of Whelan & Iben (1973): SNæ Ia, are due to the explosion of a CO white dwarf that reaches the Chandrasekhar limit by accreting material from a giant companion filling its Roche lobe. An upper limit to the mass of the primary is fixed by the requirement that it builds a degenerate CO–core before filling its Roche lobe, so that it doesn't explode as a SN II. For models with convective overshooting, this translates in

$$M_1 \leq 6M_\odot$$

where M_1 is the mass of the primary ($M_1 > M_2$); therefore, the upper limit for the total mass $M_B = M_1 + M_2$ of a binary system able to produce a SN Ia is:

$$M_{B,u} = 12M_\odot$$

Since the primary needs to accrete enough mass to reach the Chandrasekhar mass, a minimum total mass for the system is also introduced, generally $M_{B,l} \sim 3\ M_\odot$. The distribution function of the fractionary mass of the secondary $\mu = M_2/M_B$, $\mu \leq 1/2$ is (Greggio & Renzini 1983):

$$F(\mu) = 24\mu^2$$

which is normalized between 0 and 0.5 and favours systems whose components have similar masses ($M_1 \sim M_2$, Tutukov & Yungelson 1980).

As the star formation rate for single stars of mass M is $\Psi(t)\Phi(M)$, we assume that the SFR for binary system precursors of SNæ Ia is $A\,\Psi(t)\Phi(M)$. This means that a fraction A of stars between $M_{B,l}$ and $M_{B,u}$ is assumed to form binaries (with such characteristics that a SN Ia is eventually produced), rather than single stars. A is a parameter to be fixed so to match the observed rate of SNæ Ia.

In this scenario, the typical timescale for the explosion of a SN Ia is fixed by the lifetime τ_{M_2} of the secondary. The explosion rate (by number) of SNæ Ia is expressed as (Greggio & Renzini 1983):

$$R_{SNI}(t) =$$

$$A \int_{M_{B,l}}^{M_{B,u}} \frac{\Phi(M_B)}{M_B} \left[\int_{\mu_m}^{0.5} F(\mu)\Psi(t-\tau_{M_2})d\mu \right] dM_B \quad (32)$$

where μ_m is the minimum mass fraction contributing to the rate of SNæ Ia at time t:

$$\mu_m = \max\left\{ \frac{M_2(t)}{M_B},\ \frac{M_B - 0.5M_{B,u}}{M_B} \right\}$$

For Type Ia SNæ we adopt the ejecta E_{SNI} of the W7 model of Nomoto et al. (1984), in the updated version by Thielemann et al. (1993). Due to the homogeneity of SNæ Ia, we can safely assume that the same set of ejecta holds for all of these objects.

To include the contribution of SNæ Ia, we need to change the formulation of the W_i's. Following Matteucci & Greggio (1986) with some slight changes, in the range $M_{B,l}$—$M_{B,u}$ we distinguish the contribution of single stars — a fraction $(1 - A)$ of the whole — from that of binaries originating SNæ Ia — a fraction A of the whole. In the case of the binaries, we assume that their ejecta are released in two steps: after a time τ_{M_1} the primary expels its products behaving just like a single star (i.e. according to the Q_{ij} matrix suited to its mass and metallicity), while after a time τ_{M_2} the secondary pours mass on the companion originating the SN explosion. Therefore, introducing the notation:

$$\Psi\Phi R_i(M,t) = \Psi(t-\tau_M)\Phi(M)R_{Mi}(t-\tau_M)$$

we can write:

$$W_i(t) = \int_{M_l}^{M_{B,l}} \Psi\Phi R_i(M,t)\,dM +$$

$$+ (1-A) \int_{M_{B,l}}^{M_{B,u}} \Psi\Phi R_i(M,t)\,dM +$$

$$+ \int_{M_{B,u}}^{M_u} \Psi\Phi R_i(M,t)\,dM +$$

$$+ A \int_{M_{B,l}}^{M_{B,u}} \frac{\Phi(M_B)}{M_B} \left[I_1(t,M_B) + I_2(t,M_B) \right] dM_B +$$

$$+\left[\frac{d}{dt}G_i(t)\right]_{inf} \quad (33)$$

indicating with:

$$I_1(t,M_B)=\int_0^{0.5} F(\mu)\Psi(t-\tau_{M_1})R_{M_1i}(t-\tau_{M_1})M_1 d\mu$$

$$M_1=(1-\mu)M_B$$

$$I_2(t,M_B)=\int_{\mu_m}^{0.5} F(\mu)\,\Psi(t-\tau_{M_2})\,E_{SNIi}\,d\mu,$$

$$M_2=\mu M_B\ .$$

In Eq. (33), the first three terms on the right hand side represent the contribution of single stars, the fourth term represents that of binaries becoming SNæ Ia and the fifth term is the contribution of infall. Since the ejecta E_{SNIi} of SNæ Ia are assumed to be independent of M_B or μ, the term describing binaries can also be written as:

$$A\int_{M_{B,l}}^{M_{B,u}}\frac{\Phi(M_B)}{M_B}\,I_1(t,M_B)\,dM_B\ +\ R_{SNI}(t)E_{SNIi}$$

This formulation better shows how the primary star is assumed to evolve like a single star, unaffected by its companion as far as nucleosynthesis is concerned and releasing all its ejecta away from the system, while the secondary pours all its ejecta to produce the SN Ia, without any direct contribution to the enrichment of the ISM.

The term expressing the ejecta of the primary stars can also be integrated with respect to the mass of the primary M_1, if we write it as:

$$A\int_{M_{1,min}}^{M_{1,max}}\Psi(t-\tau_{M_1})\,R_{M_1i}(t-\tau(M_1)\,\mathcal{F}(M_1)\,dM_1$$

where:

$$M_{1,min}=\frac{M_{B,l}}{2}\qquad M_{1,max}=M_{B,u}$$

$$\mathcal{F}(M_1)=\int_{\nu_{min}}^{\nu_{max}} f(\nu)\ \Phi\left(\frac{M_1}{\nu}\right)\,d\nu$$

$$\nu=\frac{M_1}{M_B}=1-\mu\qquad f(\nu)=24(1-\nu)^2,\quad \nu\in[0.5,1]$$

$$\nu_{min}=\max\left\{0.5,\frac{M_1}{M_{B,u}}\right\}\qquad \nu_{max}=\min\left\{1,\frac{M_1}{M_{B,l}}\right\}$$

Integrating the W_i's with respect to time and introducing the notation:

$$\Phi R_i dM(t,t')=\left[\Phi(M)R_{Mi}(t')\left(-\frac{dM}{d\tau_M}\right)\right]_{M(t-t')}$$

$$\mathcal{F}R_i dM_1(t,t')=\left[\mathcal{F}(M_1)R_{M_1i}(t')\left(-\frac{dM_1}{d\tau_{M_1}}\right)\right]_{M_1(t-t')}$$

when we insert SNæ Ia Eq. (31) becomes:

$$\begin{aligned}W_i(t)\ =\ &\int_0^{t-\tau_{M_{B,l}}}\Psi(t')\,\Phi R_i dM(t,t')\,dt'\ +\\ &+(1-A)\int_{t-\tau_{M_{B,l}}}^{t-\tau_{M_{B,u}}}\Psi(t')\,\Phi R_i dM(t,t')\,dt'\ +\\ &+\int_{t-\tau_{M_{B,u}}}^{t-\tau_{M_u}}\Psi(t')\,\Phi R_i dM(t,t')\,dt'\ +\\ &+A\int_{t-\tau_{M_{1,min}}}^{t-\tau_{M_{1,max}}}\Psi(t')\,\mathcal{F}R_i(t')dM_1(t,t')\,dt'\ +\\ &+R_{SNI}E_{SNIi}\ +\\ &+\left[\frac{d}{dt}G_i(t)\right]_{inf}\end{aligned} \quad (34)$$

The integration is performed as described in § 8.6. Again, here we need to integrate with respect to time rather than with respect to mass if we want to include the implicit dependence on the metallicity $Z(t)$.

9. Chemical evolution in the Solar Neighbourhood

As a first application of our model, we analyze the chemical evolution in the Solar Neighbourhood. Standard observational counterparts for chemical models, such as (1) the current gas fraction, (2) the rate of Type I and Type II SNæ (3) the age–metallicity relation, (4) the past and current estimated SFR, (5) the distribution of long–lived stars in metallicity (G–dwarf problem), are used to calibrate the free parameters of the model. The abundance ratios of different elements observed in the atmospheres of nearby stars are used as a test for our nucleosynthesis prescriptions, since model predictions for most abundance ratios depend mainly on the adopted yields and IMF, and only slightly on other model parameters.
Here we list the parameters of the model:

ν	star formation efficiency
κ	exponent of the star formation law
μ	exponent of the IMF
M_u	higher limit for the IMF
ζ	mass fraction of the IMF in stars with $M \geq 1\ M_\odot$
τ	infall timescale
t_G	age of the system
A	"amplitude" factor for SNæ Ia
$r_\odot$	galactocentric radius of the Sun
$\sigma(r_\odot)$	surface mass density in the Solar Neighbourhood

Some of these parameters are directly fixed by observational determinations. We adopt $r_\odot \sim 8$ kpc, as indicated by recent estimates of the galactocentric distance of the Sun (Reid 1993; Paczynski & Stanek 1997). From a collection of independent measurements of the local surface

mass density of the disc Sackett (1997) derives a fiducial estimate of 53±13 $M_\odot$/pc^2; in this paper we therefore assume $\sigma(r_\odot)$=50 $M_\odot$/pc^2.

For the local IMF, we assume a Salpeter (1955) slope μ=1.35 for M <2 $M_\odot$ and, following Scalo (1986), μ=1.7 for M >2 $M_\odot$. Actually, the assumed slope below 1 $M_\odot$ is relatively unimportant for our models, since these stars give little contribution to the chemical enrichment and only act as a sink of matter from the gaseous phase. What actually matters in the model is the fraction of mass that each stellar generation stores in such low-mass, long lived stars, which is formulated in term of a free parameter as (1-ζ).

We further assume the infalling material to be protogalactic gas with primordial chemical composition: 76% ^{1}H and 24% ^{4}He (Walker et al. 1991); the abundance of all heavier elements is assumed to be zero in the infalling gas (in practice, we assume a negligible abundance of 10^{-11} to avoid mathematical infinities at the beginning of the model).

On the other hand, ν, κ, τ, ζ and A are treated as free parameters to be calibrated in order to match the observational constraints. In the following we discuss the space of model parameter with respect to the available empirical constraints.

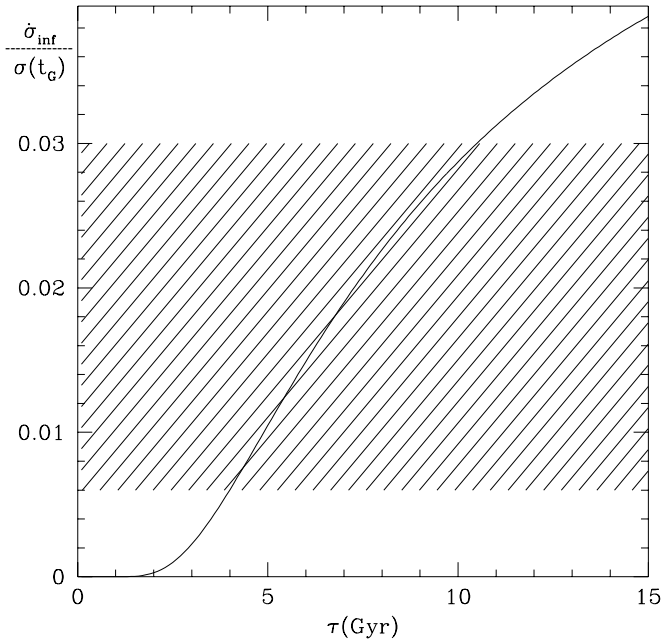

Fig. 10. Current normalized infall rate vs. infall timescale, as predicted by model equations (see text). The shaded area traces the observational estimates.

9.1. The current infall rate

In principle, an observational estimate of the current infall rate on the galactic disc could fix the infall timescale τ, since combining Eqs. (8) and Eq. (10) we get

$$\frac{\dot{\sigma_{inf}}}{\sigma}(t_G) = \left[\tau\left(e^{\frac{t_G}{\tau}} - 1\right)\right]^{-1} \quad (35)$$

independently of other model parameters.

Unluckily, current data cannot provide tight constraints in practice. Observational evidence of infall comes from High Velocity Clouds (Oort 1970) and Very High Velocity Clouds, infalling on the disk at a rate of ∼0.2 and 1.0 $M_\odot$/yr, respectively (Tosi 1988 and references therein). While there is general agreement on the primordial nature of VHVCs, the metal content displayed by some HVCs suggests a Galactic origin for at least a part of them (Schwarz et al. 1995). So, we can take the numbers above as the uncertainty range for the current global infall rate on the galactic disc. Assuming that such infall is uniform over the disc and that the radius of the disc is ∼15 kpc, we get a local infall rate of 0.3–1.5 $M_\odot$/pc^2/Gyr, or $\dot{\sigma}_{inf}/\sigma(r_\odot, t_G) \sim 6\,10^{-3} - 3\,10^{-2}$ in the Solar Neighbourhood, taking $\sigma(r_\odot)$=50 $M_\odot$/pc^2. As displayed in Fig. 10, any $\tau \geq 4$ (or even less since our estimate is rather crude) is basically allowed within the uncertainties, and τ is not properly constrained.

Better hints about the infall timescale come from the metallicity distribution of local long-lived stars: recent data indicate infall timescales longer that ∼5 Gyrs (see § 9.6). Therefore, we start our investigation of the parameter space by selecting the range $\tau = 5 \div 9$ Gyr.

9.2. The current gas fraction

The current gas fraction predicted by our models is to be compared to observational estimates. From a compilation of data on the HI and H_2 distribution, Rana (1991) quotes as the current surface gas density in the Solar Neighbourhood $\sigma_g(r_\odot)$ ∼5.7–7 $M_\odot$/pc^2, which implies a gas fraction ∼0.1–0.15 of the total surface mass density (∼50 $M_\odot$/pc^2).

The gas fraction $G(t_G)$ predicted by our models at the present age t_G=15 Gyr turns out to depend mainly on the parameters κ and ν of the star formation law, while being only slightly dependent on other model parameters. Since κ is limited to the range 1÷2 (see § 8.2), we considered the extreme cases κ =1, κ =2 and the intermediate case κ =1.5. To fulfill the constraint set by the current gas fraction, ν needs to fall within a suitable range of values, which increase with κ. For a given κ, the "good" values of ν slightly increase with the infall timescale τ and with the mass fraction ζ of short-lived stars. Here below we list our detailed results on the suitable ranges for ν as a function of κ, τ and ζ. As an example, Fig. 11 shows the evolution of the gas fraction in time for our Model B (κ =1.5, ζ =0.3, τ =9, ν =1.2, see § 9.6).

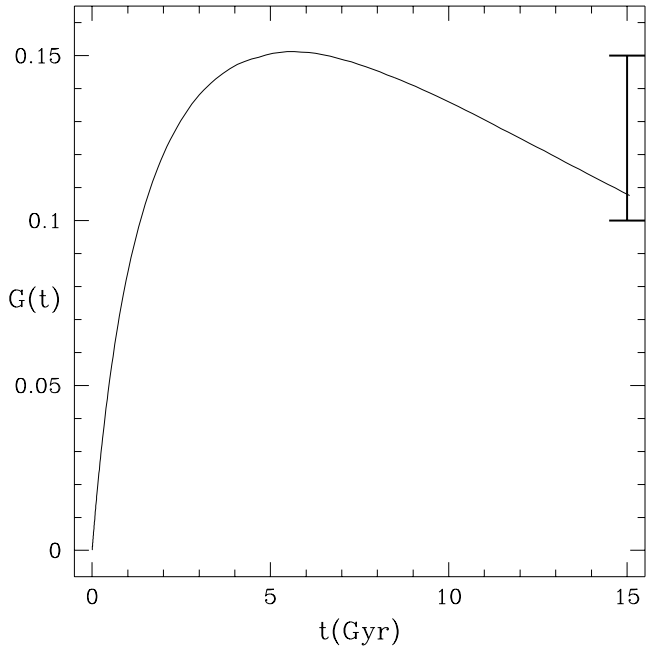

Fig. 11. Evolution of the normalized gas fraction G(t) for our model B. The vertical bar at t =15 Gyrs shows the observational constraint on the current gas fraction

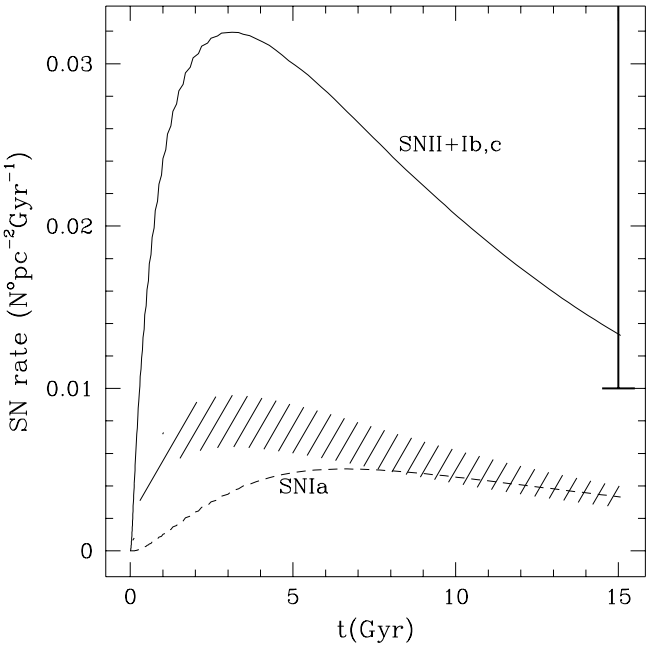

Fig. 12. Evolution of the SN II+Ib,c (solid line) and SN Ia rate (dashed line) for our model B, in SNæ/pc^2/Gyr. The vertical bar at t =15 Gyr shows the observational constraints on the local rate of SNæ II+Ib,c. The shaded area traces a factor 0.2÷0.3 of the rate of SNæ II+Ib,c in time. The observational constraints on the relative rate of SNæ Ia require that at the present age t_G=15 Gyrs the dashed line falls within the shaded area.

		τ =5	τ =7	τ =9
κ=2.0	ζ=0.2	1.2–2.5	1.5–3	2–4
	ζ=0.3	1.2–2.5	1.5–3.5	2–4
	ζ=0.4	1.5–3	2–4	2–4.5
	ζ=0.5	1.5–3	2–4	2–5
κ=1.5	ζ=0.2	0.5–0.8	0.6–1	0.7–1.2
	ζ=0.3	0.6–1	0.7–1.2	0.7–1.3
	ζ=0.4	0.6–1	0.7–1.2	0.8–1.5
	ζ=0.5	0.7–1.2	1–1.5	1–1.7
κ=1.0	ζ=0.2	0.25–0.3	0.35–0.4	0.3–0.4
	ζ=0.3	0.28–0.35	0.35–0.4	0.35–0.5
	ζ=0.4	0.3–0.4	0.4–0.5	0.4–0.5
	ζ=0.5	0.35–0.45	0.4–0.5	0.45–0.6

9.3. The supernova rates

The most recent empirical estimates of the Galactic SN rate give 14±6 (Cappellaro et al. 1997) and 21±5 (Tamman et al. 1994) SN events originating by massive stars — namely, Type II + Type Ib,c SNæ — per 1000 yrs. Taking a disc radius of ∼15 kpc, this roughly translates into (2±1)10^{-2} and (3±1)10^{-2} SNæ/pc^2/Gyr. We therefore adopt (1÷4)10^{-2} SNæ/pc^2/Gyr as the observational constraint to compare with the rate of SNæ II predicted by our models.

As far as SNæ Ia are concerned, Cappellaro et al. (1997) give a Galactic rate of 2±1 SN Ia per millennium, which leads to a ratio of 0.3±0.2 of Type Ia versus Type II+Ib,c SNæ. Tamman et al. (1994) estimate that ∼85% of the SNæ exploding in a galaxy like our own come from massive stars, which gives a value of ∼0.2 for the above mentioned ratio. We therefore require the number of SNæ Ia to be a factor 0.2÷0.3 of the number of SNæ originated by massive stars. In our models, once $M_{B,l}$ is fixed (see § 8.7) the efficiency with which binaries produce to SNæ Ia is driven by the parameter A. For $M_{B,l}$=3 $M_\odot$, A is constrained to be in the range

$$A = 0.05 \div 0.08$$

independently of other model parameters. Choosing $M_{B,l}$=2 $M_\odot$, A would be constrained in the range 0.03÷0.05, but this alternative choice of the ($M_{B,l}$,A) has little effect on any practical outcome of other model predictions. Therefore, in the following we will limit our discussion to models with $M_{B,l}$=3 $M_\odot$, A=0.05÷0.08.

As an example, Fig. 12 shows the evolution of the local rate of SNæ II+Ib,c and SNæ Ia (solid and dashed line, respectively) as predicted by our Model B (A =0.07), together with the relevant observational constraints. The observed present relative rate of SNæ Ia is reproduced if, at the present age t_G=15 Gyrs, the dashed line falls within the shaded area, which represents a factor 0.2÷0.3 of the SN II rate. We notice that this constraint does not sensitively depend on the assumed age of the disc, since the

requirement remains actually fulfilled over a long period (from 8 to 15 Gyrs).

9.4. The age–metallicity relation

The age–metallicity relation (AMR) for stars in the Solar Neighbourhood was first plotted by Twarog (1980). The data showed a large dispersion, therefore age–bins and the average metallicity per bin were used to trace the local AMR, which turned out to increase rapidly from 13 to 5 Gyrs ago, and more slowly afterwards. Part of Twarog's data were re-examined by Carlberg et al. (1985), who did not include in their sample about fifty of the lowest metallicity stars and therefore obtained a shallower slope for the AMR in the early phases, suggesting that the disc evolution started with a high initial metallicity. The bulk of Twarog's data was later analysed again by Meusinger et al. (1991), and their AMR confirmed the original result of a steep slope at old ages.

A more recent study about the local AMR, based on a new sample of 189 nearby F and G dwarfs, was performed by Edvardsson et al. (1993) using high resolution spectra with theoretical LTE atmospheres to derive the chemical compositions, and photometric fits with Vandenberg (1985) isochrones to derive ages. The resulting binned, average AMR is in good agreement with that by Meusinger et al. (Fig. 13), but the dispersion of the data about the average is so large that the AMR is not a tight constraint for chemical models. Ng & Bertelli (1997) have lately re-examined the Edvardsson et al. dataset, by means of modern isochrones including new opacity tables, of new distances from the Hipparcos dataset and giving a higher weight to stars with most reliable age determination. The resulting AMR shows a slope of ∼0.07 dex/Gyr, in agreement with Edvardsson et al., but still with a large scatter.

Additional information on the AMR comes from open clusters, whose age estimates are much more reliable than those for isolated field stars, but with the counterargument of the uncertainty on the correction for the radial metallicity gradient and the different galactocentric distance of clusters. See Carraro et al. (1997) for a more comprehensive discussion of the disc AMR.

To reproduce the large scatter in the local AMR, more complex models would be required, including various possible mechanisms responsible for the scatter (orbital diffusion, non-instantaneous mixing of enriched material, self-propagation of star formation, local infall episodes and so forth). Our model applies the standard "one-zone" scheme, therefore it is aimed at reproducing average features and can only be compared to the average trend of the AMR, regardless of the scatter.

The comparison with the observed binned AMR allows us to single out a limited range of values for the parameter ζ. Even including the highest possible contribution on iron enrichment from SNæ Ia (A=0.08), models with ζ <0.3 still predict too low metallicities for all the suitable

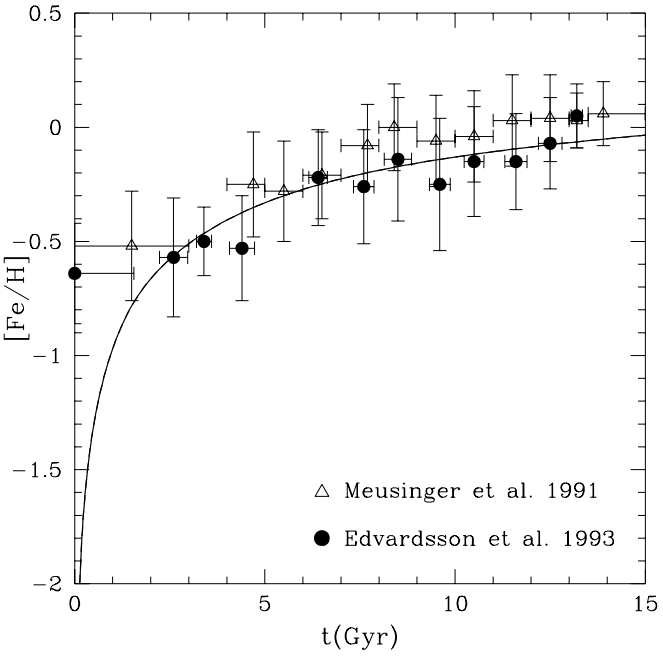

Fig. 13. Observational data on the local age-metallicity relation shown together with the predictions of our Model B.

combinations of κ, ν and τ, and are therefore ruled out. At the other end, models with ζ =0.5 are compatible with the observed AMR only if combined with the lowest allowed relative rate of SNæ Ia (A=0.05); larger values for ζ are hence ruled out, since such models would predict too high metallicities. Therefore, from now on we will only consider models with

$$\zeta = 0.3 \div 0.5$$

9.5. The Star Formation Rate

The present SFR in the Solar Neighbourhood is estimated to be ∼2–10 $M_\odot$/pc^2/Gyr (Güsten & Mezger 1982). Besides, Scalo (1986) estimates that the present SFR is within a factor 0.5÷1.5 of the average SFR in the past over the whole lifetime of the disk:

$$\frac{\Psi(t_G)}{\frac{1}{t_G}\int_0^{t_G}\Psi(t)dt} = 0.5 \div 1.5$$

By imposing these two observational constraints on the predicted SF history, we can rule out some models and further restrict the range of "good" combinations of the parameters κ, ν, τ and ζ. Notably, if we assume τ=5 Gyr, models with κ=2 or 1.5 are unable to fulfill the above requirements on the SFR.
Thus we further filtered the ranges of values for ν listed here below:

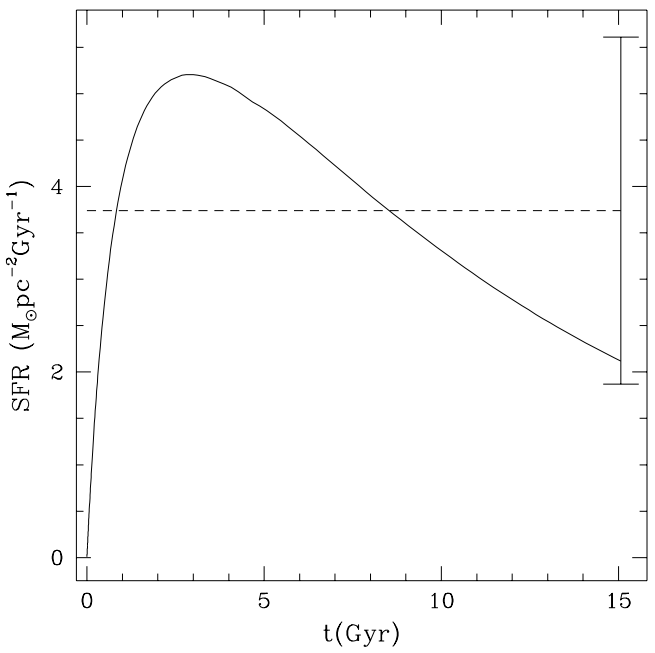

Fig. 14. Evolution of the SFR for our model B. The dashed horizontal line shows the average SFR over the lifetime of the disc, and the vertical bar at t =15 Gyrs shows the range 0.5÷1.5 times the average SFR. Observational constraint (see taxt) require that the current SFR at $t = t_G$ falls within the range indicated by the bar, as well as within the observational estimates of 2–10 $M_\odot$ pc^{-2}/Gyr^{-1}

		τ =5	τ =7	τ =9
κ=2.0	ζ=0.3	—	—	2–4
	ζ=0.4	—	∼2	2–4.5
	ζ=0.5	—	2–3	2–5
κ=1.5	ζ=0.3	—	∼0.7	0.8–1.3
	ζ=0.4	—	0.7–1.2	0.8–1.5
	ζ=0.5	∼0.7	1–1.5	1–1.7
κ=1.0	ζ=0.3	∼0.28	0.35–0.4	0.35–0.5
	ζ=0.4	∼0.3	0.4–0.5	0.4–0.5
	ζ=0.5	0.35–0.45	0.4–0.5	0.45–0.6

As an example, Fig. 14 shows the evolution of the SFR in time for our Model B, with the related observational constraints.

9.6. The G-dwarf distribution

The G-dwarf problem, i.e. the paucity of metal–poor stars in the Solar Vicinity with respect to the predictions of the "simple closed–box model", is usually interpreted as a consequence of the progressive building-up of the Galaxy through accretion of primordial gas, hence the failure of closed models in this respect (Lynden-Bell 1975; Tinsley 1980). Other solutions have actually been suggested: prompt initial enrichment from the halo or bulge providing a finite initial metallicity in the ISM, higher yields due to an IMF skewed toward massive stars in the early galactic phases, more effective star formation in high-metallicity inhomogeneities of the ISM (see Pagel 1997 for a review); but open models with progressive inflow of primordial material remain the best scheme to explain the G-dwarf problem, as well as being consistent with dynamical simulations of the formation of galactic discs and with the observation of infall of High and Very High Velocity Clouds.

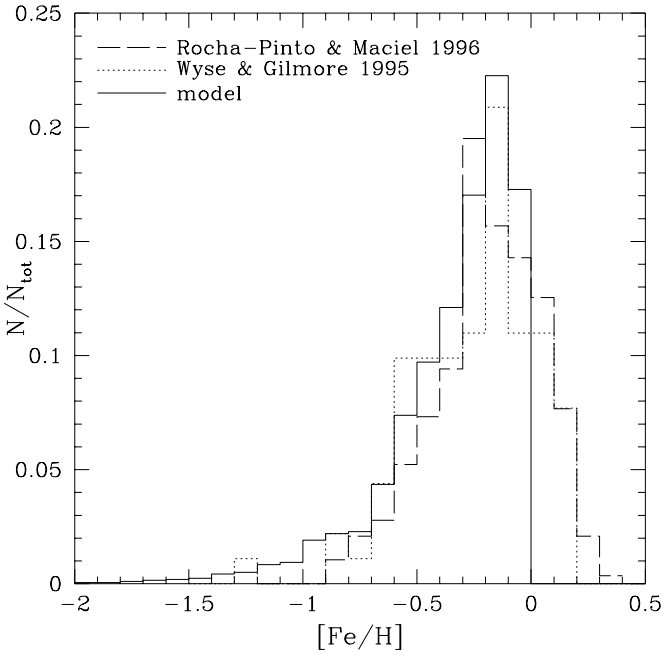

Fig. 15. Observational data on the local metallicity distribution, in relative number, of long-lived stars (dashed and dotted line) shown together with the predictions of our Model B (solid line).

Basing on a complete volume–limited sample of nearby G-dwarfs, Pagel & Patchett (1975) provided a reference dataset (later revised by Pagel 1989 and by Sommer–Larsen 1991), which was was nicely reproduced by chemical models with infall timescales of 3–4 Gyrs (e.g. Matteucci & François, 1989). The latest compilations of G–dwarf metallicities (Wyse & Gilmore 1995; Rocha–Pinto & Maciel 1996) show instead a narrower distribution with a prominent peak around [Fe/H]∼-0.2, and seem therefore to favour longer timescales (e.g. Chiappini et al. 1997 and Fig. 15). This is also consistent with dynamical studies, which indicate that a rather long time is needed to build up a galactic disc (∼6 Gyrs, Burkert et al. 1992), especially when one takes into account that primordial or low-metallicity gas in the early galactic phases has a very low cooling efficiency (Carraro et al. 1997).

In our models, the peak metallicity of the predicted distribution increases with increasing ζ and A. On the other hand, the height of the peak mainly depends on

other parameters: the distribution gets narrower with increasing τ, κ, and ν.

All calculated models with τ=5 Gyrs and τ=6 Gyr (and with the suitable combinations of κ and ν as discussed above) predict metallicity distributions of stars which are too broad with respect to the observed one. Therefore, we can rule out all these models and set the limit

$$\tau \geq 7$$

On the other hand, models with $\tau \geq$10 tend to predict too narrow distributions, therefore form now on we will consider only models with τ =7–9 Gyrs.

If ζ=0.4–0.5, whatever the iron contribution of SNæ Ia (with A=0.05 to 0.08) the predicted G-dwarf distribution remaines peaked around [Fe/H]$\geq$0, not consistent with observations. We rule these models out and set the limit

$$\zeta < 0.4$$

In the following, we discuss models with ζ=0.3 as a representative case. Here below we list, for ζ=0.3, the sets of model parameters which are able to predict a metallicity distribution in agreement with the observed one, as well as being in agreement with all the other constraints.

ζ =0.3	τ =7	κ =1.5	ν ∼0.7	A =0.06–0.07
	τ =8	κ =2	ν =2–3	A =0.07
			ν ∼3	A =0.06
		κ =1.5	ν ∼1.2	A =0.06
			ν ∼0.7	A =0.07
		κ =1.0	ν ∼0.45	A =0.06
	τ =9	κ =2	ν ∼2	A =0.06–0.08
		κ =1.5	ν =0.8–1.3	A =0.07
			ν ∼0.8	A =0.06-0.08
		κ =1.0	ν ∼0.35–0.5	A =0.06

We take as representative of the three cases κ =1, 1.5 and 2 the following models:

model	κ	ζ	τ	ν	A
A	2.0	0.3	9	2.0	0.08
B	1.5	0.3	9	1.2	0.07
C	1.0	0.3	9	0.5	0.06

We chose to use model B in Figures 11 to 15 as the representative model to plot versus the observational constraints. In Fig. 15, the model well reproduces the location and height of the peak, while it cannot reproduce the higher-metallicity tail of the observed distribution. In fact, since our one-zone model cannot reproduce scatter around the average AMR, no stars are predicted to form with a metallicity higher than the average one reached at t_G =15 Gyrs (see also Fig 13).

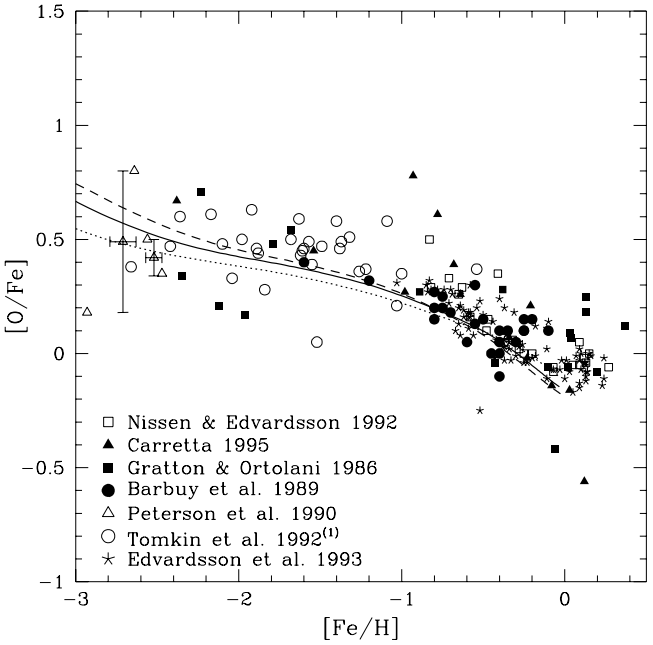

Fig. 16. Observational data on the [O/Fe] ratio vs. [Fe/H] as observed in the atmospheres of nearby stars. Predictions of model A (dotted line), B (solid line) and C (short-dashed line) are shown for comparison. (1)The data from Tomkin et al. (1992) are taken as revised by Carretta (1995)

9.7. Abundance ratios

Figures 16 to 22 display observational data on the abundance ratios of various elements with respect to iron, together with the predictions of our models A, B and C. The data refer to spectroscopic abundances in the atmospheres of nearby stars; detailed data sources are indicated in the legends of the figures.

Predictions for the α-elements (^{16}O, ^{24}Mg, ^{28}Si, ^{32}S, ^{40}Ca) seem in most cases to well reproduce the trend of the data. A remarkable exception is the [Mg/Fe] ratio. Our yields for the SN explosion are derived from those of WW95, and therefore display the same problem of ^{24}Mg underproduction (Timmes et al. 1995). As discussed by Thomas et al. (1997), uncertainties in SN calculations still allow for rather different yields among different authors, especially in the case of ^{24}Mg production. For instance, ^{24}Mg yields by Thielemann et al. (1996) are sensitively higher and better suited at explaining the [Mg/Fe] ratio observed in low–metallicity nearby stars. See, in this respect, the lower panel of Fig. 23, where we compare the ^{24}Mg ejecta from the CO–cores by WW95 with those by Thielemann et al. (1996) (these latter obtained in a similar fashion as for WW95, see App. A. As in Timmes et al. (1995), there is a ^{32}S underproduction which could not be solved by adopting Thielemann et al. 's yields,

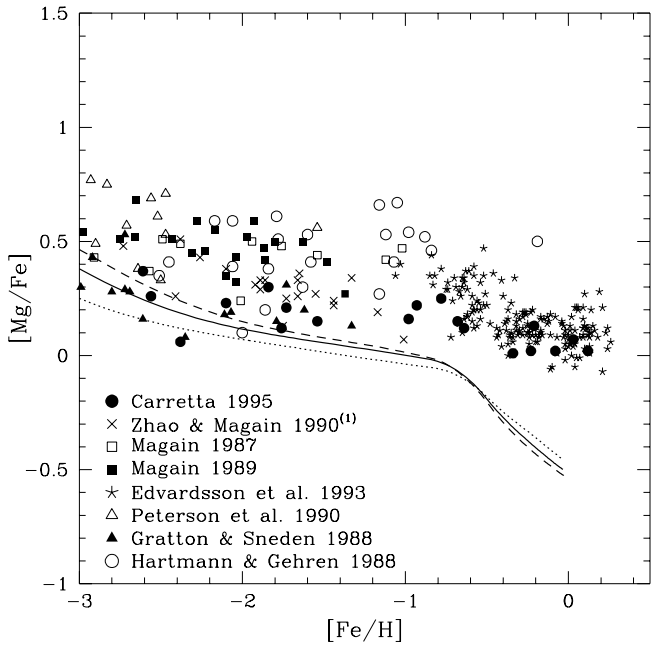

Fig. 17. Observational data on the [Mg/Fe] ratio vs. [Fe/H]. Model predictions are plotted as in Fig. 16. (1)The data from Zhao & Magain (1990) are taken as revised by Carretta (1995)

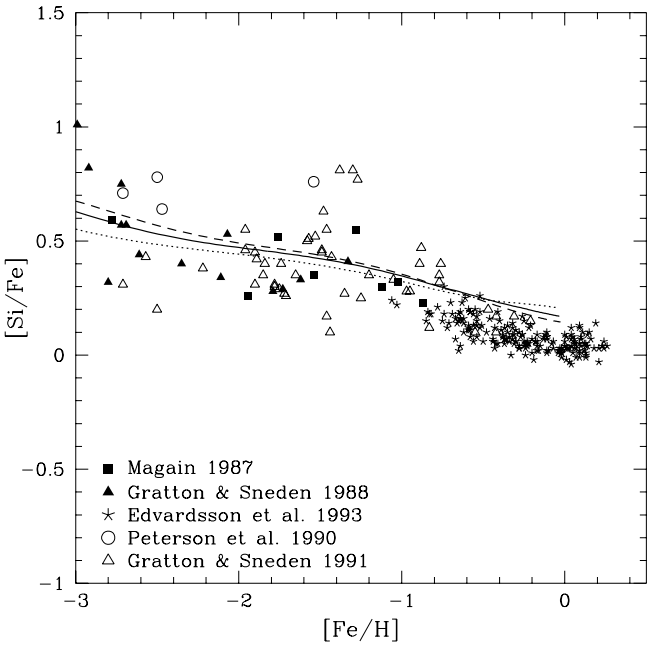

Fig. 18. Observational data on the [Si/Fe] ratio vs. [Fe/H]. Model predictions are plotted as in Fig. 16

which in the case of sulfur are even lower than those by WW95.

Our model predicts an overproduction of carbon with respect to the observational data. The mismatch with the data starts at low metallicities, indicating that the contribution of short-lived, massive stars to C-production is overestimated. Timmes et al. (1995) do not display a similar problem when using directly WW95 SN ejecta. At least two reasons might be tracked for this. (1) Stellar models with overshooting give a lower limiting mass for SN explosion (M_{up} ∼6 $M_{\odot}$ rather than 8 $M_{\odot}$) and therefore C-producing massive stars have a larger global weight in the IMF is taken into account. (2) Our link between mass-losing pre-SN structures and SN models requires some assumptions, especially relevant to the edge of the He-burning region, where carbon is produced; this might make ^{12}C yields particularly uncertain in our grid (see App. B). With respect to the data, our carbon overproduction in massive stars amounts to a factor of ∼2, which is still acceptable when taking into account the uncertainties in SNæ II yields. Again, if for instance we compare the results by WW95 and by Thielemann et al. (1996) for a given M_{CO}, the latter give ^{12}C yields up to a factor of 2 lower (see Fig. 23, upper panel).

Unlike for the α elements, the predicted [N/Fe] ratio at low metallicities depends sensitively on the past SF history. This effect is mainly due to the contribution of primary ^{14}N from intermediate mass stars, which in the range 4–5 $M_{\odot}$undergo envelope CNO–burning during

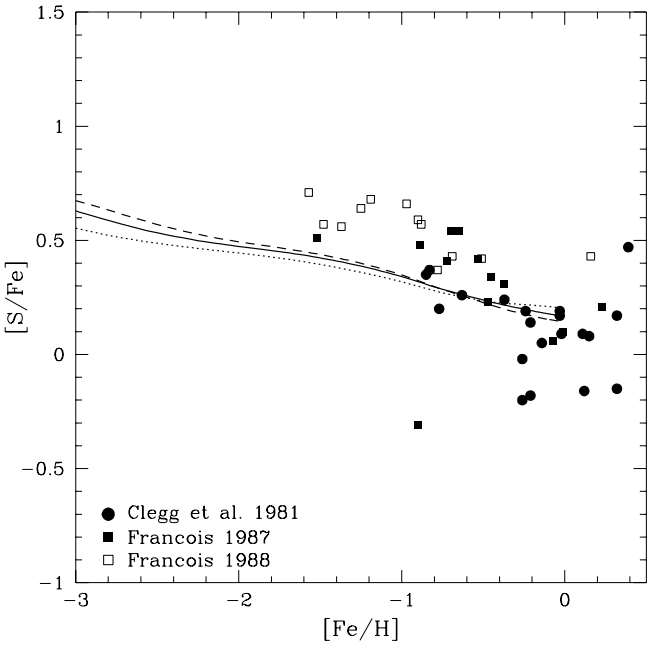

Fig. 19. Observational data on the [S/Fe] ratio vs. [Fe/H]. Model predictions are plotted as in Fig. 16

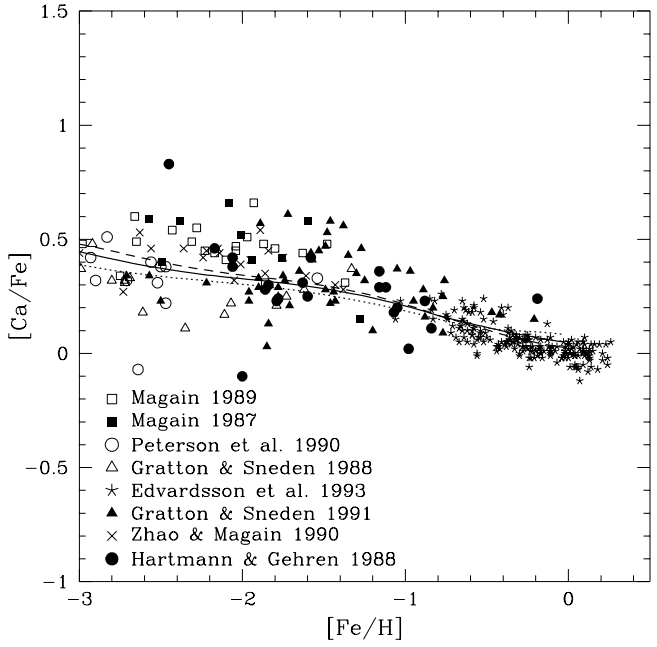

Fig. 20. Observational data on the [Ca/Fe] ratio vs. [Fe/H]. Model predictions are plotted as in Fig. 16

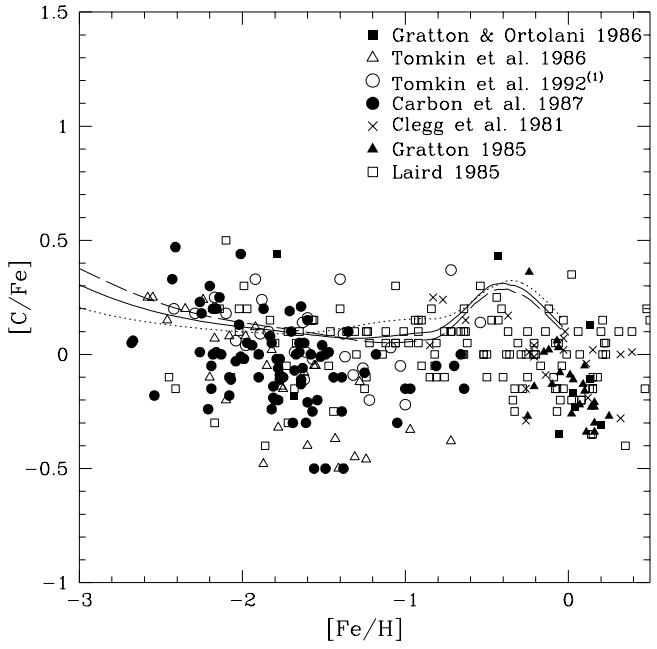

Fig. 21. Observational data on the [C/Fe] ratio vs. [Fe/H]. Model predictions are plotted as in Fig. 16. (1)The data from Tomkin et al. (1992) are taken as revised by Carretta (1995)

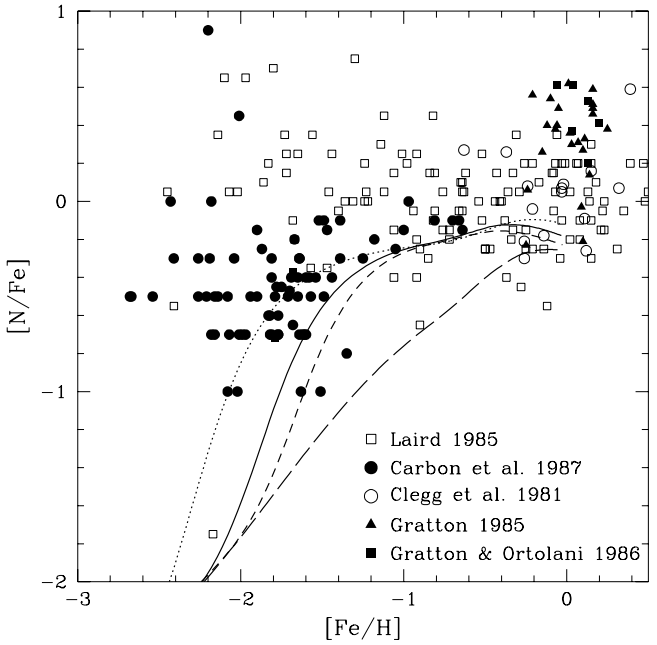

Fig. 22. Observational data on the [N/Fe] ratio vs. [Fe/H]. Model predictions are plotted as in Fig. 16. The long–dashed line shows separately the contribution of the sole secondary component for Model B (see text)

the TP-AGB phase (Marigo et al. 1997). These stars release their contribution of primary ^{14}N on timescales of $\sim 1-2\,10^8$ yrs, independently of the initial metallicity. In Fig. 22 we display the relevant data versus the the predictions of our models A, B, C. As κ decreases (from C to A), the SF gets less efficient in the early phases, and the metallicity [Fe/H] evolves more slowly. Therefore, the [N/Fe] ratio increases more rapidly in the early phases if κ is lower.

Abundance ratios of α elements do not show a similar dependence on the SF efficiency in the early phases, since in the first Gyr or so iron and α elements are produced by the same source (massive stars), and their relative abundance is determined by the adopted yields and IMF for massive stars, irrespectively of the SF history. On the contrary, in the case of ^{14}N the effect is related to the competition between different sources for the two elements: if κ is higher, more gas is recycled through successive generations of massive stars in the first $\sim 10^8$ yrs, and intermediate mass stars contribute to the rise of the [N/Fe] ratio when the metallicity [Fe/H] is already relatively high. In Fig. 22 we also display the contribution of secondary ^{14}N alone (long dashed line); unlikely the primary component, the [N/Fe] ratio due to the bare secondary component is basically independent of the SF history, therefore we just show Model B for the secondary component. Evidently, primary ^{14}N from intermediate mass stars is a major component in the overall ^{14}N production, and must be properly taken

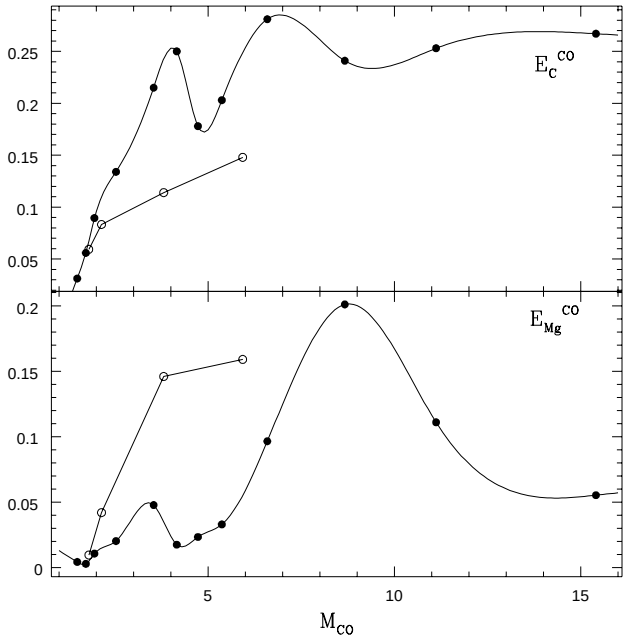

Fig. 23. Ejecta of ^{12}C (upper panel) and ^{24}Mg (lower panel) of the CO–core vs. M_{CO} as deduced from Thielemann et al. 1996 (open circles) compared with those from WW95 (case $Z = Z_{\odot}$, filled circles)

into account. Still, even including this component, models seem to underproduce ^{14}N with respect to ^{56}Fe, especially in the low-metallicity range. A classical suggestion to overcome this mismatch is to assume some primary ^{14}N contribution by massive stars (Matteucci 1986). This might be possible in very low-metallicity massive stars if some peculiar mixing event is allowed to occur (Timmes et al. 1995). Fig. 22 might also suggest, as an alternative, that a slow SF history (κ =1) combined with a more efficient production of primary ^{14}N in intermediate mass stars might solve the problem. A more extreme alternative might be an initial IMF skewed to massive stars, which quickly provide the ISM with a minimum amount of CNO isotopes so that secondary production of ^{14}N becomes effective already at very low metallicities. But this alternative should need to be tested also with respect to the other abundance ratios and the other model constraints.

10. Summary and conclusions

We have presented a detailed study of the ejecta and chemical yields from stars of different mass and initial chemical composition, taking into account modern results of hydrostatic and explosive nucleosynthesis. The analysis is made for stars that avoid the AGB phase. i.e. from 6 $M_{\odot}$up 1000 $M_{\odot}$.

In this range of mass we distinguish three main groups: (i) the 6 to 9 $M_{\odot}$ stars, which are not significantly affected by mass loss by stellar wind and terminate their evolution by the electron capture instability and consequent supernova explosion; (ii) the 9 to 120 $M_{\odot}$ stars, which suffer from mass loss by stellar wind starting from the zero age main sequence and terminate as iron-core collapse or PC supernovæ; and finally (iii) the rather hypothetical range of very massive objects (120 to 1000 $M_{\odot}$), which are characterized by pulsational instability and violent mass loss during the core H-burning phase and may terminate the evolution either as iron-core collapse or "PC" supernovæor black holes, depending on the size of their CO–core

We start from the sets of hydrostatic stellar models by the Padua group that are calculated in presence of mild convective overshoot. This explains why the upper mass limit for the occurrence of the AGB phase is set at about 5 $M_{\odot}$ depending on the initial chemical composition. All these evolutionary sequences are carried out from the ignition of the core H-burning till the start of central C-burning, taking into account mass loss by stellar wind wherever appropriate. These sets of models span a wide range of initial masses and chemical composition and are fully homogeneous as far as the input physics, accuracy and numerical methodology are concerned. So they are the ideal tool to construct equally homogeneous sets of ejecta and stellar yields.

From the models we derive the basic relationships between the initial and final (namely, at the onset of C-burning in the core) mass of the stars, and between the initial mass and the final mass of the helium and carbon–oxygen core. The subsequent evolutionary stages are so short-lived that the above relationships will not change at all. If mass loss occurs by stellar wind during the core H- and He-burning stages, the amounts of mass in the various species lost in the wind are calculated.

Adopting the CO core mass as the driving parameter we link the hydrostatic structure at early core C-burning to the final explosive stage. Using literature data on supernova models, we calculate the amount of mass ejected by each CO core at the time of explosion for each species under consideration, to which the contribution from the overlying layers still existing in the star at this stage, and the contribution from stellar wind in the earlier stages are added.

The results are summarized in a series of tables, and all details relative to construction of the ejecta and yields for massive and very massive stars are given in the main text and Appendices A and B.

The corresponding ejecta and yields for low and intermediate mass stars (those passing though the AGB phase) can be found in Marigo et al. (1996, 1997). They are based on the same stellar models in usage here up to the end of the E-AGB, and are derived from an original semi-analytical method suitably tailored to follow the TP-AGB phase in presence of envelope burning in the most massive stars of this group. So the ejecta and yields for massive and very massive objects presented here together with those

by Marigo et al. (1996, 1997) constitute a dataset of unprecedented homogeneity.

Our results about stellar nucleosynthesis and ejecta have been applied to study the chemical enrichment of the Solar Neighbourhood by means of the infall model of Chiosi (1980), in which the matrix formalism developed by Talbot & Arnett (1973) to calculate the fraction of a star of initial mass M that is ejected in form of chemical species i has been incorporated. This matrix formalism is particularly useful to understand what fraction of a star originally in form of species j is eventually ejected as species i. The numerical method to solve the set of model equations governing the chemical evolution of the ISM is the same as in Talbot & Arnett (1971), however adapted to the infall scheme.

The chemical model contains a number of parameters, some of which are directly fixed by the observations or estimated independently (e.g. the distance of the Sun from the Galactic center, the local surface mass density and the age of the galactic disk). Other parameters are let vary so that some basic observational constraints are met. All our results refer to the Scalo IMF with fixed slope and upper mass limit M_u=100 $M_\odot$.

Constraints of the models are (i) the current gas fraction; (ii) the rate of type I and type II SNæ; (iii) the age metallicity relation; (iv) the past and present estimated star formation rate; (v) the distribution of long-lived stars in metallicity (G-dwarf problem).

Free parameters of the models are: (i) the efficiency and exponent of the SFR (ν and κ, respectively); (ii) the infall time-scale τ; (iii) the mass fraction ζ of the IMF in stars with $M \geq 1\ M_\odot$; (iv) the amplitude factor A and minimum mass of the binary $M_{B,l}$ for Type Ia SNæ.

A careful comparison of model results with the observational constraints allows us to disentangle the effects of different parameters on the model predictions and put successive limits on them. We are finally left with the following "good ranges" for the various parameters: $1 \leq \kappa \leq 2$, $0.3 \leq \nu \leq 3$ (in suitable combination with κ), $0.3 \leq \zeta \leq 0.4$, $7 \leq \tau \leq 9$ Gyrs, $0.05 \leq A \leq 0.08$ (for $M_{B,l}$=3 $M_\odot$).

Predictions for most elemental ratios as a function of [Fe/H] seem to reproduce the trend of the data, but for [Mg/Fe] and to a less extent for [C/Fe] and [N/Fe]. Possible reasons for this disagreement are briefly discussed. In the case of ^{24}Mg and ^{12}C, they might be reconduced to uncertainties in the ejecta of SNæ. In the case of ^{14}N, the predicted [N/Fe] is crucially dependent on the past SF history due to the contribution of primary ^{14}N from intermediate mass stars. Possible ways out to the low predicted ^{14}N abundance are briefly recalled: either primary ^{14}N from massive stars of low metallicity (Matteucci 1986) or an IMF more skewed toward massive stars than predicted by a Salpeter–like law during the very early stages of galaxy formation and evolution (cf. Chiosi et al. 1997). Both hypotheses need to be thoroughly investigated. The problem is open.

Finally, we like to remark our effort to derive metallicity and hence time dependent stellar yields, since limiting to consider constant yields is not compatible with our current understanding of stellar evolution. But we also need to underline that for some elements many uncertainties still exist on the nucleosynthetic yields of stars in the different mass ranges. These uncertainties display already when considering model predictions for the Solar Neighbourhood, and should be borne in mind when applying chemical models to external galaxies, where detailed tests of the predictions are more difficult.

Acknowledgements. L.P. warmly thanks Paola Marigo for stimulating and helpful discussions on stellar evolution and nucleosynthesis, and acknowledges kind hospitality from the Nordita Institute of Copenhagen. C.C. is pleased to acknowledge the hospitality and stimulating environment provided by ESO in Garching where this paper was finished during sabbatical leave from the Astronomy Department of the Padua University. This study has been financed by the Italian Ministry of University, Scientific Research and Technology (MURST), the Italian Space Agency (ASI), and the European Community (TMR grant ERBFMRX-CT-96-0086).

Appendix A: the link with SN models

Here we describe in detail the method we adopt to establish the relations between M_{CO} and the amount of different elements expelled by the core, so that we can "complete" the total ejecta of our models with the outcome of the final iron–core collapse SN. To this aim, we need to deduce the contribution of the sole CO–core E_i^{CO} to the total ejecta of the SN models by WW95. In the following, we adopt this notation:

M	total mass of the model by WW95
M_{CO}	mass of the CO–core of the model
Z	metallicity of the model
E_i	total ejected amount of species i, taken from WW95 tables
E_i^{new}	newly synthesized and ejected amount of species i
X_i^0	initial abundance of species i in the model
E_i^{ext}	amount of species i contained in the layers external to M_{CO}
E_i^{CO}	amount of species i ejected by the CO–core, i.e. contribution of the CO–core to the global ejecta of i
M_{env}	mass of the region unaffected by CNO burning (roughly corresponding to the mass of the envelope, apart from dredge-up episodes)

First of all, for each tabulated total mass we need to deduce the relevant value of M_{CO}. We assume that the expelled amounts of H and He originate solely in the layers overlying M_{CO}, that is to say (1) in the H–rich envelope, possibly enriched in ^{4}He and in ^{14}N by convective dredge-up episodes, and (2) in the fraction of the He–core that was not involved in the He $\rightarrow$ CO burning, M_{He^-} M_{CO}. (With these assumptions we neglect a possible contribution in He from an α rich freeze–out, which anyway should contribute only a small fraction of the total He ejecta.) The global metallicity in the layers external to M_{CO} is assumed to correspond to the initial one, since

in these layers no nuclear burning takes place but H–burning and the CNO cycle, though altering the relative abundances of CNO isotopes, leaves the overall metallicity substantially unchanged. Therefore, on the base of the expelled amount of H and He, and correcting for the initial fraction of metals, we can derive the mass of the layers over the CO–core; then we derive M_{CO} as:

$$M_{CO} = M - \frac{E_H + E_{He}}{1 - Z} \quad \text{(A1)}$$

In the 15 and 25 $M_\odot$, Z=$Z_\odot$ cases (Tab. S in WW95), we get $M_{CO} = 2.53$ and 6.59 $M_\odot$ respectively; these values look reasonable when compared to Figs. 10a,b of WW95, that illustrate the chemical profiles of the corresponding pre-SN structures. This gives us confidence in the method we adopt (but see § 10). Once we get M_{CO}we consider the production sites of the various elements, so that we can distinguish the ejecta originating in the CO–core from the contribution of the overlying layers.

^{14}N—^{13}C are produced in the CNO cycle and destroyed by α capture during He–burning. No ^{14}N and ^{13}C are left inside the CO–core, and they are not produced by explosive nucleosynthesis (see also Tab. 7 in WW95, comparing the chemical composition of a 25 $M_\odot$ model before and after explosion). These species can come only from layers outside M_{CO}, which doesn't contribute to their ejecta; see also Fig. 13a,b of WW95.

$E^{CO}_{C13} = 0$

$E^{CO}_{N} = 0$

^{12}C—^{16}O are synthesized during He–burning inside M_{CO}. In order to remove the contribution of the outer layers, we need to estimate carbon and oxygen abundances outside M_{CO}. In layers experiencing the CNO cycle, their original abundances are altered in favour of ^{14}N and ^{13}C. Consequently, we estimate first the amount of newly synthesized ^{14}N and ^{13}C. Since these are located only outside M_{CO}, by subtracting the initial amounts within M–M_{CO} to their total ejecta we directly get the newly synthesized amounts:

$E^{new}_{C13} = E_{C13} - X^0_{C13}(M - M_{CO})$

$E^{new}_{N} = E_{N} - X^0_{N}(M - M_{CO})$

^{13}C is synthesized in the CNO cycle starting from ^{12}C, while ^{14}N is synthesized starting from ^{12}C and ^{16}O. Assuming that the new ^{14}N originates from ^{12}C and ^{16}O proportionally to their initial abundances, the amount of ^{12}C and ^{16}O lying outside M_{CO} can be expressed as:

$$E^{ext}_C = X^0_C(M - M_{CO}) - E^{new}_{C13} - E^{new}_N \frac{X^0_C}{X^0_C + X^0_O}$$

$$E^{ext}_O = X^0_O(M - M_{CO}) - E^{new}_N \frac{X^0_O}{X^0_C + X^0_O}$$

Here, the first term is the amount of ^{12}C and ^{16}O present outside M_{CO} since the beginning, from which we remove the amount that has been converted into ^{14}N and ^{13}C. The contribution of the CO–core to carbon and oxygen ejecta is:

$E^{CO}_C = E_C - E^{ext}_C$

$E^{CO}_O = E_O - E^{ext}_O$

^{15}N is quickly destroyed by the CNO cycle, which reduces its abundance by an order of magnitude. The SN explosion can produce ^{15}N by neutrino nucleosynthesis on ^{16}O (^{16}O($\nu_x, \nu_x' p$)^{15}N). We assume that the abundance of ^{15}N is negligible where the CNO cycle takes place, unaltered with respect to the initial one elsewhere. We estimate the mass not involved in H–burning as:

$$M_{env} = \frac{E_H}{X^0}$$

Starting with the total ejecta of ^{15}N, we subtract the contribution of the "envelope" (mass unaffected by the CNO cycle) with the initial abundance of ^{15}N. Whatever is left comes from neutrino nucleosynthesis on ^{16}O, both on the ^{16}O in the CO–core and on the ^{16}O in the outer layers; we further scale the resulting amount of ^{15}N with respect to the fraction of ^{16}O within M_{CO}. The resulting contribution of M_{CO} to the ejecta of ^{15}N is expressed as:

$$E^{CO}_{N15} = (E_{N15} - M_{env}\, X^0_{N15})\, \frac{E^{CO}_O}{E_O}$$

^{17}O abundance within M_{CO} is negligible because ^{17}O is destroyed by α capture during He–burning — see also Figs. 13a,b of WW95.

$E^{CO}_{O17} = 0$

^{18}O is destroyed in the CNO cycle and later produced, but also rapidly destroyed, during He–burning; no ^{18}O is left inside the CO–core.

$E^{CO}_{O18} = 0$

^{20}Ne—^{24}Mg—^{28}Si—^{32}S—^{40}Ca are produced during He– and C–burning; we assume that out of the CO–core their abundances are unaltered with respect to the initial ones. To get the contribution of the CO–core, we simply remove from the total ejecta the contribution of the overlying layers, where the initial abundances hold:

$E^{CO}_{Ne} = E_{Ne} - (M - M_{CO})\, X^0_{Ne}$

$E^{CO}_{Mg} = E_{Mg} - (M - M_{CO})\, X^0_{Mg}$

$E^{CO}_{Si} = E_{Si} - (M - M_{CO})\, X^0_{Si}$

$E^{CO}_{S} = E_{S} - (M - M_{CO})\, X^0_{S}$

$E^{CO}_{Ca} = E_{Ca} - (M - M_{CO})\, X^0_{Ca}$

^{56}Fe is produced in the very last hydrostatic burning stage (Si–burning), but most of the ejected amount of iron originates in the radioactive decay of ^{56}Ni. The tables from WW95 list the ejecta at a time immediately after explosion, when the decay hasn't taken place yet; since all the released ^{56}Ni should later decay in ^{56}Fe, we add the ejecta of ^{56}Ni to those of ^{56}Fe:

$E^{CO}_{Fe} = [E_{Fe} - (M - M_{CO})\, X^0_{Fe}] + E_{Ni}$

In the case of 30, 35 and 40 $M_\odot$ WW95 calculate several models (A, B, C) differing in the energy of the ejected material at infinity. This results mainly in different ejecta of ^{56}Fe, since this element is sensitive to the location of the *mass cut*, which changes with the explosion energy. In our link we referred to the A models of WW95; the effect of different assumptions about the explosion energy can be included in the uncertainty of a factor of two upon the amount of ejected iron, mentioned by WW95.

Appendix B: some warnings about the link

Here we discuss possible drawbacks or incoherences of the method we adopted to link our stellar models with WW95 SN models.

(1) We have implicitly assumed that explosive nucleosynthesis only involves the CO–core leaving the overlying layers unaffected, as they are added from our pre-SN models. This sounds a reasonable approximation, but we neglect a possible production of ^{15}N from neutrino nucleosynthesis over the ^{16}O lying out of M_{CO} and a possible contribution of an α rich freeze–out in the ejecta of ^{4}He.

(2) One of the basic parameters in the adopted SN models is the kinetic energy of the ejecta at infinity (WW95): the shockwave generating the explosion is simulated by means of a piston, regulated so that the final energy assumes a typical value, $\sim 1.2 \times 10^{51}$ erg. Outside M_{CO}, the layers in our pre-SN models have a different mass and structure from those of WW95, both because we include mass loss and because of the different physical treatment of details of stellar evolution (especially the inclusion of convective overshooting). Therefore, for a given M_{CO}, the kinetic energy of our ejecta at infinity can be different from that imposed in WW95 models. This affects mainly the remnant mass, which depends on the explosion energy, on the pre-SN structure, on the stellar mass and on metallicity (WW95). Most of all, the extent of a possible *reverse shock* as found in WW95 models may not be directly transferred to our models, because it depends on the density structure of the layers over the core. A reverse shock can induce a fall back of material toward the collapsed core, which increases the mass of the final remnant. Since we do not know how the remnant mass in WW95 models depends on this physical effect in detail, we can't correct for it. The choice of adopting the same remnant mass for the same M_{CO} as in WW95 models can influence our ejecta of ^{28}Si, ^{32}S and ^{56}Fe, that are the elements produced next to the mass cut of the SN.

(3) An inconsistency between the two sets of models is the different cross-section adopted for the fundamental reaction ^{12}C(α,γ)^{16}O. In our tracks the adopted value is from Caughlan & Fowler (1988), while WW95 adopt 1.7 times that value. Both values are within current uncertainties, but they result in a sensitively different composition of the CO–core: in our models the resulting core consists of a 30% of ^{12}C and a 70% of ^{16}O, while in WW95 models the carbon abundance in the core is as low as $\sim$10% (see Figs. 5ab, 10ab, 12ab, 14ab and 16ab of WW95). In a way, by "replacing" our CO–cores with the cores of WW95, we adopt their value of the cross-section, since that reaction is important only from He–burning on, i.e. inside the CO–core. However, in cases where mass loss is so efficient as to reveal He–burning processed material on the surface and disperse it in the wind, the carbon/oxygen abundance ratio in the expelled material is due to a cross-section value which is different from that used inside the core; this gives some inconsistency in case of extreme mass-loss.

(4) Most of all, our method neglects the finite extension of the He–burning shell: when we separate the CO–core contribution from the contribution of the overlying layers, we somehow assume a sudden jump in the chemical composition between the CO–core and the outer layers, as if He–burning defined M_{CO} as a sharp edge. Actually, there is a gradient of chemical profile between the regions where helium is still abundant and those where it has been completely processed. In cases where the He–burning shell is not thin and/or a shallow gradient of chemical composition has been established, our assumption about a clean separation between the CO–core and the rest of the star may lead to inconsistency. This would mainly affect the early products of He–burning, such as carbon, whose abundance can change sensitively even in the outer regions of He–burning, where the process is only partial. This brings some scatter in the C–production vs. M_{CO} relation, since at the time of explosion most of the carbon is located at the edge of the CO–core or even outside it, and its distribution is sensitive to past history especially in stars which suffered from efficient mass loss (M92). Therefore, the linking method can be less reliable in the case of carbon, and this might explain our problems in reproducing the observed [C/Fe] ratio (see § 9.7). To check this effect, we apply the method outlined in App. A to derive the ejecta of the CO–cores of the mass–losing helium stars calculated by Woosley et al. (1995). These stars build up a shallow gradient of carbon and helium abundance at the outer edge of the CO–core, and for these stars the assumption of a sharp–edged core is not properly correct. By applying Eq. (A1), we tend to overestimate the size of the CO–core for these stars, as shown in Tab. 15 where the estimated core masses are compared with the real ones as tabulated in Woosley et al. (1995, Tab. 6). In Fig. 24 we plot the ejecta versus M_{CO} for these helium stars and we compare these relations to those obtained for WW95 models of Z=$Z_{\odot}$ (App. A and Fig. 4). While carbon evidently behaves in quite a different way in the two cases, the ejecta of other elements and the remnant mass seem to follow a better defined relation with M_{CO}.

Table 15. 1^{st} column: model masses of mass–losing helium stars of Woosley et al. 1995; 2^{nd} column: corresponding CO–core masses as listed in Tab. 6 of Woosley et al. 1995; 3^{rd} column: CO–core masses as deduced according to the outlined method (see text)

M	$M_{CO}(1)$	$M_{CO}(2)$
4	1.53	1.60
5	1.87	2.05
7A	2.30	2.73
7B	2.30	2.80
7C	2.30	2.80
10A	2.50	3.26
10S	2.50	3.26
20	2.53	3.31

Appendix C: calculating the Q_{ij} matrix

Here we explain the definition and the meaning of the non–zero elements of the Q_{ij} matrix (Tab. 13) and show how the fundamental quantities entering the matrix are calculated.

^{1}H For any stellar mass, all the hydrogen which remains unburnt in the interiors is eventually ejected. The only non–zero matrix element for ^{1}H is $Q_{1,1}$, corresponding to the

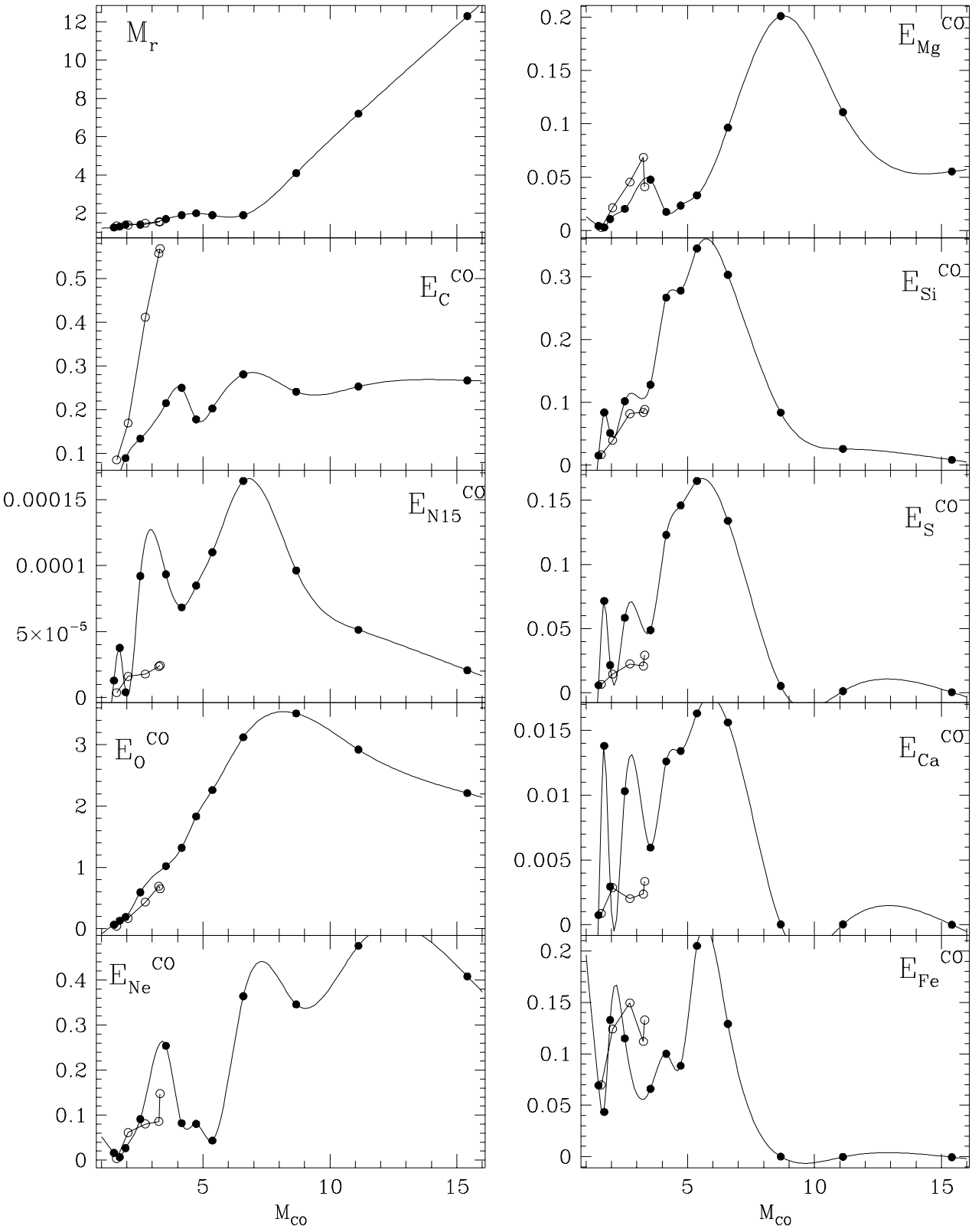

Fig. 24. Remnant mass and ejecta of the CO–core vs. M_{CO}as deduced for mass-losing helium stars of Woosley et al. 1995 (open circles) compared with the analogous relations deduced for the case Z=$Z_{\odot}$ of WW95 (filled circles).

initial ^{1}H which hasn't been processed. As q_4 is the mass fraction where ^{1}H is turned to ^{4}He,

$Q_{1,1} = 1 - q_4$

^{2}He Helium is synthesized on ^{1}H within q_4 and later turned to ^{12}C, ^{16}O and heavier species within q_C. All the surviving ^{4}He (at least for stars of some interest, $M > 0.5\ M_\odot$) is eventually ejected. The term corresponding to the newly synthesised and ejected ^{4}He is

$Q_{2,1} = q_4 - q_C$

while the term corresponding to the original unprocessed and ejected ^{4}He is

$Q_{2,2} = 1 - q_C$

^{12}C Carbon is turned to ^{13}C and later to ^{14}N within q_{C13s}, by the CNO cycle; later, it is synthesised on ^{4}He within q_C. The original ^{12}C which is ejected is represented by

$Q_{3,3} = 1 - q_{C13s}$

Also the newly synthesized ^{12}C within $w_C = q_C - d$ is not locked in the remnant and can be ejected:

$Q_{3,1} = Q_{3,2} = \chi_C w_C$

The matrix element $Q_{3,1}$ is non–zero because the 3α chain turns to ^{12}C both the original ^{4}He and the ^{4}He which had been previously synthesized on the original ^{1}H.

^{13}C The ejected original ^{13}C is the one outside q_{Ns}, where it is turned to ^{14}N by the CNO cycle:

$Q_{4,4} = 1 - q_{Ns}$

Some new ^{13}C can also be synthesized on ^{12}C by the CN cycle within q_{C13s}, and the corresponding ejected fraction is represented by:

$Q_{4,3} = q_{C13s} - q_{Ns}$

In intermediate mass stars some primary ^{13}C can also be produced, due to the combined effect of III dredge-up and CNO envelope burning, so for these stars further non–zero matrix elements can be:

$Q_{4,1} = Q_{4,2} = \chi_{C13} w_C$

^{14}N Only the original ^{14}N outside the He–burning region can be eventually expelled, otherwise it is turned to neutron–rich isotopes:

$Q_{5,5} = 1 - q_C$

Secondary ^{14}N is synthesized on ^{12}C, ^{16}O and ^{13}C during the CNO cycle; the fraction which remains outside q_C is eventually ejected for any stellar mass:

$Q_{5,3} = Q_{5,4} = Q_{5,6} = q_{Ns} - q_C$

We point out that, by taking $Q_{5,3} = Q_{5,4} = Q_{5,6}$, we implicitly assume that in the CNO cycle secondary ^{14}N comes from original ^{12}C, ^{16}O and ^{13}C in the same proportions as their initial abundances.

In intermediate mass stars some primary nitrogen is produced by CNO envelope burning over dredged-up ^{12}C, so for these stars we also have:

$Q_{5,1} = Q_{5,2} = \chi_N w_C$

^{16}O The ejected original oxygen is that outside q_{Ns}, where it is turned to ^{14}N by the ON cycle:

$Q_{6,6} = 1 - q_{Ns}$

New oxygen is produced within q_C; the fraction which isn't locked in the remnant d is expelled:

$Q_{6,1} = Q_{6,2} = \chi_O w_C$

nr We indicate with *nr* the body of neutron rich isotopes synthesized on ^{14}N during He–burning (^{18}O, ^{22}Ne, ^{25}Mg) within q_C. All the original and newly synthesized nr isotopes are eventually ejected; the corresponding matrix elements are:

$Q_{7,7} = 1 - d$

$Q_{7,3} = Q_{7,4} = Q_{7,5} = Q_{7,6} = w_C$

^{20}Ne—^{24}Mg—^{28}Si—^{32}S—^{40}Ca—^{56}Fe All these species are produced in the He–burning stage or in later stages, within q_C. The fraction of the original amount of each of these species which is eventually ejected is represented by:

$Q_{i,i} = 1 - d \qquad i = 8 \div 13$

while the ejected fraction of the newly synthesized amount is:

$Q_{i,1} = Q_{i,2} = \chi_i w_C \qquad i = 8 \div 13$

The relevant quantities entering the Q_{ij} matrix (§ 8.4) are calculated on the base of the stellar ejecta derived from the tracks of the Padua library and discussed in this paper. We impose, species after species, Eq. (23), so that by re-inserting the proper abundance set $\{X_j,\ j = 1, ...13\}$ the original values of stellar ejecta are preserved.

d The remnant mass fraction d is, by definition:

$$d = \frac{M_r}{M} \tag{C1}$$

q_4 By definition, q_4 is the mass fraction involved in the ^{1}H→ ^{4}He burning. If we simply considered the mass fraction of the He–core, $q_4 = M_{He}/M$, we would neglect that the core may have receded or varied in size in the course of evolution and that some material has been dredged-up in the envelope and/or lost in stellar winds. On the contrary, by applying Eq. (23) to the case of hydrogen (i=1):

$$(1 - q_4)\, X = \frac{E_H}{M}$$

we get an "effective" q_4 which automatically takes into account the whole mass where hydrogen has been burnt, both the mass lying in the core and the mass dredged-up to the surface. So we assume:

$$q_4 = 1 - \frac{E_H}{XM} \tag{C2}$$

q_C By definition, q_C is the mass fraction where ^{4}He is turned to ^{12}C, ^{16}O and heavier species. Again, if we simply took the mass fraction of the CO–core, $q_C = M_{CO}/M$, we would neglect the material dredge-up in the envelope and/or ejected with mass loss. In the case of low and intermediate mass stars, we would lose completely the contribution of the III dredge-up, since we'd find $q_C = d$ and $w_C = 0$. On the contrary, by applying Eq. (23) to the case of helium (i=2), we get an "effective" q_C which automatically takes into account the role of dredge-up episodes:

$$(q_4 - q_C)\, X + (1 - q_C)\, Y = \frac{E_{He}}{M}$$

$$q_C = \left[q_4 X + Y - \frac{E_{He}}{M}\right] \frac{1}{X + Y} \tag{C3}$$

where q_4 is known from Eq. (C2). Now we can also determine:

$$w_C = q_C - d \tag{C4}$$

q_{Ns} We obtain the mass fraction q_{Ns} where secondary nitrogen is produced by imposing Eq. (23) to the case of *secondary* ^{14}N. This corresponds to all the ejected ^{14}N in the case of massive stars, while in low and intermediate mass stars we keep the ejecta of primary and secondary ^{14}N apart, since they involve distinct matrix elements.

$$(q_{Ns}-q_C)(X_C+X_{C13}+X_O)+(1-q_C)X_N=\frac{E_{Ns}}{M}$$

$$q_{Ns} = \frac{E_{Ns}}{(X_C+X_{C13}+X_O)M} - (1-q_C)\frac{X_N}{X_C+X_{C13}+X_O} + q_C \quad \text{(C5)}$$

where q_C is known from Eq. (C3).

q_{C13s} We obtain the mass fraction q_{C13s} where the CN cycle turns ^{12}C to ^{13}C in the same way as q_{Ns}, i.e. by imposing Eq. (23) to the case of *secondary* ^{13}C:

$$(q_{C13s}-q_{Ns})\,X_C+(1-q_{Ns})\,X_{C13}=\frac{E_{C13s}}{M}$$

$$q_{C13s}=\frac{E_{C13s}}{X_C M}-(1-q_{Ns})\frac{X_{C13}}{X_C}+q_{Ns} \quad \text{(C6)}$$

where q_{Ns} is known from Eq. (C5).

χ_N The abundance χ_N of the ^{14}N synthesized within w_C by envelope burning in intermediate mass stars is defined by Eq. (23), applied to *primary* ^{14}N:

$$(\chi_N w_C)(X+Y)=\frac{E_{Np}}{M}$$

$$\chi_N=\frac{E_{Np}}{(X+Y)Mw_C} \quad \text{(C7)}$$

where w_C is known from Eq. (C4).

χ_{C13} Similarly, by imposing Eq. (23) to *primary* ^{13}C we get:

$$\chi_{C13}=\frac{E_{C13p}}{(X+Y)Mw_C} \quad \text{(C8)}$$

χ_C The abundance χ_C of new ^{12}C synthesized within w_C is obtained by applying Eq. (23) to carbon (i=3)

$$(\chi_C w_C)(X+Y)+(1-q_{C13s})\,X_C=\frac{E_C}{M}$$

$$\chi_C=\frac{E_C}{(X+Y)Mw_C}-\frac{1-q_{C13s}}{w_C}\frac{X_C}{X+Y} \quad \text{(C9)}$$

where q_{C13s} is known from Eq. (C6).

χ_O Similarly, by applying Eq. (23) to ^{16}O (i=6) we get:

$$\chi_O=\frac{E_O}{(X+Y)Mw_C}-\frac{1-q_{Ns}}{w_C}\frac{X_O}{X+Y} \quad \text{(C10)}$$

where q_{Ns} is known from Eq. (C5).

χ_{Ne}—χ_{Mg}—χ_{Si}—χ_S—χ_{Fe} The abundances of the newly synthesized component of these elements within w_C is obtained by imposing Eq. (23) to the cases i=8÷13.

$$(\chi_i w_C)(X+Y)+(1-d)\,X_i=\frac{E_i}{M}$$

$$\chi_i=\frac{E_i}{(X+Y)Mw_C}-\frac{1-d}{w_C}\frac{X_i}{X+Y} \quad \text{(C11)}$$

We can now derive a Q_{ij} matrix for each star whose ejecta have been determined; then, using Eq. (21), we get the "restitution fractions" R_{Mi} entering Eq. (7). We have derived stellar ejecta and Q_{ij} matrices for 5 different sets of metallicities; therefore in Eq. (21) we have an explicit dependence on the initial composition of the star through the X_j's, and also an indirect dependence through $Q_{ij}=Q_{ij}(M,Z)$. That's why the restitution fractions R_{Mi}'s in Eq. (7) are to be evaluated as a function of the birth-time of the star, to take the effect of initial composition into account:

$$R_{Mi}(t-\tau_M)=\sum_j Q_{ij}(M,Z(t-\tau_M))X_j(t-\tau_M)$$

It is worth here underlining the advantages of this "Q_{ij} matrix" formalism. It was originally introduced in order to compensate for the lack of stellar model of different metallicities, by assuming that the influence of the initial chemical composition over the R_{Mi}'s was included in the linear dependence on the X_j's, while the dependence of the Q_{ij}'s on Z was negligible (Talbot & Arnett 1973). Now that stellar models and corresponding ejecta for different metallicities are available, using the Q_{ij} matrix allows to take into account also possible differences of chemical composition *within* a given Z. Indeed, stellar models with different metallicities generally assume solar *relative* abundances of the various species within a given Z; but abundance ratios are not constant in the course of galactic evolution, nor they are in the evolution of a chemical model. The Q_{ij} matrix links any ejected species to all its different nucleosynthetic sources, allowing the model to scale the ejecta with respect to the detailed initial composition of the star through the X_j's.

References

Adouze J., 1986, in *Nucleosynthesis and chemical evolution*, 16^{th} Advanced Course, Saas-Fee, p.431

Arnett D.W., 1978, ApJ 219, 1008

Arnett D.W., 1991, in *Frontiers of stellar evolution*, Lambert D.A. (ed.), ASP Conf. Ser. 20, p.389

Baraffe I., El Eid M.F., 1991, A&A 245,548

Barbuy B., Erdelyi-Mendes M., 1989, A&A 214, 239

Bond J.R., 1984, in *Stellar nucleosynthesis*, C. Chiosi C., Renzini A. (eds.), Dordrecht:Reidel, Astrophysics and Space Science Library, vol. 109, p.297

Bond J.R., Arnett D.W., Carr B.J., 1984, ApJ 280, 825

Bressan A., Fagotto F., Bertelli G., Chiosi C., 1993, A&A Suppl. 100, 647

Burkert A., Truran J.W., Hensler G., 1992, ApJ 391, 651

Cappellaro E., Turatto M., Tvetkov D.Yu., et al., 1997, A&A 322, 431

Carbon D.F., Barbuy B., Kraft R.P., Friel E.D., Suntzeff N.B., 1987, PASP 99, 335

Carlberg R.G., Dawson P.C., Hsu T., VandenBerg D.A., 1985, ApJ 294, 674

Carr B.J., Bond J.R., Arnett D.W., 1984, ApJ 277, 445

Carraro G., Lia C., Chiosi C., 1997, MNRAS submitted

Carraro G., Ng Y.K., Portinari L., 1997, MNRAS submitted (astro-ph 9707185)

Carretta E., 1995, PhD Thesis, University of Padua

Caughlan G.R., Fowler W.A.,1988, Atomic Data Nuc. Data Tables 40, 283

Chiappini C., Matteucci F., Gratton R.G., 1997, ApJ 477, 765

Chiosi C., 1979, A&A 80, 252

Chiosi C., 1980, A&A 83, 206

Chiosi C., 1986, in *Nucleosynthesis and chemical evolution*, 16^{th} Advanced Course, Saas-Fee, p. 201

Chiosi C., 1997, in *Stellar Astrophysics for the Local Group: A First Step to the Universe*, Aparicio A.J., Herrero A. (eds.), Cambridge University Press
Chiosi C., Caimmi R., 1979, A&A 80, 234
Chiosi C., Maeder A., 1986, ARA&A 24, 329 (CM86)
Chiosi C., Matteucci M., 1982, A&A 105, 140
Chiosi C., Bertelli G., Bressan A., 1992, ARA&A 30, 235
Chiosi C., Bressan A.G., Portinari L., Tantalo R., 1997, A&A submitted (astro-ph 9708123)
Clegg R.E.S., Lambert D.L., Tomkin J., 1981, ApJ 250, 262
de Jager C., Nieuwenhuijzen H., van der Hucht K.A., 1988, A&A Suppl. 72, 259
Edvardsson B., Andersen J., Gustaffson B., et al., 1993, A&A 275, 101
El Eid M.F., Fricke K.J., Ober W.W., 1983, A&A 119, 54
Fagotto F., Bressan A., Bertelli G., Chiosi C., 1994a, A&A Suppl. 105, 29
Fagotto F., Bressan A., Bertelli G., Chiosi C., 1994b, A&A Suppl. 104, 365
Ferrini F., Matteucci F., Pardi C., Penco U., 1992, ApJ 387, 138
Fowler W.A., Hoyle F., 1964, ApJS 9, 201
François P., 1987, A&A 176, 294
François P., 1988, A&A 195, 226
Garcia-Berro E., Iben I., 1994, ApJ 434, 306
Gratton R.G., 1985, A&A 148, 105
Gratton R.G., Ortolani S., 1986, A&A 169, 01
Gratton R.G., Sneden C., 1988, A&A 204, 193
Gratton R.G., Sneden C., 1991, A&A 241, 501
Greggio L., Renzini A., 1983, A&A 118, 217
Güsten R., Mezger P.G., 1982, Vistas in Astr. 26, 159
Gutierrez J., Garcia-Berro E., Iben I., et al., 1996, ApJ 459, 701
Hartmann K., Gehren T., 1988, A&A 199, 269
van den Hoek L.B., de Jong T., 1997, A&A 318, 231
Kudritzki R.P., 1997, in *Stellar Astrophysics for the Local Group: a First Step to the Universe*, Aparicio A.J., Herrero A. (eds.), Cambridge University Press
Kudritzki R.P., Pauldrach A., Puls J., & Abbott D.C., 1989, A&A 219, 205
Laird J.B., 1985, ApJ 289, 556
Lamers H., Cassinelli J., 1996, in *From stars to galaxies: the impact of stellar physics on galaxy evolution*, Leitherer C., Fritze-von Alvensleben U., Huchra J. (eds.), ASP Conf. Ser. 98, 162
Langer N., 1989, A&A 220, 135
Langer N., Woosley S.E., 1996, in *From stars to galaxies: the impact of stellar physics on galaxy evolution*, Leitherer C., Fritze-von Alvensleben U., Huchra J. (eds.), ASP Conf. Ser. 98, 220
Larson R.B., 1976, MNRAS 176, 31
Larson R.B., 1991, in *Frontiers of stellar evolution*, Lambert D.A. (ed.) ASP Conf. Ser. 20, 539
Leitherer C., Langer N., 1991, in *The Magellanic Clouds*, IAU Symp. 148, Haynes R., Milne D. (eds.), Kluwer Acad. Publ., p. 480
Lynden-Bell D., 1975, Vistas in Astr. 19, 229
Maeder A., 1981, A&A 101, 385
Maeder A., 1983, A&A 120, 113
Maeder A., 1984, in *Stellar nucleosynthesis*, Chiosi C., Renzini A. (eds.), Dordrecht: Reidel
Maeder A., 1992, A&A 264, 105 (M92)
Maeder A., 1993, A&A 268, 833
Maeder A., Conti P.S., 1994, ARA&A 32, 227
Magain P., 1987, A&A 179, 176
Magain P., 1989, A&A 209, 211
Malinie G., Hartmann D.H., Mathews G.J., 1991, ApJ 376, 520
Malinie G., Hartmann D.H., Clayton D.D., Mathews G.J., 1993, ApJ 413, 633
Marigo P., Bressan A.G., Chiosi C., 1996, A&A 313, 545
Marigo P., Bressan A.G., Chiosi C., 1997, A&A in press (astro-ph 9710093)
Matteucci F., 1986, MNRAS 221, 911
Matteucci F., 1991, in *Frontiers of stellar evolution*, Lambert D.A. (ed.) ASP Conf. Ser. 20, 539
Matteucci F., François P., 1989, MNRAS 239, 885
Matteucci F., Greggio L., 1986, A&A 154, 279
Mayle R., Wilson J.R., 1988, ApJ 334, 909
Meusinger H., Reimann H.G., Stecklum B., 1991, A&A 245, 57
Miller G.E., Scalo J.M., 1979, ApJS 41, 513
Nissen P.E., Edvardsson B., 1992, A&A 261, 255
Ng Y.K., Bertelli G., 1997, A&A in press
Nomoto K., 1984, ApJ 277, 791
Nomoto K., 1987, ApJ 322, 206
Nomoto K., Hashimoto M., 1986, Progr. Part. Nucl. Phys. 17, 267
Nomoto K., Thielemann F.K., Yokoi K., 1984, ApJ 286, 644
Nomoto K., Shigeyama T., Tsujimoto T., 1991, in *Evolution of stars: the photospheric abundance connection*, IAU Symp. 145, Michaud G., Tutukov A. (eds.), Kluwer Acad. Publ., p.21
Ober W.W., El Eid M.F., Fricke K.J., 1983, A&A 119, 61
Oort J.H., 1970, A&A 7, 381
Paczynski B., Stanek K.Z., 1997, ApJL submitted, astro-ph/9708080
Pagel B.E.J., 1989, in *Evolutionary phenomena in galaxies*, Beckman J.E., Pagel B.E.J. (eds.), Cambridge University Press, p.201
Pagel B.E.J., 1997, *Nucleosynthesis and chemical evolution of galaxies*, Cambridge University Press
Pagel B.E.J., Patchett B.E., 1975, MNRAS 172, 13
Peterson R.C., Kurucz R.L., Carney B.W., 1990, ApJ 350, 173
Pilyugin L.S., Edmunds M.G., 1996, A&A 313, 792
Rana N.C., 1991, ARA&A 29,129
Reid M.J., 1993, ARA&A 31, 345
Ritossa C., Garcia-Berro E., Iben I., 1996, ApJ 460, 489
Rocha-Pinto H.J., Maciel W.J., 1996, MNRAS 279, 447
Sackett P.D., 1997, ApJ 483, 103
Salpeter E., 1955, ApJ 121, 161
Scalo J.M., 1986, Fund. Cosmic Phys. 11, 3
Schmidt M., 1959, ApJ 129, 243
Schwarz U.J., Wakker B.P., Van Woerden H., 1995, A&A 302,364
Sneden C., Lambert D.L., Whitaker R.W., 1979, ApJ 234, 864
Sommer-Larsen J., 1991, MNRAS 249. 368
Talbot R.J., Arnett D.W., 1971, ApJ 170, 409
Talbot R.J., Arnett D.W., 1973, ApJ 186, 51
Talbot R.J., Arnett D.W., 1975, ApJ 197, 551
Tammann G.A., Löffler W., Schröder A., 1994, ApJS 92,487
Thielemann F.K., Nomoto K., Hashimoto M.K., 1993, in *Origin and evolution of the elements*, Prantzos N., Vangioni-

Flam E., Cassé M. (eds.), Cambridge University Press, p.297
Thielemann F.K., Nomoto K., Hashimoto M.K., 1996, ApJ 460, 408
Thomas D., Greggio L., Bender R., 1997, MNRAS submitted (astro-ph/9710004)
Timmes F.X., Woosley S.E., Weaver T.A., 1995, ApJS 98, 617
Tinsley B., 1980, Fund. Cosmic Phys. 5, 287
Tomkin J., Sneden C., Lambert D.L., 1986, ApJ 415, 420
Tomkin J., Lemke M., Lambert D.L., Sneden C., 1992, AJ 104, 1568
Tosi M., 1988, 197, 47
Tutukov A.V., Yungelson L.R., 1980, in *Close binary stars*, IAU Symp. 88, p.15
Twarog B.A., 1980, ApJ 242, 242
Walker T.P., Steigman G., Kang H., Schramm D.N., Olive K.A., 1991, ApJ 376, 51
Whelan J.C., Iben I., 1973, ApJ 186, 1007
Woosley S.E., 1986, in *Nucleosynthesis and chemical evolution*, 16^{th} Advanced Course, Saas-Fee, p. 1
Woosley S.E., Weaver T.A., 1982, in *Supernovæ: a survey of current research*, Rees M.J., Stoneham R.J. (eds.), Dordrecht:Reidel, p.79
Woosley S.E., Weaver T.A., 1986, ARA&A 24, 205
Woosley S.E., Weaver T.A., 1995, ApJS 101, 181 (WW95)
Woosley S.E., Langer N., Weaver T.A., 1993, ApJ 411, 823
Woosley S.E., Langer N., Weaver T.A., 1995, ApJ 448, 315
Wyse R.F.G., Gilmore G., 1995, AJ 110, 2771
Zhao G., Magain P., 1990, A&A 238, 242

This article was processed by the author using Springer-Verlag LaTeX A&A style file *L-AA* version 3.